Studies on the Interactions of Water Waves(Dissertation_全文)

AUTHOR(S):

Funakoshi, Mitsuaki

Studies on the Interactions of Water Waves

Mitsuaki Funakoshi

Studies on the Interactions of Water Waves

Mitsuaki Funakoshi

Abstract

Some results about the interactions of water waves are presented. In chapter 1, some theories and experiments about the nonlinear effect in water waves are reviewed.

In chapters 2 and 3, the reflection problem of a solitary wave in shallow water at the rigid vertical wall is examined. This problem is closely related to the interaction of two solitary waves. In chapter 2, the nonlinear effect in the one-dimensional reflection of a solitary wave is examined numerically in detail. It is shown that the larger phase shift associated with the reflection is obtained for the larger ε. Here ε is the amplitude of an incident wave nondimensionalized by the water depth h. Furthermore, the phase shift tends to zero as $\varepsilon \to 0$ in agreement with the existing theory based on the perturbation method. It is also found that an incident solitary wave suffers the slight distortion of its shape from the reflection. That is, a reflected wave has the amplitude slightly smaller than that of an incident wave, and is followed by the small oscillating part. This distortion nondimensionalized by h is at most of $O(\varepsilon^3)$.

In chapter 3, the reflection of an obliquely incident solitary wave is examined. The equations which govern the shallow-water wave motion in two dimensions are derived and solved numerically. If the angle of incidence α satisfies $\alpha > (3\varepsilon)^{1/2}$ a regular reflection pattern emerges, while if $\alpha < (3\varepsilon)^{1/2}$ a Mach reflection pattern (geometrically similar to the corresponding shock-wave reflection pattern) is found. The

solution for the latter case agrees well with the solution composed of three resonantly interacting solitary waves predicted by Miles.

In chapters 4 and 5, the long-short wave interactions between an internal gravity wave and a surface gravity wave packet in two-layer fluid are examined. This interaction occurs when the phase speed of an internal wave coincides with the group velocity of a surface wave packet. The equations which govern the time development of a long wave and the envelope of a short wave packet are derived and are solved numerically.

In chapter 4, the shallow-fluid case, in which the wavelength l of an internal wave is much larger than the fluid depths, is considered. It is found that a coupled soliton composed of the depression of a long wave and a hump of short wave packet emerges from a wide class of localized initial distributions. In chapter 5, the deep-fluid case, in which l is much larger than the fluid depth of the upper layer and is much smaller than that of the lower layer, is considered. The governing equations for this case have the extra term representing the dispersion of internal waves in comparison with those for shallow-fluid case. The solitary wave solutions to the equations are obtained numerically.

Ackowledgement

The author would like to express his sincere thanks to Professor Akira Ueda for his kind advice and continued encouragement. The author also would like to express his sincere thanks to Dr. Masayuki Oikawa for his kind guidance and for helpful advice and discussions in the course of this work.

The author is very grateful to Professor Jun-ichi Okabe for his continued encouragement. Finally the author wishes to thank Miss Kyoko Tsuchiya for typing the manuscript.

Contents

Chapter 1

Introduction

The nonlinear effects in water waves have been one of the most interesting subjects in fluid dynamics since they began to be taken into account in the nineteenth century. The problem of interactions of water waves, which can be considered as one manifestation of these effects, is examined in the present thesis.

The history of nonlinear theories and the related experiments for water waves are reviewed briefly in this chapter. The developments in the investigations on surface waves and on the waves in two-layer fluid are described in §1.1 and in §1.2 respectively. Several basic results for the interactions of these water waves are reviewed in § 1.3.

§ 1.1 Surface Waves

The irrotational motion of incompressible and inviscid fluid of uniform density on the horizontal bed is considered under the existence of a free surface. Although this situation is fairly simple, many interesting phenomena related to the nonlinearity have been predicted and observed.

The x and y coordinates are taken to be in a horizontal plane and the z axis vertically upwards from the free surface in quiet state. The geometrical configuration is shown in Fig.1. If we take (u,v,w) as the velocity of the fluid particle in the (x,y,z) direction, and p as the pressure, the governing equation

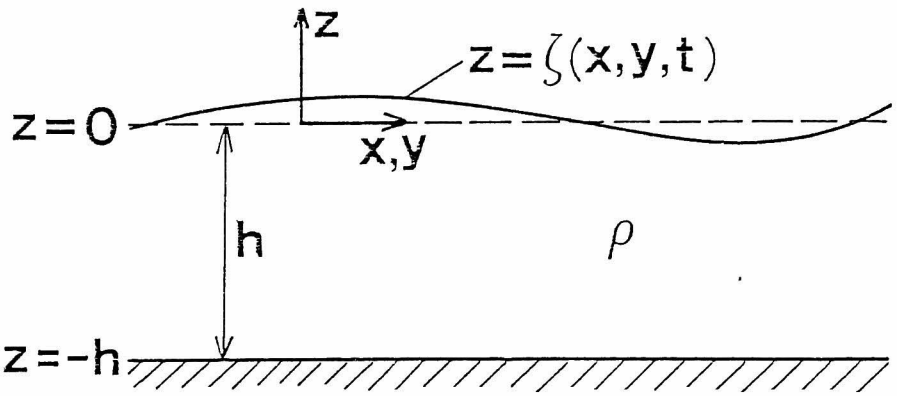

Fig.1 The geometrical configuration.

for the fluid motion can be written as

$$\frac{\partial u}{\partial t} + \frac{\partial}{\partial x}(u^2) + \frac{\partial}{\partial y}(uv) + \frac{\partial}{\partial z}(uw) = -\frac{1}{\rho}\frac{\partial p}{\partial x}, \tag{1.1a}$$

$$\frac{\partial v}{\partial t} + \frac{\partial}{\partial x}(uv) + \frac{\partial}{\partial y}(v^2) + \frac{\partial}{\partial z}(vw) = -\frac{1}{\rho}\frac{\partial p}{\partial y}, \tag{1.1b}$$

$$\frac{\partial w}{\partial t} + \frac{\partial}{\partial x}(uw) + \frac{\partial}{\partial y}(vw) + \frac{\partial}{\partial z}(w^2) = -\frac{1}{\rho}\frac{\partial p}{\partial z} - g, \tag{1.1c}$$

$$\frac{\partial u}{\partial x} + \frac{\partial v}{\partial y} + \frac{\partial w}{\partial z} = 0, \tag{1.1d}$$

where t denotes the time, and g and ρ are the gravitational acceleration and the fluid density respectively. The boundary conditions for the wave motion are given by

$$\frac{\partial \zeta}{\partial t} + u\frac{\partial \zeta}{\partial x} + v\frac{\partial \zeta}{\partial y} = w, \qquad \text{at} \quad z=\zeta \tag{1.2a}$$

$$p + T(R_1^{-1}+R_2^{-1}) = \text{const.}, \qquad \text{at} \quad z=\zeta \tag{1.2b}$$

$$w=0, \qquad \text{at} \quad z=-h \tag{1.2c}$$

under the assumption of constant atmospheric pressure. Here $z=\zeta(x,y,t)$ denotes the free surface displacement, h is the water depth in quiet state, and T is the surface tension, and R_1 and R_2 are the principal radii of curvature of the free surface. For the irrotational motion eqs.(1.1) and boundary conditions (1.2) can be reduced to

$$\frac{\partial^2\phi}{\partial x^2}+\frac{\partial^2\phi}{\partial y^2}+\frac{\partial^2\phi}{\partial z^2}=0, \qquad -h<z<\zeta \tag{1.3a}$$

$$\frac{\partial\zeta}{\partial t}+\frac{\partial\phi}{\partial x}\frac{\partial\zeta}{\partial x}+\frac{\partial\phi}{\partial y}\frac{\partial\zeta}{\partial y}=\frac{\partial\phi}{\partial z}, \qquad \text{at} \quad z=\zeta \tag{1.3b}$$

$$\frac{\partial\phi}{\partial t}+\frac{1}{2}\left[\left(\frac{\partial\phi}{\partial x}\right)^2+\left(\frac{\partial\phi}{\partial y}\right)^2+\left(\frac{\partial\phi}{\partial z}\right)^2\right]+g\zeta-\frac{T}{\rho}(R_1^{-1}+R_2^{-1})$$

$$=\text{const.} \qquad \text{at} \quad z=\zeta \tag{1.3c}$$

$$\frac{\partial\phi}{\partial z}=0, \qquad \text{at} \quad z=-h \tag{1.3d}$$

where ϕ is the velocity potential satisfying

$$\frac{\partial\phi}{\partial x}=u, \quad \frac{\partial\phi}{\partial y}=v, \quad \frac{\partial\phi}{\partial z}=w. \tag{1.4}$$

The linearized forms of eqs.(1.3) have the following solution which propagates in the x direction :

$$\zeta=a\cos(kx-\omega t), \tag{1.5a}$$

$$\phi=\frac{a\omega\cosh k(z+h)}{k\sinh kh}\sin(kx-\omega t). \tag{1.5b}$$

Here the wavenumber k and the frequency ω satisfy the dispersion relation

$$\omega=\sqrt{gk(1+Tk^2/\rho g)\tanh kh}. \tag{1.6}$$

The length scales which are important in the linear theory

of surface waves are the water depth h, the characteristic wavelength l ($\sim k^{-1}$), and the number $(T/\rho g)^{1/2}$. In the nonlinear theory, the wave amplitude a as well as the above three length scales must be taken into account. The theoretical treatment of surface waves differs according to the ratios of these length scales.

The nonlinear effects in the gravity wave in non-shallow water ($h \gtrsim l \gg (T/\rho g)^{1/2}$, a:finite) are reviewed in § 1.1.1, and those in shallow water ($l \gg h$, $l \gg (T/\rho g)^{1/2}$, a:finite) in § 1.1.2. The brief comments on the nonlinear theory of the capillary-gravity wave ($l \lesssim (T/\rho g)^{1/2}$, a:finite) are made in § 1.1.3.

1.1.1. Surface gravity waves in non-shallow water

The nonlinear effect in surface gravity waves was first investigated by Stokes [1], [2]. He considered a steady progressive one-dimensional wave of the amplitude a and of the wavelength l ($=2\pi/k$). Using a systematic perturbation technique with respect to the wave steepness $\varepsilon_s \equiv ak$, he calculated the solution of the equations obtained by the neglect of the surface tension in eqs.(1.3) for finite depth to $O(\varepsilon_s^3)$. It can be written as

$$k\zeta = \varepsilon_s \cos\theta + \frac{1}{2}\varepsilon_s^2 \coth kh \left(1 + \frac{3}{2\sinh^2 kh}\right)\cos 2\theta + O(\varepsilon_s^3), \qquad (1.7a)$$

$$\frac{k^2}{\omega}\phi = \varepsilon_s \frac{\cosh k(z+h)}{\sinh kh}\sin\theta + \frac{3}{8}\varepsilon_s^2 \frac{\cosh 2k(z+h)}{\sinh^4 kh}\sin 2\theta + O(\varepsilon_s^3), \qquad (1.7b)$$

where $\theta = kx - \omega t$. The dispersion relation for k and ω is

$$\omega = \sqrt{gk\tanh kh}\{1 + \frac{1}{2}\varepsilon_s^2(1 + \frac{1}{\sinh^2 kh} + \frac{9}{8\sinh^4 kh})\}. \qquad (1.8)$$

It is noted that the lowest-order terms of the solution (1.7) and the dispersion relation (1.8) are the same as the solution (1.5) and the dispersion relation (1.6) in the linear theory under the neglect of the surface tension. The higher-order terms in eqs.(1.7) modify the sinusoidal wave form of the free surface in the linear theory into that composed of steep crests and flat troughs. The higher-order term in eq.(1.8) represents the amplitude dispersion.

Stokes [2] also obtained the solution for deep-water case ($l << h$) to $O(\varepsilon_s^5)$, and many workers computed the solution of higher order by means of more sophisticated procedures for finite depth [3]~[5], and for infinite depth, [6] [7].

Benjamin and Feir [8] examined the stability of a weakly nonlinear uniform wavetrain in deep water given by

$$\zeta = a\cos\theta + \frac{1}{2}ka^2\cos 2\theta, \qquad (1.9a)$$

$$\phi = \frac{a\omega}{k}e^{kz}\sin\theta, \qquad (1.9b)$$

$$\theta = kx - \omega t, \qquad (1.9c)$$

$$\omega^2 = gk(1+k^2a^2), \qquad (1.9d)$$

which is derived from Stokes' solution (1.7) and (1.8) by the neglect of terms of $O(\varepsilon_s^3)$ and by taking the limit $kh\to\infty$. They found that the wavetrain (1.9) is unstable to modulational disturbances with wavenumber K in the range

$$0 < K < 2\sqrt{2}k^2a.$$

Furthermore, they obtained the wavenumber of maximum instability and the maximum growth rate. They also reported experimental data in fairly good agreement with the prediction regarding the wavenumber and the growth rate of instability. This modulational instability was also predicted by Lighthill [9] and by Whitham [10] by making use of Whitham's averaging technique [11] Benjamin [12] and Whitham [10] showed that in the finite-depth case this modulational instability occurs only for $kh > 1.363$. It will be shown in § 1.3 that this instability has the close relation to the resonant interaction of surface gravity waves.

Next the equation which describes the long-time development of the weakly nonlinear wavetrain was attempted to derive. Hasimoto and Ono [13] considered the following slowly modulated wavetrain in finite-depth water :

$$\zeta = \varepsilon_s A(\xi, \tau) e^{i(kx-\omega t)} + \text{c.c.} + O(\varepsilon_s^2), \tag{1.10a}$$

where

$$\xi = \varepsilon_s(x - c_g t), \tag{1.10b}$$

$$\tau = \varepsilon_s^2 t, \tag{1.10c}$$

$$\omega^2 = gk\tanh kh, \tag{1.10d}$$

$$c_g = \frac{d\omega}{dk}, \tag{1.10e}$$

and c.c. denotes complex conjugate of the preceding term. They

then showed that the complex wavetrain envelope A is governed by the so-called nonlinear Schrödinger equation

$$i\frac{\partial A}{\partial \tau} + \mu\frac{\partial^2 A}{\partial \xi^2} + \nu|A|^2 A = 0, \qquad (1.11)$$

where

$$\mu = \frac{1}{2}\frac{d^2\omega}{dk^2} < 0.$$

The coefficient ν depends on k and h, and is negative for $kh > 1.363$ and positive for $kh < 1.363$. Equation (1.11) had been discussed by Benney and Newell [14] and by Taniuti and Yajima [15] in the general context. Both of them showed that if $\mu\nu<0$ ($\mu\nu>0$) the uniform wavetrain solution of eq.(1.11) is stable (unstable) Therefore, the results for the modulational instability of a uniform wavetrain in finite-depth water are again obtained by invoking the results about the signs of μ and ν.

The nonlinear Schrödinger equation (1.11) with $\mu\nu>0$ was solved exactly by Zakharov and Shabat [16] by means of the inverse scattering method for the initial conditions which decay sufficiently rapidly as $|\xi|\to\infty$. They also considered the interaction between the following envelope soliton solutions of eq.(1.11) :

$$A = a_1 \mathrm{sech}\left[\left(\frac{\nu}{2\mu}\right)^{1/2} a_1(\xi - c_1\tau)\right] \exp\left\{i\left[\frac{c_1}{2\mu}\xi + \left(\frac{\nu}{2}a_1^2 - \frac{1}{4\mu}c_1^2\right)\tau\right]\right\}, \qquad (1.12)$$

where a_1 and c_1 are real constants. They then found that the envelope solitons of different velocities pass through one another without any permanent loss of identity and suffer only phase shifts. This theoretical prediction of soliton properties

was confirmed by experiments [17]. Some initial-value problems of eq.(1.11) with $\mu\nu>0$ were examined by Satsuma and Yajima [18] for localized distributions and by Yuen and Ferguson [19] for an unstable wavetrain.

1.1.2 Surface gravity waves in shallow water

It has been shown by Ursell [20] that the linear solution (1.5) is valid only if $U_r\equiv(l/h)^3a/l$ as well as the wave steepness ε_s, is small. Therefore, the waves which are too long relative to the water depth must be treated by means of an approach different from Stokes' theory based on the expansion with respect to ε_s.

The nonlinear theory for shallow-water gravity waves ($l\gg h, l\gg(T/\rho g)^{1/2}$) was developed by Boussinesque [21] and by Rayleigh [22] by taking account of weak dispersion as well as weak nonlinearity. The theory was put forward by Korteweg and de Vries [23], who considered the time evolution of a unidirectional shallow-water wave on the assumption that $\varepsilon\equiv a/h\sim(h/l)^2$ (which means $U_r=O(1)$) and $\varepsilon\ll1$. The equation derived from eqs.(1 3) by them can be reduced to

$$\frac{\partial B}{\partial\tau}+\mu_1 B\frac{\partial B}{\partial\xi}+\nu_1\frac{\partial^3 B}{\partial\xi^3}=0, \qquad (1\ 13)$$

where $\zeta=aB(\xi,\tau)$, $\xi=\varepsilon^{1/2}(x-c_pt)$, $\tau=\varepsilon^{3/2}t$, $c_p=(gh)^{1/2}$, and $\mu_1=3c_p/2$ and $\nu_1=c_ph^2/6$ are positive constants. Equation (1.13) is referred to as the Korteweg-de Vries equation (the K-dV equation).

Korteweg and de Vries [23] then obtained a solution of eq.(1.13) describing a steady progressive periodic wave and called it as a "cnoidal wave". This solution comprises the following solitary wave solution in the limit of infinite

period:

$$B = a_1 \mathrm{sech}^2 \left[\left(\frac{\mu_1 a_1}{12 \nu_1} \right)^{1/2} \left(\xi - \frac{1}{3} \mu_1 a_1 \tau \right) \right], \qquad (1.14)$$

where a_1 is a positive constant. The K-dV equation (1.13) can be solved exactly by the inverse scattering method for initial data which vanish at $\xi = \pm\infty$. The N-soliton solution, [24]~[27] of eq.(1.13) indicates that the solitary wave solutions (1.14) behave as solitons, that is, the solutions with different amplitudes preserve their identities through collisional interaction between them except for the phase shifts. Other many interesting results related to the K-dV equation were reviewed by Miura [28].

Shallow-water waves of large amplitude were investigated by the integral-equation formulation or by the series-expansion method with respect to ε (or $(h/l)^2$). The former method was used for the examination of a solitary wave by many workers, [29]~[36]. Based on the latter method Laitone [37], Chappelear [38] and Fenton [39] obtained higher-order periodic solutions. Higher-order solitary wave solutions were computed by Laitone [37], Fenton [40], and Longuet-Higgins and Fenton [41].

The stability of the solitary wave (1.14) as a solution of the K-dV equation (1.13) has been established by Benjamin [42]. Jeffrey and Kakutani [43] had earlier demonstrated stability with respect to small one-dimensional perturbations. Kadomtsev and Petviashvili [44] and Oikawa *et al.* [45] have shown that the one-dimensional solitary wave (1.14) is neutrally stable with respect to small transverse perturbations.

1.1.3 Capillary-gravity waves

When l (the wavelength of a wave) is comparable to or much less than $(T/\rho g)^{1/2}$, the effect of surface tension must be taken into account.

Crapper [46] investigated pure capillary waves in deep water ($h \gg l, l \ll (T/\rho g)^{1/2}$) and obtained an exact closed-form solution for steady progressive waves of arbitrary amplitude. Unlike (pure) gravity waves, steep capillary waves are characterized by deep troughs and broad flat crests.

Harrison [47] and Wilton [48] treated the problem of a capillary-gravity wave in deep water ($h \gg l \sim (T/\rho g)^{1/2}$) by using Stokes' expansion introduced in § 1.1.1, and obtained higher-order solutions. Harrison [47] showed that the sinusoidal wave form in the linear theory is modified by the effect of nonlinearity in a similar way to a gravity wave or to a pure capillary wave according as k ($=2\pi/l$) is smaller or larger than $(\rho g/2T)^{1/2}$ respectively. Wilton [48] found that when $k=(\rho g/nT)^{1/2}$ ($n=2,3,\ldots$) Stokes' expansion fails because certain series coefficients become infinite. This breakdown is closely related to the resonant interaction of a fundamental wave with a higher harmonics as will be shown in § 1.3.

§ 1.2 Gravity Waves in Two-Layer Fluid

When the density of a fluid is not uniform, there exists the wave motion called an internal wave. In this section we consider only the special case of two-layer fluid, which is composed of two immiscible fluids of uniform densities.

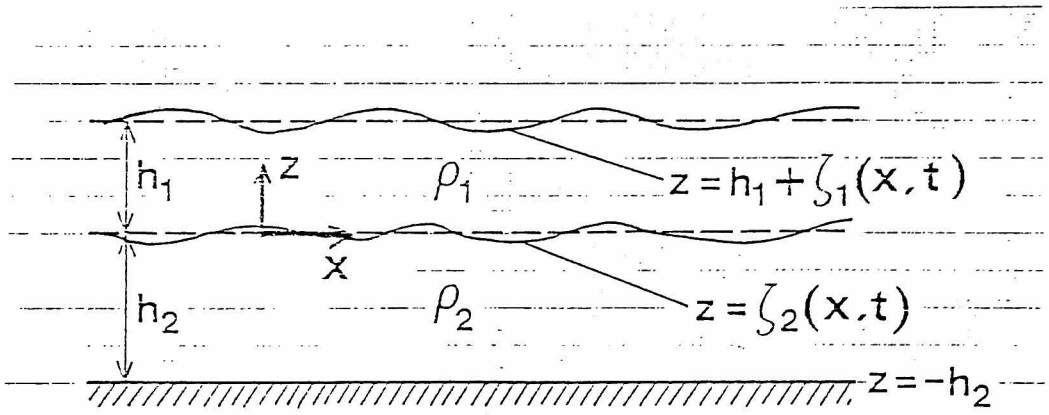

Fig.2 The geometrical configuration.

We assume that the fluid in each layer is incompressible and inviscid and makes a one-dimensional irrotational motion, and that the densities of the upper and lower layers are ρ_1 and $\rho_2(>\rho_1)$, and that the thicknesses of the upper and lower layers are h_1 and h_2 respectively. The x and z are taken as the horizontal and vertical coordinates. The geometrical configuration is shown in Fig.2. If the disturbed free surface is specified by $z=h_1+\zeta_1(x,t)$, the disturbed interface by $z=\zeta_2(x,t)$, the horizontal rigid bottom by $z=-h_2$, and the velocity potentials in the upper and lower layers by $\phi_1(x,z,t)$ and $\phi_2(x,z,t)$, the basic equations and the boundary conditions are written as

$$\frac{\partial \zeta_1}{\partial t} + \frac{\partial \phi_1}{\partial x}\frac{\partial \zeta_1}{\partial x} - \frac{\partial \phi_1}{\partial z} = 0, \quad \text{at} \quad z=h_1+\zeta_1 \tag{1.15a}$$

$$\frac{\partial \phi_1}{\partial t} + g\zeta_1 + \frac{1}{2}\left(\frac{\partial \phi_1}{\partial x}\right)^2 + \frac{1}{2}\left(\frac{\partial \phi_1}{\partial z}\right)^2 = 0, \quad \text{at} \quad z=h_1+\zeta_1 \tag{1.15b}$$

$$\frac{\partial^2\phi_1}{\partial x^2} + \frac{\partial^2\phi_1}{\partial z^2} = 0, \qquad \zeta_2<z<h_1+\zeta_1 \tag{1.15c}$$

$$\frac{\partial^2\phi_2}{\partial x^2} + \frac{\partial^2\phi_2}{\partial z^2} = 0, \qquad -h_2<z<\zeta_2 \tag{1.15d}$$

$$\frac{\partial\zeta_2}{\partial t} + \frac{\partial\phi_2}{\partial x}\frac{\partial\zeta_2}{\partial x} - \frac{\partial\phi_2}{\partial z} = 0, \qquad \text{at} \quad z=\zeta_2 \tag{1.15e}$$

$$\frac{\partial\zeta_2}{\partial t} + \frac{\partial\phi_1}{\partial x}\frac{\partial\zeta_2}{\partial x} - \frac{\partial\phi_1}{\partial z} = 0, \qquad \text{at} \quad z=\zeta_2 \tag{1.15f}$$

$$\rho_1\{\frac{\partial\phi_1}{\partial t} + g\zeta_2 + \frac{1}{2}(\frac{\partial\phi_1}{\partial x})^2 + \frac{1}{2}(\frac{\partial\phi_1}{\partial z})^2\} - \rho_2\{\frac{\partial\phi_2}{\partial t} + g\zeta_2$$

$$+ \frac{1}{2}(\frac{\partial\phi_2}{\partial x})^2 + \frac{1}{2}(\frac{\partial\phi_2}{\partial z})^2\} = 0, \qquad \text{at} \quad z=\zeta_2 \tag{1.15g}$$

$$\frac{\partial\phi_2}{\partial z} = 0. \qquad \text{at } z=-h_2 \tag{1.15h}$$

Here we assumed that the surface tension is negligible.

The linearized forms of eqs.(1.15) have the following solution :

$$\zeta_1 = ae^{i\theta} + \text{c.c.}, \tag{1.16a}$$

$$\zeta_2 = (\cosh kh_1 - \frac{gk}{\omega^2}\sinh kh_1)ae^{i\theta} + \text{c.c.}, \tag{1.16b}$$

$$\phi_1 = \frac{i\omega}{k}\{\sinh k(h_1-z) - \frac{gk}{\omega^2}\cosh k(h_1-z)\}ae^{i\theta} + \text{c.c.}, \tag{1.16c}$$

$$\phi_2 = -\frac{i\omega}{k\sinh kh_2}(\cosh kh_1 - \frac{gk}{\omega^2}\sinh kh_1)\cosh k(z+h_2)ae^{i\theta} + \text{c.c.}, \tag{1.16d}$$

$$\theta = kx - \omega t, \tag{1.16e}$$

where k and ω satisfy the dispersion relation

$$\omega^2 = gk\frac{\sigma_1+\sigma_2\pm\{(\sigma_1+\sigma_2)^2-4\Delta\sigma_1\sigma_2\{1+(1-\Delta)\sigma_1\sigma_2\}\}^{1/2}}{2\{1+(1-\Delta)\sigma_1\sigma_2\}}\ , \qquad (1.$$

$$\sigma_1 = \tanh kh_1, \quad \sigma_2 = \tanh kh_2, \quad \Delta = 1 - \frac{\rho_1}{\rho_2}\ .$$

Unlike the case of continuous stratification, only the fundamental mode of an internal wave (which corresponds to the negative sign in eq.(1.17)) can exist in addition to the surface mode (which corresponds to the positive sign in eq.(1.17)).

The case of a rigid upper boundary, in which $\zeta_1 \equiv 0$, is sometimes considered in order to examine an internal wave without unnecessary complexity. The equations obtained by the linearization in eqs.(1.15c~ h) and

$$\frac{\partial \phi_1}{\partial z} = 0, \qquad \text{at } z=h_1 \qquad (1.18)$$

have the solution of the form

$$\zeta_2 = a_0 e^{i\theta} + \text{c.c.}, \qquad (1.19a)$$

$$\phi_1 = \frac{i\omega \cosh k(z-h_1)}{k \sinh kh_1} a_0 e^{i\theta} + \text{c.c.}, \qquad (1.19b)$$

$$\phi_2 = -\frac{i\omega \cosh k(z+h_2)}{k \sinh kh_2} a_0 e^{i\theta} + \text{c.c.}, \qquad (1.19c)$$

$$\theta = kx-\omega t, \qquad (1.19d)$$

where

$$\omega^2 = gk\frac{\Delta\sigma_1\sigma_2}{\sigma_1 + \sigma_2(1-\Delta)}. \qquad (1.20)$$

Kakutani and Yamasaki [49] considered the case of a free upper boundary on the assumption that $\varepsilon \equiv a/h_1 \sim (h_1/l)^2 \ll 1$, $h_1 \sim h_2$. Here l is the characteristic wavelength of a wave. They then derived the K-dV eq.(1.13) both for a surface mode and for an internal mode. In this case the variables in eq.(1.13) are defined by $\zeta_2 = aB(\xi, \tau)$, $\xi = \varepsilon^{1/2}(x - c_p t)$, $\tau = \varepsilon^{3/2} t$. Furthermore, $c_p = \omega/k$ is obtained from eq.(1.17) by taking the long wave limit $kh_1 \to 0$, $kh_2 \to 0$. They found that for an internal mode the coefficient ν_1 in eq.(1.13) is always positive and μ_1 in eq.(1.13) changes sign depending on h_1/h_2 and Δ. They then showed that the solitary wave solution of eq.(1.13) describes a depression of the free surface and an elevation of the interface for $h_1/h_2 > m$ and *vice versa* for $h_1/h_2 < m$. Here m depends on Δ and is between 1 and 1.25. The same result for the critical value of h_1/h_2 had been obtained also by Walker [50].

Tanaka [51] considered the long-time evolution of the wave (1.19) in the case of a rigid upper boundary under the assumption $l \sim h_1 \sim h_2$, and derived the nonlinear Schrödinger equation (1.11). In this case the variables in eq.(1.11) are defined by $A(\xi, \tau) = a_0/\varepsilon_s$, $\xi = \varepsilon_s(x - c_g t)$, $\tau = \varepsilon_s^2 t$. Furthermore, $c_g = d\omega/dk$ is computed from eq.(1.20) By the examination of the signs of μ and ν in eq.(1.11) he found that the existence of the upper layer slightly supresses the modulational instability of a uniform wavetrain.

§ 1.3 Wave-Wave Interactions

The problem of interactions between wavetrain or solitary waves (introduced in the previous sections) is one of the most

important branches in the nonlinear theory of water waves.

In the shallow-water case, solitary waves are observed usually and are generated from a wide range of initial conditions. Therefore, the interaction between solitary waves has been investigated by many workers. The results about this interaction in one and two dimensions are reviewed in § 1.3.1.

On the other hand, if l (the wavelength) is comparable to or much smaller than the water depth, only a slowly-modulated wavetrain can survive for a long time because the dispersion is strong. The results about the interaction of wavetrains are reviewed in § 1.3.2.

1.3.1. Interactions between solitary waves in shallow water

The problem of the interaction between two solitary waves propagating to the same direction with different velocities can be described by the K-dV eq.(1.13) to the first order. The theory of the K-dV eq. predicts that two solitary waves of different amplitudes pass through one another without any permanent loss of identity and suffer only a forward phase shift of the larger solitary wave and a backward phase shift of the smaller one. Experimental confirmation of this prediction has been provided by Zabusky and Galvin [52], by Hammack and Segur [53], and by Weidman and Maxworthy [54].

Another interaction problem in one dimension is the head-on collision of two solitary waves. The reflection of a solitary wave at the vertical rigid wall can be regarded as the special case of this problem. The second-order solution for the head-on collision of two solitary waves was obtained by Byatt-Smith [55] and by Oikawa and Yajima [56]. Oikawa and

Yajima found that two solitary waves suffer only phase shifts of $O(\varepsilon l)$ from the interaction. This phase shift is also included implicitly in the results of Byatt-Smith. However, the experiments made by Maxworthy [57] gave the phase shifts quite different from the above theoretical prediction. The study on the nonlinear effect in the reflection of a solitary wave at the vertical wall is made by the author, and the results are mentioned in chapter 2.

The problem of oblique interactions between solitary waves has been investigated theoretically or experimentally by many workers. Miles [58] considered the case in which the intersection angle φ between two solitary waves is much larger than $\varepsilon^{1/2}$. He then found that the first approximation to the solution describing an oblique interaction is obtained by superimposing the solutions for the individual solitary waves.

On the other hand, when $\varphi=O(\varepsilon^{1/2})$ the solution made by the above superposition is found to be not valid even as the lowest-order solution for the oblique interaction. Kadomtsev and Petviashvili [44] derived the following equation in order to examine the stability of a solitary wave propagating to the x direction with respect to small transverse perturbations :

$$\frac{\partial}{\partial\xi}\left(\frac{\partial B}{\partial\tau}+\mu_1 B\frac{\partial B}{\partial\xi}+\nu_1\frac{\partial^3 B}{\partial\xi^3}\right)+\mu_1\frac{\partial^2 B}{\partial\eta^2}=0, \tag{1.21}$$

where $\zeta=aB(\xi,\tau)$, $\xi=\varepsilon^{1/2}(x-c_p t)$, $\eta=3^{1/2}\varepsilon y$, $\tau=\varepsilon^{3/2}t$, $c_p=(gh)^{1/2}$, $\mu_1=3c_p/2$ and $\nu_1=c_p h^2/6$. This equation is called two-dimensional K-dV equation or Kadomtsev-Petviashvili equation, and was also derived by Oikawa *et al.* [45]. The oblique interaction between solitary waves is governed by this equation (1.21) to the first

order if $\varphi=O(\varepsilon^{1/2})$. The solution of eq.(1.21) for intersecting solitons has been obtained by Chen [59], Satsuma [60], Hirota [61] and Miles [58]. Miles [58] found that this solution is non-singular only if $\varphi>\varphi_+$ or $\varphi<\varphi_-$. Here φ_+ and φ_- are determined from the amplitudes of two solitary waves. In this non-singular case the solution describes the phase shift of magnitude comparable to l similarly to the case of one-dimensional interaction between two solitary waves propagating to the same direction. Miles [58] also found that the condition $\varphi=\varphi_+$ or $\varphi=\varphi_-$ is precisely that necessary for a resonant interaction among three solitary waves.

The problem of oblique interactions between two solitary waves is closely related to the reflection problem of a solitary wave obliquely incident to the vertical rigid wall. Based on the results about the oblique interactions Miles [62] predicted that a regular reflection pattern appears only when the angle of incidence α is larger than $(3\varepsilon)^{1/2}$ and that a Mach reflection pattern (geometrically similar to the corresponding shock-wave reflection pattern) appears for $\alpha<(3\varepsilon)^{1/2}$ The latter reflection pattern is composed of three resonantly interacting solitary waves.

Numerical study on the reflection of obliquely incident solitary waves with arbitrary α is made by the author. In chapter 3, the results are shown and compared with the above Miles' theory and with available experiments made by Melville [63].

1.3.2 Wave-wave interactions in non-shallow water

In the case of weak nonlinearity the linear solutions

written by

$$\zeta = a_i \cos(k_i x - \omega_i t), \quad (i=1,2,\ldots) \tag{1.22a}$$

$$\omega = \omega(k), \quad \text{(linear dispersion relation)} \tag{1.22b}$$

are regarded as fundamental waves. It is well known that if the dispersion relation (1.22b) allows the satisfaction of the resonance condition

$$\begin{cases} \sum_{i=1}^{n} s_i \omega_i = 0, \\ \sum_{i=1}^{n} s_i k_i = 0, \\ s_i = \pm 1, \quad n \geqq 3 \end{cases} \tag{1.23}$$

there exists the $(n-1)$th-order resonant interaction among n fundamental waves of wavenumber vector k_i and frequency ω_i. If the resonance condition (1.23) is satisfied significant energy transfer among these n wave components is possible in spite of weak nonlinearity.

In one-dimensional case the resonance condition of lowest order is written by

$$k_1 \pm k_2 = k_3, \tag{1.24a}$$

$$\omega_1 \pm \omega_2 = \omega_3. \tag{1.24b}$$

This second-order resonant interaction is possible among capillary-gravity waves [64], among different modes of internal waves in a continuously stratified fluid, and between two

surface modes and one internal mode in two-layer fluid [65], [66]. Using a model equation displaying the property of second-order resonance, Bretherton [67] derived equations which govern time development of amplitudes a_i (i=1,2,3) of wave components satisfying (1.24). He then examined the property of the solution. Based on the same equation Hasselman [68] showed that a uniform wavetrain in the system which allows second-order resonance is always unstable.

The problem of resonant interactions between a short wavetrain of wavenumber k_1 and a long wave of wavenumber k_3 also has been investigated by many workers. This interaction can be regarded as the second-order resonance among the wave components of wavenumbers k_1, $k_2(=k_1)$ and k_3. In this case the resonance condition (1.24) with the minus sign is reduced to

$$c_g = c_p, \tag{1.25}$$

where

$$c_g = \left(\frac{d\omega}{dk}\right)_{k=k_1}$$

is the group velocity of a short wavetrain, and

$$c_p = \left(\frac{\omega}{k}\right)_{k=k_3}$$

is the phase speed of a long wave. This long-short resonant interaction was investigated by Djordjevic and Redekopp [69] for capillary-gravity waves, and by Grimshaw [70] for long and short internal waves in continuously stratified fluid.

The long-short resonant interactions between a short wavetrain of surface mode and a long internal wave in two-layer

fluid are examined by the author. The results for the case $l \gg h_1, h_2$ are shown in chapter 4, while those for the case $h_2 \gg l \gg h_1$ are shown in chapter 5. Here l is a characteristic length scale of a long internal wave, and h_1 and h_2 are the thicknesses of the upper and lower layers respectively.

For capillary-gravity waves the interaction called harmonic resonance is also possible. McGoldrick [71] and Simmons [72] pointed out that if $k_1=(\rho g/2T)^{1/2}$ the triad k_1, $k_2(=k_1)$ and k_3 $(=2k_1)$ satisfies the resonance condition (1.24). Therefore the initial wave of wavenumber k_1 is expected to become increasingly distorted as it propagates due to the energy transfer to the component of wavenumber $2k_1$. This prediction was confirmed experimentally by McGoldrick [71]. The nth-order resonant interaction with higher harmonics is possible for the fundamental wave of wavenumber $(\rho g/nT)^{1/2}$. Nayfeh [73] and McGoldrick [74] examined this interaction. The breakdown of Stokes' expansion found by Wilton [48] for these special wavenumbers is due to the inappropriateness of the assumption in Stokes' expansion that the nth Fourier component is of nth order.

For gravity waves in deep water there exists no nontrivial solution to the second-order resonance condition (1.24). It was shown that the third-order resonance represented by

$$k_1 + k_2 = k_3 + k_4 \tag{1.26a}$$

$$\omega_1 + \omega_2 = \omega_3 + \omega_4 \tag{1.26b}$$

is possible for this case, [75]~[77]. The significant energy

transfer among wave components satisfying (1.26) was observed in experiments [78] [79]. In one-dimensional case Benney [80] considered the weak interaction among four wave components satisfying the resonance condition (1.26) and derived equations which govern the time development of wave amplitudes $a_i (i=1,\ldots,4)$. The modulational instability of a uniform wavetrain of wavenumber k_1 in deep water mentioned in § 1.1.1 can be regarded as the phenomena caused by the third-order resonant interaction between wave components of wavenumbers k_1, $k_2(=k_1)$, $k_3(=k_1+\delta)$, and $k_4(=k_1-\delta)$. Here δ is of $O(\varepsilon_s)$ and is determined so as to satisfy the condition (1.26) under the use of nonlinear dispersion relation (1.9d). The nonlinear Schrödinger equation (1 11) derived for the description of the long-time evolution of a slowly-modulated wavetrain is closely related to the above third-order resonant interaction. In fact eq.(1.11) can be derived from the above Benney's equation on the assumption of narrow band ($|k_1-k_i| \ll k_1$, $i=2,3,4$), [81]

Chapter 2

Normal Reflection of a Solitary Wave in Shallow Water

§ 2.1. Introduction

Solitary waves in shallow water have been studied by many research workers and are typical examples which exhibit soliton phenomena in small amplitude [82].

In the present chapter, the reflection problem of a solitary wave at a rigid vertical wall is solved numerically under the assumption that the fluid is inviscid. Then, the problem is equivalent to that of head-on collision between two solitary waves with the same amplitude. Head-on collisions between two solitary waves were investigated by several authors by means of perturbation methods [55], [56], [58], [83], [84]. Benney and Luke [83] gave a systematic expansion procedure although their final results for the reflection problem of a solitary wave are incorrect. Byatt-Smith [55] obtained the second order solution for the head-on collision of two solitary waves on the basis of an integral equation for unsteady surface waves. The solution gives implicitly the phase shifts of the solitary waves due to collision. Oikawa and Yajima [56] introduced the phase variables into their expansion scheme to give the explicit result for the phase shifts and they also investigated the interaction of the quasi-simple waves in a general weak nonlinear and weak dispersive system. The phase shift obtained by them becomes $\sqrt{\varepsilon/3}h$ for the reflection problem (for phase shift, see Fig.7), here h is the undisturbed fluid

depth and εh the amplitude of the incident solitary wave. Up to the second order of ε, the theoretical solution of the reflection problem predicts that far after reflection the solitary wave undergoes no effect of the interaction with the wall except for the phase shift $\sqrt{\varepsilon/3h}$ and the wave changes its shape only during its stay near the wall.

The experiments on the head-on collision and the reflection were made by Maxworthy [57]. In the experiments it was found that the phase shift of the solitary wave is independent of the initial wave amplitude for both the head-on collision and the reflection in contradiction to the above theoretical results (see Fig.9). The secondary reflected wave following the primary wave was also observed for a moderate or large initial amplitude. Maxworthy [57] suggested two possible reasons for this discrepancy between the experiment and the above theories. First, the scaling procedure adopted in the theories may be inappropriate for the present problem. Secondly, if the scaling procedure is appropriate, the higher order terms in the expansion may be needed. Recently, Su and Mirie [84] gave the third order solution for the head-on collision problem through a perturbation method similar to that of Oikawa and Yajima [56]. The solution contains non-uniform phase shifts which cause a distortion of the wave form of $O(\varepsilon^3)$. Then, they examined the time evolution of this distorted wave and showed that it eventually recovers its original form with the shedding of a secondary wave group which propagates with diminishing amplitude. Through this procedure they obtained the uniform phase shift $\sqrt{\varepsilon/3}(1+7\varepsilon/8)h$ for the reflection problem. With

regard to the shedding of a secondary wave their result agrees qualitatively with the experiments, but the discrepancy about the phase shift still remains.

In the present chapter, we examine the reflection problem by solving the Euler equations numerically with high accuracy. The numerical solutions permit us to determine the validity of the scaling procedure adopted in the above theories and of the approximate solutions. It is also useful to compare the numerical solutions with the results of the experiment in order to find a cause of the discrepancy about the phase shift. A numerical study of the reflection problem was made by Chan and Street [85]. However, they laid emphasis on the numerical method itself, so that did not pay attention to the phase shift. They did not find the difference between the wave form of the incident wave and that of the reflected wave.

In § 2.2 the formulation of the problem and the numerical procedures are described along with the discussion on the accuracy of the numerical solutions. The numerical results for the phase shift and the wave form of the reflected waves are described and compared with the theoretical and the experimental results in § 2.3.

§ 2.2. Numerical Procedure and Accuracy

2.2.1 Formulation

The situation considered is shown in Fig.3. The undisturbed fluid depth is denoted by h. The disturbed free surface is specified by $z = \zeta(x,t)$, the horizontal bottom by $z = -h$ and the rigid vertical walls are by $x = 0$ and $x = L_1 h$. The

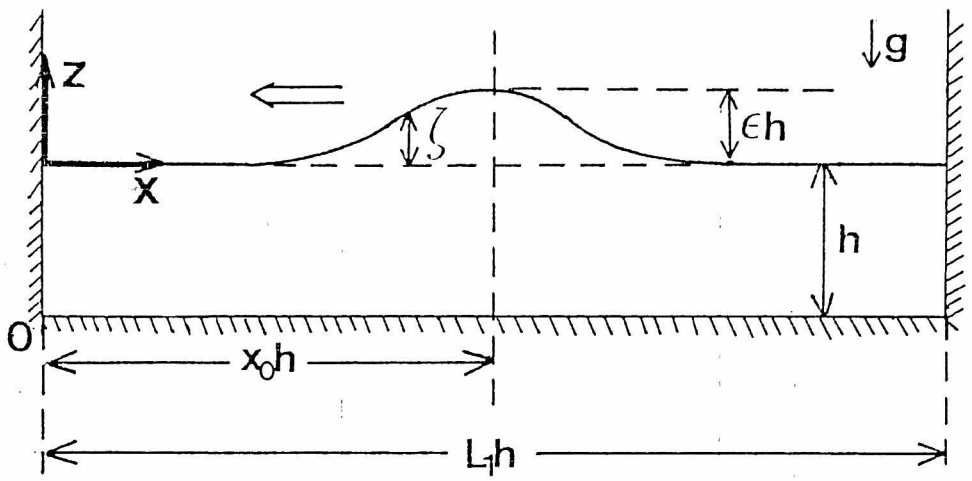

Fig.3 Configuration of the problem.

fluid is assumed to be inviscid and the motion to be two-dimensional and irrotational. The basic equations (1.1) can then be reduced to the following dimensionless form :

$$\frac{\partial u'}{\partial t'} + \frac{\partial}{\partial x'}(u'^2) + \frac{\partial}{\partial z'}(u'w') = -\frac{\partial p'}{\partial x'}, \tag{2.1}$$

$$\frac{\partial w'}{\partial t'} + \frac{\partial}{\partial x'}(u'w') + \frac{\partial}{\partial z'}(w'^2) = -\frac{\partial p'}{\partial z'} - 1, \tag{2.2}$$

$$D \equiv \frac{\partial u'}{\partial x'} + \frac{\partial w'}{\partial z'} = 0, \tag{2.3}$$

where the dimensionless variables are defined by the relations $(x',z')=(x,z)/h$, $t' = t/(h/g)^{1/2}$, $(u',w') = (u,w)/(gh)^{1/2}$ and $p' = p/\rho gh$, and g and ρ denote the gravitational acceleration and the uniform fluid density respectively. From eqs.(2.1) and (2.2) the following Poisson equation for the pressure is obtained :

$$\frac{\partial^2 p'}{\partial x'^2} + \frac{\partial^2 p'}{\partial z'^2} = -R, \tag{2.4}$$

where

$$R = \frac{\partial^2}{\partial x'^2}(u'^2) + \frac{\partial^2}{\partial z'^2}(w'^2) + 2\frac{\partial^2}{\partial x' \partial z'}(u'w') + \frac{\partial}{\partial t'}D.$$

The boundary conditions on the rigid walls are derived by use of the irrotational condition and eqs.(2.1) and (2.2), and written as

$$u' = 0, \quad \frac{\partial w'}{\partial x'} = 0 \quad \text{on} \quad x'=0,\ L_1, \tag{2.5}$$

$$\frac{\partial p'}{\partial x'} = 0 \quad \text{on} \quad x'=0,\ L_1, \tag{2.6}$$

$$w' = 0, \quad \frac{\partial u'}{\partial z'} = 0 \quad \text{on} \quad z'=-1, \tag{2.7}$$

$$\frac{\partial p'}{\partial z'} = -1, \quad \text{on} \quad z'=-1. \tag{2.8}$$

The dynamical condition (1.2b) at the free surface can be chosen as

$$p' = 0 \quad \text{on} \quad z'=\zeta'. \quad \left(\zeta'=\frac{\zeta}{h}\right) \tag{2.9}$$

under the neglect of the surface-tension effect.

In the remaining part of this chapter the primes in nondimensionalized variables are omitted.

2.2.2 Numerical procedure

In order to solve the reflection problem of a solitary wave, we use the improved MAC (SUMMAC) method introduced by Chan and Street [85]. In this method the values of the velocity field (u,w) and pressure field p are given at fixed points of rectangular mesh, and the values of them at intermediate points are given by certain interpolation. The free surface is

specified by a distribution of many massless "marker particles". The outline of the computational procedure is as follows. (i) The initial values of (u,w,p) and the initial locations of the marker particles are determined from the solitary wave solution described in the next subsection. (ii) The values of (u,w) at the next time are calculated by means of the finite-difference equations with the forward time and centered space difference scheme derived from eqs.(2.1) and (2.2). (iii) New locations of the marker particles (new location of the free surface) are determined from this new velocity field. (iv) New values of p are obtained by solving the Poisson eq.(2.4) under the boundary conditions (2.6), (2.8) and (2.9) The procedure (ii)~ (iv) is repeated as many as necessary.

2.2.3. Steady solitary wave solution

The initial data is given by the solitary wave solution, it being required to be accurate enough to obtain the solution of high accuracy. For this purpose, we used the ninth order solution of Fenton [40]. It is of the form

$$\zeta = \sum_{i=1}^{9}\sum_{j=1}^{i}\zeta_{ij}\varepsilon^{i}\mathrm{sech}^{2j}\theta,$$

$$u=\sum_{i=1}^{9}\sum_{j=1}^{i}\sum_{k=1}^{i}u_{ijk}\varepsilon^{i}(z+1)^{2k-2}\mathrm{sech}^{2j}\theta,$$

$$w=\tanh\theta\sum_{i=1}^{9}\sum_{j=1}^{i}\sum_{k=1}^{i}w_{ijk}\varepsilon^{i+1/2}(z+1)^{2k-1}\mathrm{sech}^{2j}\theta,$$

where

$$\theta = \alpha(x-x_0+U_0 t),$$

$$\alpha = \sqrt{3\varepsilon/4}\left(1+\sum_{i=1}^{8}\alpha_i \varepsilon^i\right)$$

and

$$U_0^2 = 1 + \sum_{i=1}^{9} U_i \varepsilon^i.$$

Here ε is the ratio of the amplitude of the wave to h, and x_0 is the location of the peak of the initial wave, and U_0 is the velocity of the wave. He obtained the coefficients ζ_{ij}, α_i and U_i numerically, and gave the procedure for obtaining the coefficients u_{ijk} and w_{ijk}. We calculated these coefficients explicitly and found that the solution is not so accurate for large ε though it includes many higher order terms. We used this solution only for $\varepsilon \leqq 0.2$, because for ε in this range the solution is sufficiently accurate for our purpose. The values of p were calculated through Bernoulli's equation.

2.2.4. Accuracy of the calculations

The reflection problem was solved for $\varepsilon = 0.05 \sim 0.2$, and the head-on collision problem of two solitary waves with equal amplitude $\varepsilon = 0.2$ was also solved in order to check the results of the reflection problem. We defined λ as the difference of two values of x for which $\zeta = \varepsilon/2$ for the initial solitary wave. The values of the mesh size Δx were chosen so that $\lambda/\Delta x \fallingdotseq 32$. Much larger value of $\lambda/\Delta x$ was chosen for a comparatively smaller ε in order to keep the sufficient accuracy of the computation of the phase shift. The values of the mesh size Δz were chosen so that $5 \leqq \varepsilon/\Delta z \leqq 11$. The time increment Δt was determined so as to

satisfy the approximate stability criterion $\Delta t<2\Delta x\Delta z/(\Delta x+\Delta z)$. The initial distribution of the marker particles was taken for the x coordinates of them to have the equal interval $\Delta x/4$. The values of x_0 and L_1 were chosen so that the vertical walls have only a negligible effect on the initial stage of the evolution of the wave.

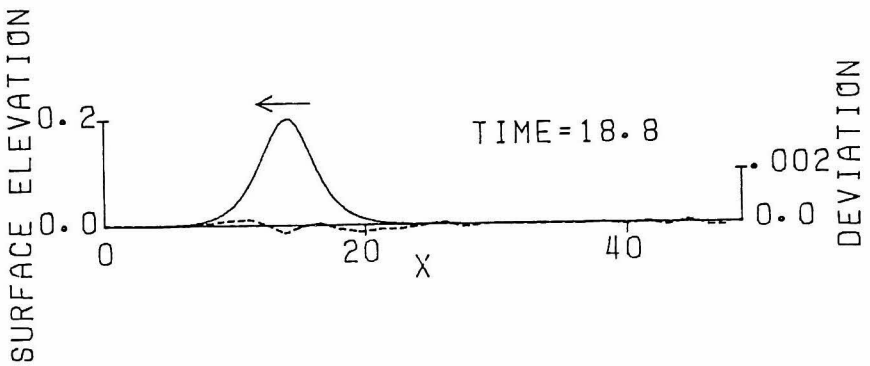

Fig.4 Profile of the solitary wave propagating in the region far from the vertical walls. ε = 0.2, x_0 = 34.6, L_1 = 48.6, Δt = 0.0039, Δx = 0.16, Δz = 0.022. ———: Wave profile at t = 18.8. — —: Deviation of the wave profile from the steady soitary wave solution.

As a preliminary calculation, we examined the evolution of the solitary wave with ε = 0.2 given in the previous subsection in the region far from the vertical walls. The profile of the wave (propagating to the left) at t = 18.8 is shown in Fig.4. The broken line denotes its deviation from Fenton's solution. The value of maximum deviation 0.00031, or $0.04\varepsilon^3$ indicates that the wave propagates with a negligible distortion. The obtained wave speed 1.0939 agrees well with U_0 = 1.0943.

Next we computed the total mass above the still water level, Z and the total wave energy, Q which are conserved

quantities. Both Z and Q decreased slowly in all calculations. We suppressed the decrease of them by the choice of sufficiently small Δt. The relative decreases of them at the end of each computation were less than 0.3% in most computations.

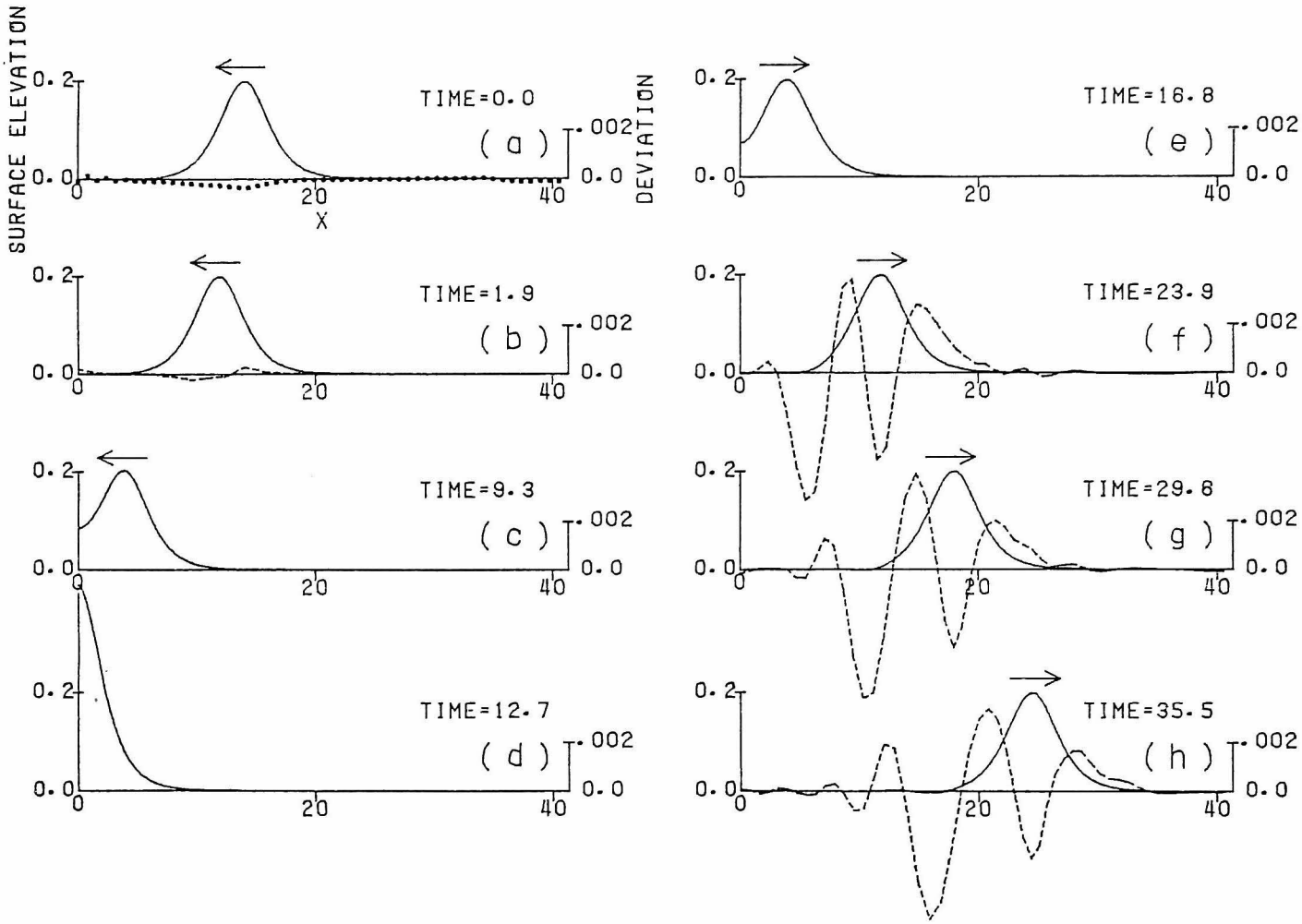

Fig.5 Wave profiles resulting from the reflection at the vertical wall. $\varepsilon = 0.2$, $x_0 = 14$, $L_1 = 41.3$, $\Delta t = 0.0039$, $\Delta x = 0.16$, $\Delta z = 0.022$. ———: Wave profile. — — —: Deviation of the wave profile from the steady solitary wave solution. ·····: Deviation of the wave profile at t = 0 in the time-reversal solution from the initial solitary wave.

§ 2.3. Results and Discussion

The numerical results about the reflection of the solitary wave with $\varepsilon = 0.2$ at the vertical wall are shown in Fig.5. The wave profiles at several instants are drawn with solid lines. Small distortion of the reflected wave was found and will be discussed on in § 2.3.3.

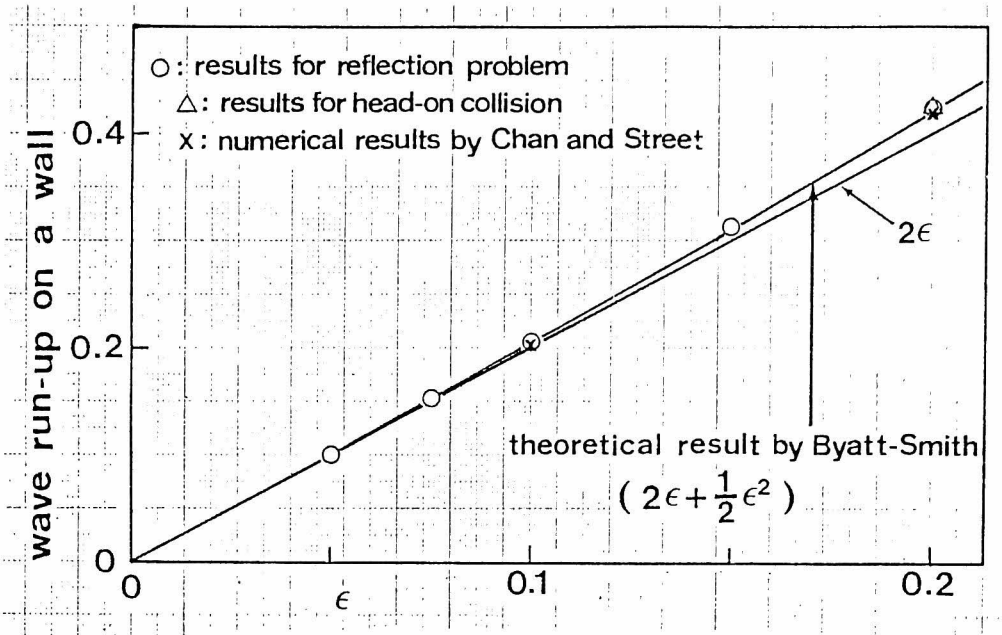

Fig.6 Wave run-up on a vertical wall.

2.3.1 Wave run-up on a vertical wall

The values of wave run-up on the vertical wall in the present calculations agree well with the theory and with the numerical results of Chan and Street [85] (see Fig.6). The calculated value for $\varepsilon = 0.2$ is 0.424, while the corresponding theoretical values of the second and third order are 0.420 and 0.426 respectively. The maximum wave amplitude for the head-on collision of two solitary wave with $\varepsilon = 0.2$ was 0.423, which is consistent with the case of reflection.

2.3.2 Phase shift

The phase shifts were computed from the data of x_{max}, the x-coordinate of the peak of the wave. The value of x_{max} varies during the reflection as is shown in Fig.7. Far from the wall, x_{max} can be written approximately as $x_{max} = -c_i t + d_i$ (before reflection) and $x_{max} = c_r t + d_r$ (after reflection). The coefficients were determined from the data of x_{max} by use of the

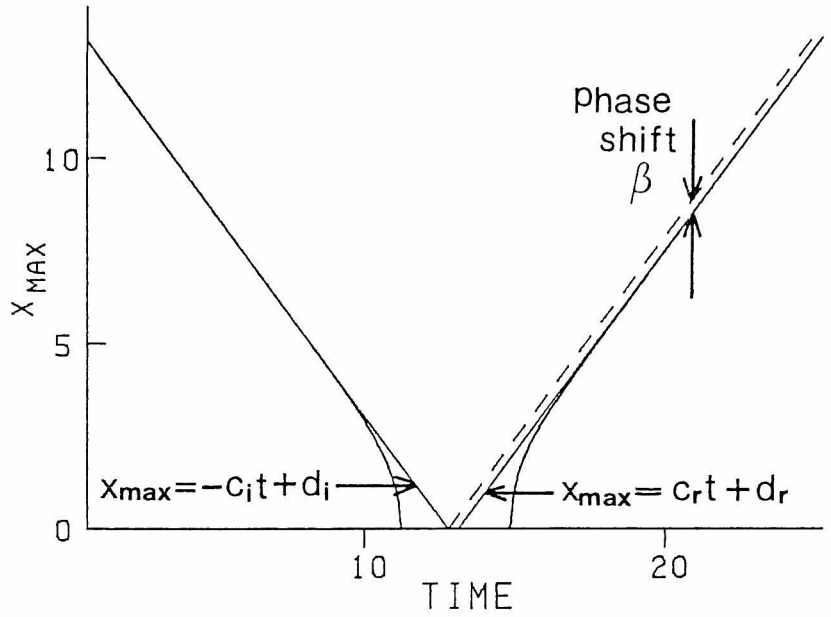

Fig.7. Trajectory of x_{max}. $\varepsilon = 0.2$.

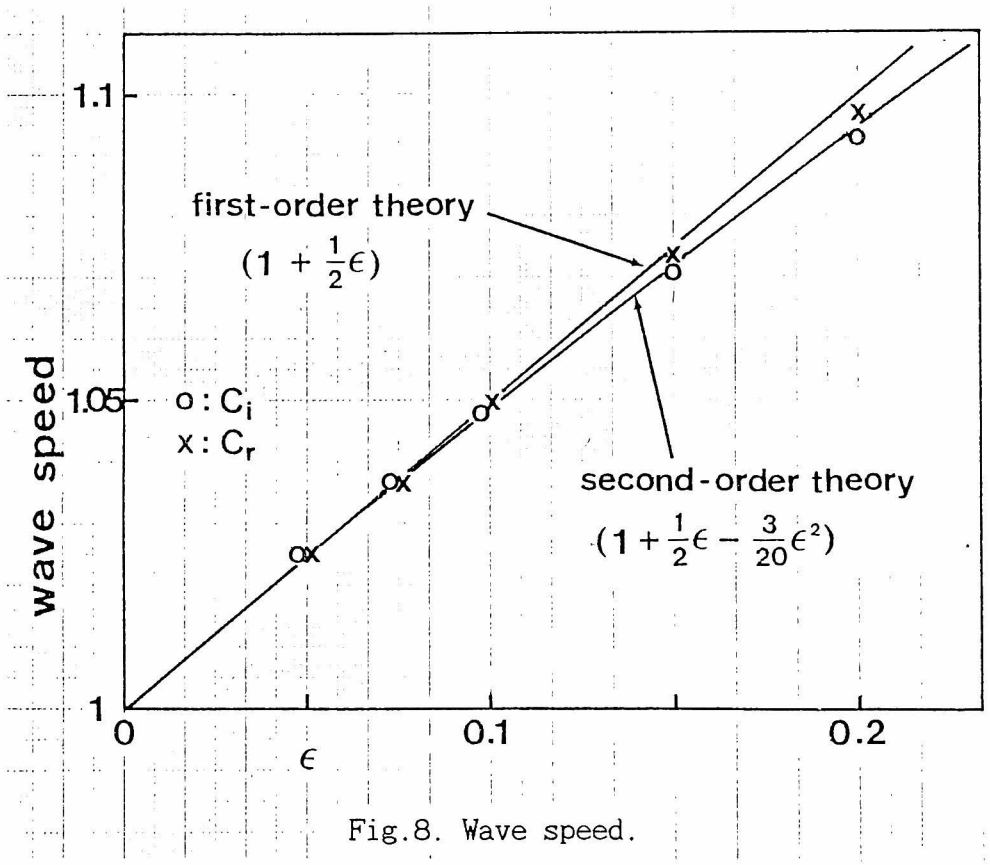

Fig.8. Wave speed.

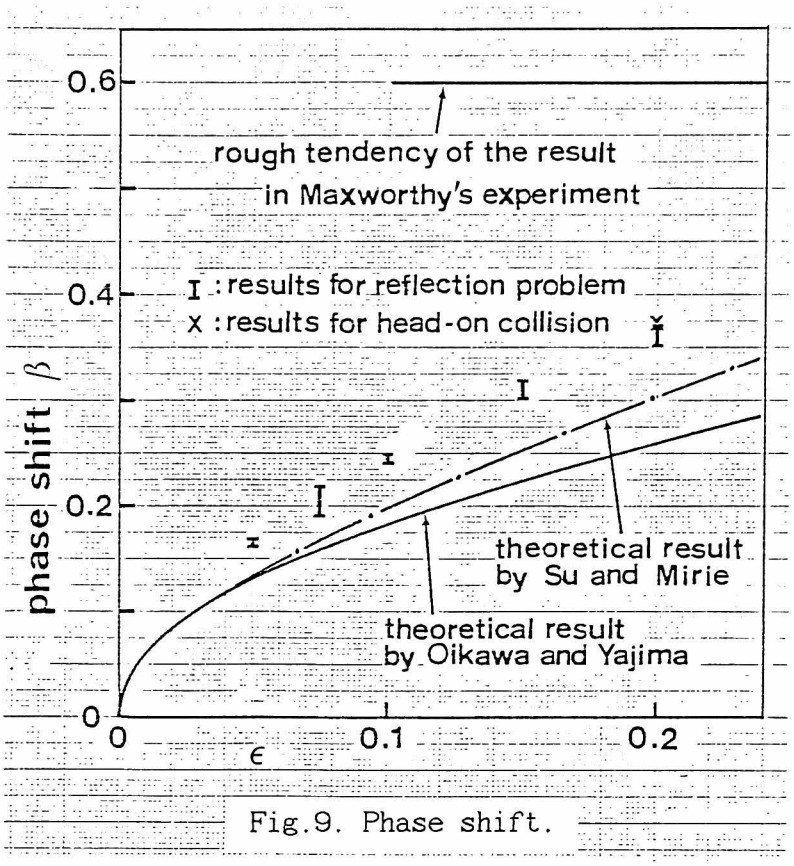

Fig.9. Phase shift.

method of least-squares. The velocities c_i and c_r are shown in Fig.8. The values of c_i are close to the theoretical values. On the other hand, the values of c_r are slightly larger than those of c_i. The reason for this is probably that the reflected wave continues to change its profile very slowly and c_r is determined from the position of the peak of the slowly varying wave. Strictly speaking, the phase shift varies in time. However, it is approximately constant in a considerably long interval far after the reflection. Therefore, we define here the phase shift β by the relation $\beta = -c_r d_i/c_i - d_r$. It is such a quantity that was measured as a phase shift in the experiment. The calculated results of β are shown in Fig.9 and seem to vanish as ε tends to zero in agreement with the theory. The values of β are a little

larger than the theoretical results. The phase shift for the head-on collision with $\varepsilon = 0.2$ agreed well with that for the corresponding reflection problem. These results show that the reason for the discrepancy between the experiment and the theories for the phase shift cannot be attributed to inappropriateness of the scaling adopted in the theories. In fact, the velocity fields obtained in our computation always satisfied the scaling. Maxworthy's [57] order-of-magnitude argument to explain for the phase shift to be independent of ε is invalid because according to his argument, the phase shift will be $O(\varepsilon^{-1/2})$ if w is $O(\varepsilon^{3/2})$ as assumed in the theories.

2.3.3 **Distortion of the reflected wave**

In Fig.5, the broken lines designate the deviation of the wave form of the numerical solution from that of the initial solitary wave shifted in the x-direction so as to have the same value of x_{max}. It is noted that the deviation at $t = 23.9$ (after reflection) is much larger than that at $t = 1.9$ (before reflection) and the deviation at x_{max} is negative after reflection. Maximum value of the magnitude of the deviation and the magnitude of the deviation at x_{max} are decreasing very slowly in time. The part of the deviation behind the main wave tends to go slowly away from the main wave. These properties of the reflected wave were found also for smaller ε and for the head-on collision of two waves.

In order to show that the distortion of the reflected wave observed above is not due to the numerical error, we made for $\varepsilon = 0.2$ the time reversal calculation starting from the data at $t = 30.1$. The solution of this time-reversal calculation agreed

well at $t = 0$ with the initial solitary wave. The deviation of the wave form is designated by the dotted line in Fig.5(a).

Consequently we conclude that the distortion of the profile of the reflected wave does exist. However, the computations suggest that the distortion is at most $O(\varepsilon^3)$. This result is consistent with the third-order theory of Su and Mirie [84]. However, the form of the reflected wave in our calculation is different from the wave form predicted to emerge immediately after the reflection in their theory. The time evolution of the reflected wave is so slow that the information about the asymptotic state of it was not obtained in our calculations The most acceptable prediction is that the distorted reflected wave evolves to a steady solitary wave with shedding a secondary wave behind it. The amplitude of this solitary wave is expected to be slightly less than that of the incident wave in consideration of the wave energy (As far as the amplitude of a solitary wave is not too large, the wave energy increases monotonically as the amplitude increases). As the shedding of a secondary wave accelerates the main wave, which reflects that $c_i < c_r$, it decreases the phase shift. Therefore, a sufficiently long time computation would have produced a little lower values of phase shift than our. Our numerical computations show that the theoretical approximate solutions are valid for sufficiently small ε and the discrepancy of the theory and the experiment for the phase shift cannot be resolved in the framework of the inviscid theory.

Chapter 3

Oblique Reflection of a Solitary Wave in Shallow Water

§ 3.1. Introduction

We are concerned with the problem of oblique reflection of solitary waves at the wall in shallow water. This problem is very interesting in consideration of a close relation to the problem of two-dimensional interaction of solitary waves.

Let ε_1 and ε_2 be the non-dimensional amplitudes of two solitary waves (divided by an undisturbed depth), and φ be the relative inclination between the normals of these solitary waves. Theoretical treatment of the oblique interaction of two solitary waves differs according as $\sin^2(\varphi/2) \gg \varepsilon_{1,2}$ or $\varphi^2 = O(\varepsilon_{1,2})$. Miles [58] called the former case 'weak interaction', and the latter case 'strong interaction'.

In the case of weak interaction, the first order approximation can be described simply by the superposition of two solitary waves [58], [83].

However, if $\varphi^2 = O(\varepsilon_{1,2})$, the weak interaction approach breaks down. The equations which describe strong interaction are similar to the two-dimensional K-dV equation. Chen [59] found the Bäcklund transformation for the two-dimensional KdV equation. Satsuma [60] solved the two-dimensional KdV equation to obtain an N-soliton solution.

Miles [58] also obtained an explicit solution, which is equivalent to that obtained by Satsuma, for strong interaction of two solitary waves in shallow water. He found that this

solution describes singular behaviour when φ is smaller than a certain critical angle and that the resonance conditions among three solitary waves are satisfied at this critical angle.

Yajima *et al.* [86] showed that the previous situation for shallow water waves is quite analogous for ion-acoustic waves.

In the theoretical treatment, the problem of oblique reflection of a solitary wave is interpreted as a special case of the oblique interaction of solitary waves (that is, $\varepsilon_1 = \varepsilon_2 = \varepsilon = a/h$ and $\varphi = 2\alpha$ for the reflection problem, where a is the amplitude of an incident solitary wave, h is an undisturbed depth, and α is the angle of incidence). We call the case of $\alpha \gg \sqrt{\varepsilon}$ (which corresponds to weak interaction) as 'non-grazing reflection', and the case of $\alpha = O(\sqrt{\varepsilon})$ (which corresponds to strong interaction) as 'grazing reflection' in this chapter.

The theoretical solution for non-grazing reflection is derived from that for weak interaction, and it describes an incident solitary wave I and a reflected solitary wave R far away from the wall (see Fig.10(a)).

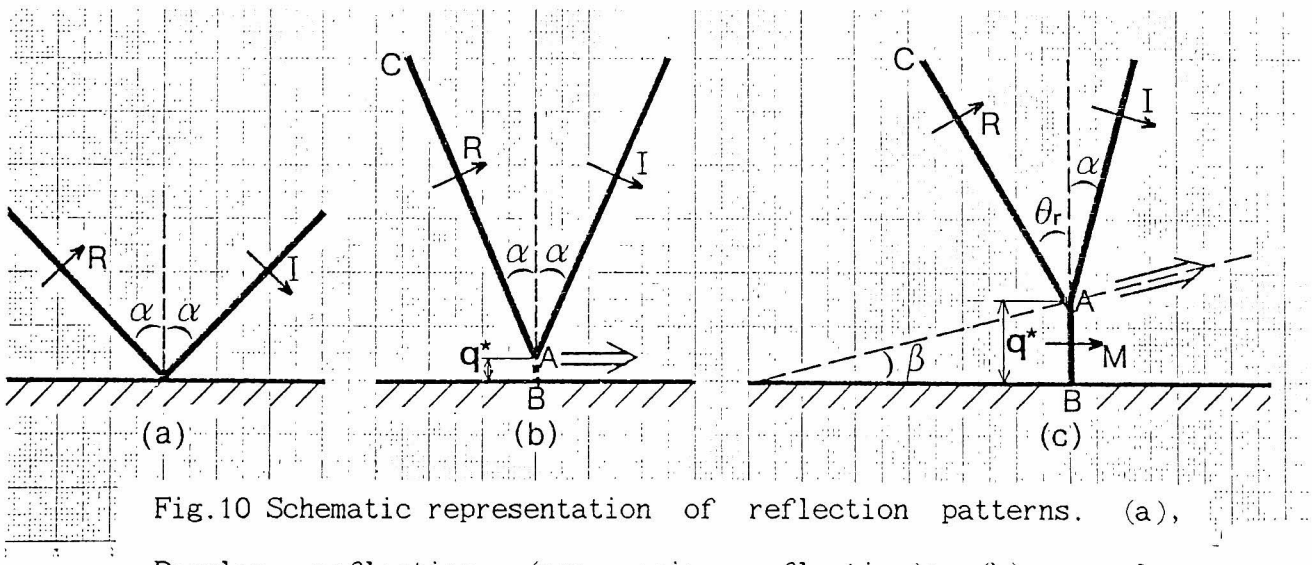

Fig.10 Schematic representation of reflection patterns. (a), Regular reflection (non-grazing reflection); (b), regular reflection (grazing reflection); (c), Mach reflection.

The angle which corresponds to the critical angle in the previous results for strong interaction is $\sqrt{3\varepsilon}$ for the reflection problem. The grazing reflection solution for $\alpha>\sqrt{3\varepsilon}$ obtained by Miles also describes a regular reflection pattern (see Fig.10(b)). However, there is a stem of the length O(1) perpendicular to the wall.

On the other hand, it was shown by Miles [58] that the solution becomes singular for $\alpha<\sqrt{3\varepsilon}$ under the assumption of regular reflection. For this case, he predicted in consideration of experiments (Perroud [87] ; Wiegel [88]) that the singular solution does not appear really, but that a resonantly interacting solution appears as an asymptotic solution for the initial-value problem of reflection [62]. The resonantly interacting solution describes three solitary waves I, R and M (see Fig.10(c)) and is called a 'Mach reflection' solution, and M is called a 'Mach stem'. The intersection of these waves, A in Fig.10(c), moves away from the wall along a straight line with the angle β to the wall contrary to the case of regular reflection. This solution, however, satisfies the boundary condition of zero normal velocity at the wall only asymptotically, and it is not clear whether the Mach stem appears and has the profile of a true solitary wave when the initial-value problem is solved.

Recently Melville [63] made experiments on this problem. He obtained the critical angle which is close to $\sqrt{3\varepsilon}$ through a double extrapolation of the measured data. However, the measured maximum run-up on the wall and the profile of a reflected wave indicated the discrepancy with the above Miles' prediction.

In this chapter, the initial-value problem of oblique reflection of a solitary wave shown in Fig.11 is solved numerically in order to make it clear whether the Mach reflection solution predicted by Miles does appear asymptotically if $\alpha<\sqrt{3\varepsilon}$ and to examine the behaviour of the solution for a wide range of α. In § 3.2, the initial and boundary value problem to be solved is presented. The numerical procedure for the problem is explained in § 3.3. The results of the numerical calculations are described and compared with the Miles' prediction and with Melville's experiments in § 3.4. Then it is concluded that the Mach reflection solution predicted by Miles does appear as an asymptotic solution of the initial-value problem for $\alpha<\sqrt{3\varepsilon}$.

§ 3.2. Formulation

We assume that the fluid is inviscid and incompressible, and that the motion is irrotational. Let $(x,y)\equiv(lx',ly')$ and $z\equiv hz'$ be horizontal and vertical co-ordinates, $t\equiv lt'/\sqrt{gh}$ the time, $\zeta\equiv a\zeta'$ the free-surface displacement and $\phi\equiv la\phi'\sqrt{g/h}$ the velocity potential, where h is an undisturbed depth, l is a characteristic wavelength and a is a characteristic amplitude. Then the parameters relevant to the problem are $\varepsilon = a/h$ and $\delta = h^2/l^2$. As we are concerned with shallow water waves of small amplitude, we assume that $\delta/\varepsilon = O(1)$ and $\varepsilon \ll 1$. Neglecting the terms of $O(\varepsilon^2)$, we get from eqs.(1.3) through the well known procedure, [58], [83], [89]

$$\frac{\partial \zeta'}{\partial t'} + \left(\frac{\partial^2}{\partial x'^2} + \frac{\partial^2}{\partial y'^2}\right) f' + \varepsilon \left[\frac{\partial}{\partial x'}\left(\zeta' \frac{\partial f'}{\partial x'}\right) + \frac{\partial}{\partial y'}\left(\zeta' \frac{\partial f'}{\partial y'}\right)\right]$$
$$- \frac{1}{6}\delta \left(\frac{\partial^2}{\partial x'^2} + \frac{\partial^2}{\partial y'^2}\right)^2 f' = 0, \qquad (3.1)$$

$$\frac{\partial}{\partial t'}\left[f' - \frac{1}{2}\delta \left(\frac{\partial^2}{\partial x'^2} + \frac{\partial^2}{\partial y'^2}\right) f'\right] + \zeta' + \frac{1}{2}\varepsilon \left[\left(\frac{\partial f'}{\partial x'}\right)^2 + \left(\frac{\partial f'}{\partial y'}\right)^2\right]$$
$$= 0, \qquad (3.2)$$

under the neglect of the surface tension Here f' is the nondimensional velocity potential at the bottom.

The boundary condition on the vertical wall is reduced to

$$\frac{\partial f'}{\partial n} = 0, \quad \frac{\partial^3 f'}{\partial n^3} = 0, \quad \frac{\partial \zeta'}{\partial n} = 0, \qquad (3.3a,b,c)$$

up to $O(\varepsilon)$, where $\partial/\partial n$ implies the normal derivative to the vertical wall.

In one-dimensional case of $\partial/\partial y=0$, the following solution [37] satisfies eqs.(3.1) and (3.2) with the error of $O(\varepsilon^2)$:

$$\zeta' = \left(1 - \frac{3}{4}\varepsilon \tanh^2\theta\right)\mathrm{sech}^2\theta, \qquad (3.4a)$$

and

$$f' = \frac{1}{k_0}\left[1 - \frac{\varepsilon}{12}(5+4\mathrm{sech}^2\theta)\right]\tanh\theta, \qquad (3.4b)$$

where

$$\theta = k_0(x'-x_0'-ct'), \qquad k_0 = \sqrt{3\varepsilon/(4\delta)}\left(1 - \frac{5}{8}\varepsilon\right),$$

and

$$c = 1 + \frac{1}{2}\varepsilon - \frac{3}{20}\varepsilon^2, \qquad (3.5)$$

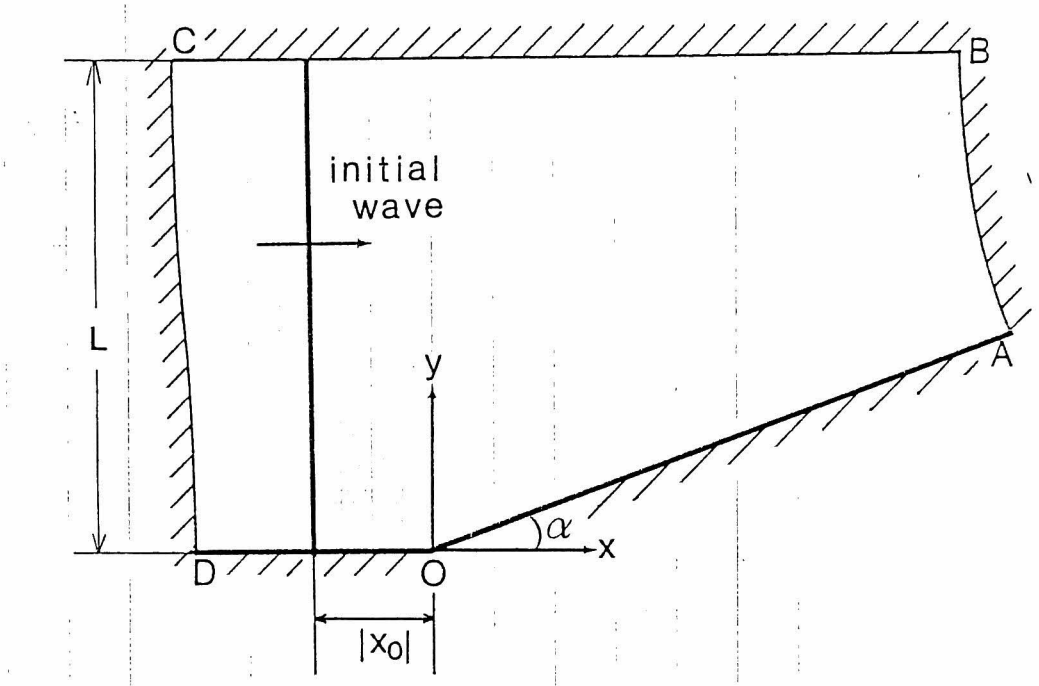

Fig.11. Schematic diagram showing the geometry of calculations.

where x_0($\equiv l x_0'$) is an initial position of the solitary wave. This solution is taken as the initial condition.

§ 3.3 The Numerical Procedure

Evolution eqs.(3.1) and (3.2) for f' and ζ' are integrated with a finite-difference method under the boundary conditions (3.3) and the initial conditions (3 4).

In eqs.(3.1) and (3.2), space derivatives were approximated using centered differences, and the time evolution was calculated with the method which is similar to the leapfrog method. Calculations were made in a rectangular region which was transformed from the region shown in Fig.11 by certain conformal mapping. Certain non-uniform mesh size which is finer near the wall AOD was used. The boundary AOD in Fig.11 was removed inward

by a small amount in order to avoid the singularity of coefficients of the difference equations at the corner O caused by the mapping. The details of the procedure are described in Appendix.

In one series of calculations (Series A), the region of calculation was restricted by a fixed boundary where the conditions (3.3) were imposed (see Fig.11). In another series of calculations (Series B), the rigion of calculation was shifted according as the movement of the wave to save computational works. In this case, the boundaries AB and CD in Fig.11 were shifted to the right by one mesh size when the wave traveled to the right by one mesh size. The values of f' and ζ' at the old AB boundary were used as those at the new AB boundary. The boundary conditions (3.3) were also imposed on the new boundaries AB and CD. Furthermore, the boundaries were kept sufficiently far from the 'interaction region', the region where an incident wave and a reflected wave (and a Mach stem) interact, so as not to affect the development of the wave in the interaction region.

For most calculations, the position of an initial wave x_0 was taken as $5.6\sqrt{h^3/a}$. Since the variation of the ratio δ/ε changes only the scales of the normalization of the horizontal co-ordinates and of the time, the ratio can be chosen arbitrarily if it is O(1). The ratio was chosen as 0.75 or 0.2 in the present calculations.

The accuracy of calculations was checked up with two methods. First, the initial wave (3.4a) is expected to travel along the wall BC in Fig.11 at the velocity (3.5) without changing its shape so long as the distance between BC and AO is not small. Deviations of the mean velocities on BC from the theoretical value (3.5) were less than 0.2%. The wave amplitude on BC increased slowly with the time, but the deviation of it from the initial amplitude was less than 3%. This increase of amplitude seems to be due to numerical error because the rate of increase decreased as the mesh size decreased.

Secondly, it is shown from eqs.(3.1) and (3.2) and the boundary conditions (3.3) that

$$Z = \int_V \zeta' dV,$$

and

$$Q = \int_V \{\frac{1}{2}\zeta'^2+\frac{1}{2}(1+\varepsilon\zeta')[(\frac{\partial f'}{\partial x'})^2+(\frac{\partial f'}{\partial y'})^2]+\frac{1}{3}\delta[(\frac{\partial^2}{\partial x'^2}+\frac{\partial^2}{\partial y'^2})f']^2\}dV,$$

are conservative quantities which correspond to the excess mass of fluid and the wave energy, where the terms of $O(\varepsilon^2)$ are neglected in the expression of Q. The variations of Z and Q were less than 0.23% and 0.75% respectively in the calculations of Series A. On the other hand, the values of Z and Q vary with the time for the calculations of Series B. The results of Series B, however, agreed well with those of corresponding calculations of Series A as to the behaviour of the solutions in the interaction region.

§ 3.4. Discussion of Results

Calculations were made for ε=0.05~0.2 and for $\alpha=\pi/40\sim\pi/3$, and the properties of the solutions were examined in detail for ε = 0.05. Furthermore, the results are compared with Melville's experiments.

3.4.1 Reflection pattern

Figure 12 (a)~ (d) show the time evolution of the surface displacement ζ' for the oblique reflection of a solitary wave. This calculation is made with ε = 0.05 and $\alpha = \pi/6$, and then the ratio $\alpha/\sqrt{3\varepsilon}$ is 1.35. A reflected wave appears and develops into a straight stems. The run-up at the wall increases monotonically with the time and tends to a certain constant The intersection of an incident and a reflected wave continues to be close to the wall, thus the solution represents the regular reflection pattern. Figure 12(e) shows the theoretical grazing reflection solution for the same values of ε and α.

A similar calculation is shown in Fig.13 for ε = 0.05 and $\alpha = \pi/20$ (these parameters satisfy the condition $\alpha<\sqrt{3\varepsilon}$). In this case, the intersection of an incident and a reflected wave moves away from the wall contrary to the result in Fig.12, and a Mach stem develops to join this intersection to the wall. Then the solution represents the Mach reflection pattern and approaches the solution predicted by Miles for $\alpha<\sqrt{3\varepsilon}$ (shown in Fig.13(e)).

In most calculations the solutions have reached stationary states. Here a solution is considered to be in the stationary state when the values of the maximum run-up at the wall, the amplitude of a reflected wave and the angle of reflection do not

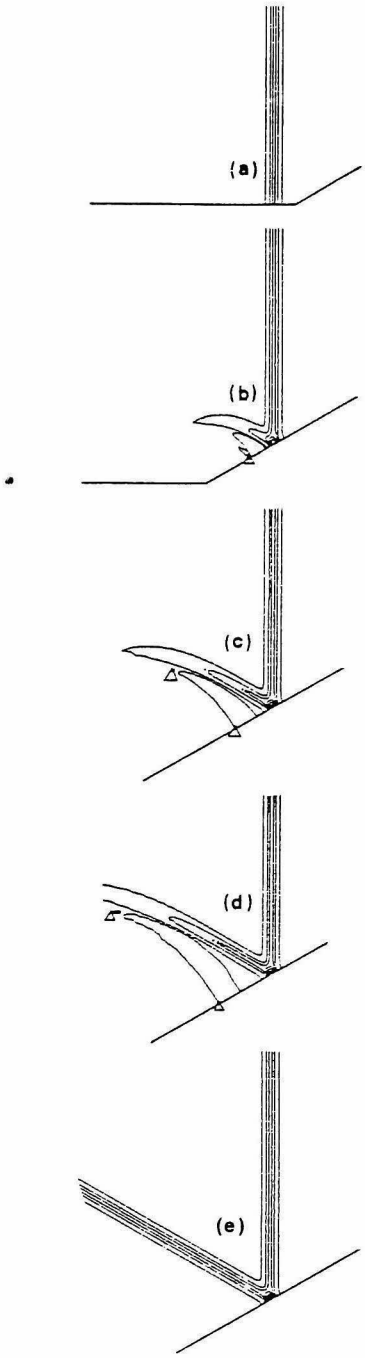

Fig.12

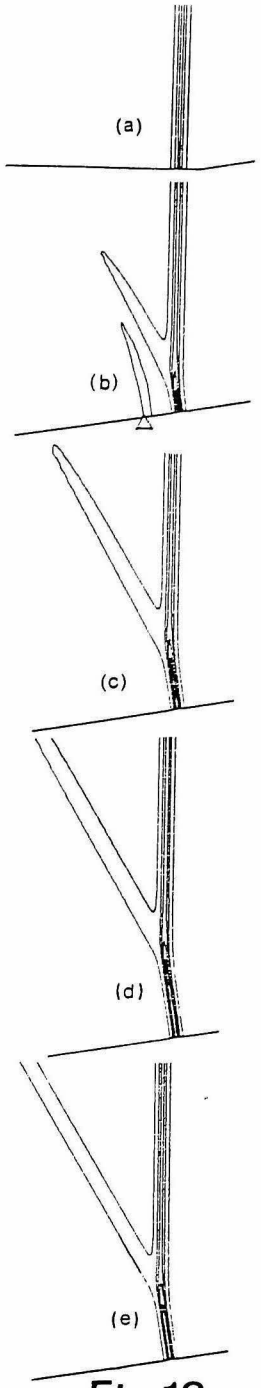

Fig.13

Fig.12. Time evolution of free-surface displacement which represents regular reflection pattern ($\varepsilon = 0.05$, $\delta = 0.01$, and $\alpha=\pi/6$). Solid curves represent the contour lines of ζ' of constant intervals ($\zeta' = 0.1, 0.5, 0.9, \ldots$), and the contour line with $\triangle$ represents $\zeta' = -0.07$. (a), $t' = 0$; (b), $t' = 10$; (c), $t' = 20$; (d), $t' = 30$ (the solution has reached a stationary state at $t' = 30$). (e), Theoretical solution with the same parameters predicted by Miles.

Fig.13. Time evolution of free-surface displacement which represents Mach reflection pattern ($\varepsilon = 0.05$, $\delta = 0.01$, and $\alpha=\pi/20$). Solid curves represent the contour lines of ζ' of constant intervals ($\zeta' = 0.1, 0.5, 0.9, \ldots$), and the contour line with $\triangle$ represents $\zeta' = -0.07$. (a), $t' = 0$; (b), $t' = 50$; (c), $t' = 105$ (the solution has reached a stationary state at $t' = 105$); (d), $t' = 150$. (e), Theoretical solution with the same parameters predicted by Miles ($t' = 105$).

depend on the time (although the tip of the reflected wave continues to advance).

The time $T_S h/\sqrt{ag}$ required to reach the stationary state since an incident wave passes the line $x = 0$ in Fig.11 is shown in Fig.14 for $\varepsilon = 0.05$. The value of T_S contains a fairly large margin of error because it is difficult to determine when the solution has reached the stationary state without ambiguity. The value of it is about 200~ 400 if $\alpha<\sqrt{3\varepsilon}$, and decreases rapidly as α increases if $\alpha>\sqrt{3\varepsilon}$.

In order to classify the solutions into regular and Mach reflection, we introduce a time-dependent variable $q^* = q\sqrt{h^3/a}$ which is the distance between two points A and B in Fig.10(b) and (c). Here, B is the point of maximum run-up, and A is the intersection of the crest line of an incident wave and the normal to the wall at the point B. The solution is concluded to be of regular reflection type if q tends to a constant asymptotically and be of Mach reflection type if q increases linearly with the time asymptotically.

The results of classification of the solution for each pair of (α,ε) are shown in Fig.15. The results are consistent with the boundary line $\alpha = \sqrt{3\varepsilon}$ predicted by Miles when $\varepsilon \leqq 0.2$.

If α is slightly larger than $\sqrt{3\varepsilon}$, the theoretical solution for grazing reflection implies that q diverges logarithmically as α tends to $\sqrt{3\varepsilon}$. In this case, the solution describes a 'Mach stem' in the vicinity of the wall although the intersection of an incident and a reflected wave does not move away from the wall. The calculated values of q for $\alpha>\sqrt{3\varepsilon}$ increase rapidly as α decreases to $\sqrt{3\varepsilon}$, but they are about 50%

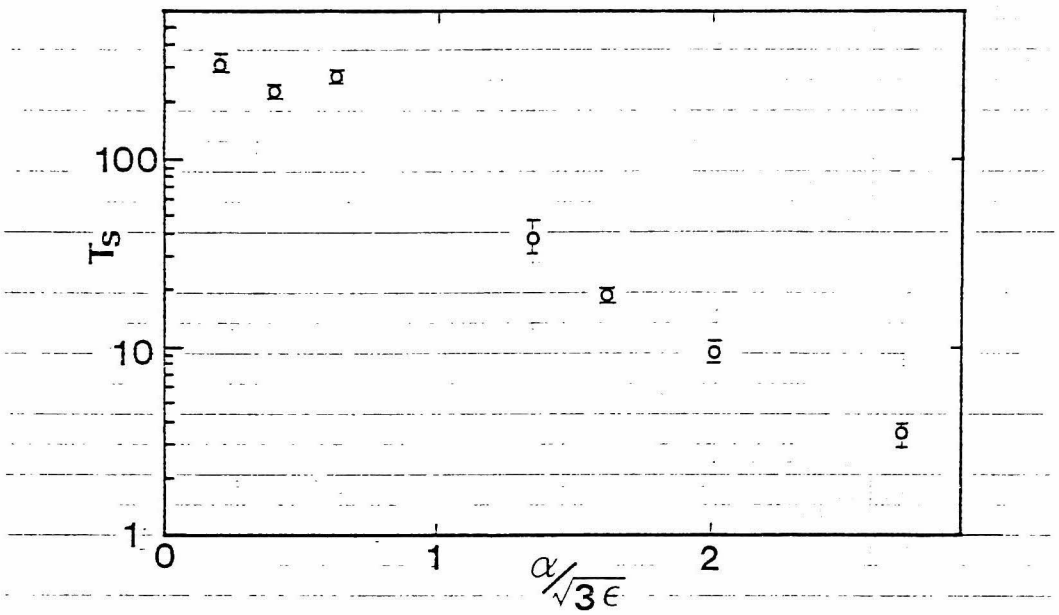

Fig.14. The time required to reach the stationary state since an incident wave begins to be reflected. $\varepsilon = 0.05$.

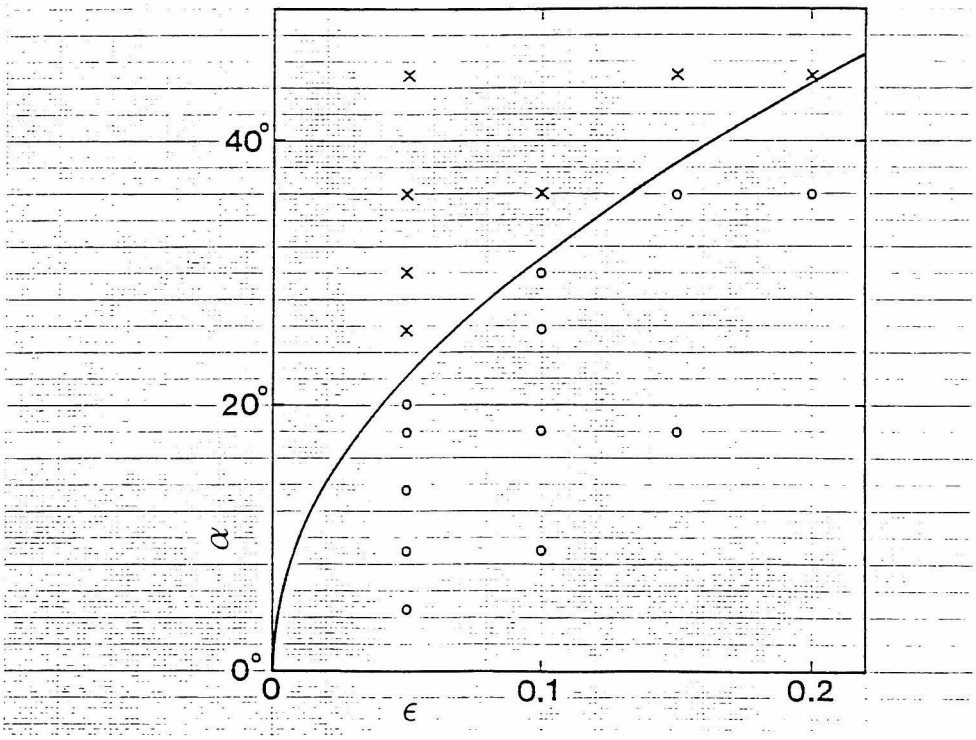

Fig.15. Reflection patterns of the solution for each pair of parameters (ε,α). ○: Mach reflection. ×: Regular reflection. The solid line is the boundary between these reflection patterns predicted by Miles.

of the theoretical values.

The angle β in Fig.10(c) may be calculated from the asymptotic values of dq^t/dt and the velocity of the point B (β = 0 for regular reflection). The values of β are shown in Fig.16 for ε = 0 05. They increase linearly as α decreases from $\sqrt{3\varepsilon}$ to zero and agrees well with Miles' prediction $\beta = \sqrt{\varepsilon/3}(1 - \alpha/\sqrt{3\varepsilon})$.

3.4.2. The maximum run-up at the wall

The maximum run-up at the wall is the most interesting quantity partly because it is important in the investigation of the reflection of ocean wave and partly because Miles predicted that it is much larger than that in linearized theory when α is close to $\sqrt{3\varepsilon}$. The maximum run-up at the wall $\alpha\zeta^*_{max}(t)$ increases monotonically with the time and then tends to a constant approximately for most calculations (see Fig.17 as examples). We define this asymptotic value as the maximum run-up at the wall for stationary state $\alpha\zeta_{max}$. The value of it is shown in Fig.18 for ε = 0.05. If $\alpha<\sqrt{3\varepsilon}$, then ζ_{max} decreases to 1 as α decreases to zero (corresponding to a wave moving parallel to the wall) and agrees well with Miles' result $(1+\alpha/\sqrt{3\varepsilon})^2$. On the other hand, if the value of $\alpha/\sqrt{3\varepsilon}$ is 1.3~ 2.7, then ζ_{max} is slightly larger than 2 (the value in linearized theory) and agrees better with the result $\zeta_{max} = 2 + \varepsilon\{ 3/(2\sin^2\alpha) - 3 + 2\sin^2\alpha \}$ for non-grazing reflection rather than the result $\zeta_{max} = 4/(1 + \sqrt{(\alpha^2-3\varepsilon)/\alpha^2})$ for grazing reflection.

Stationary state was not attained when α is close to $\sqrt{3\varepsilon}$ ($\alpha/\sqrt{3\varepsilon}$ = 1 01 and 0.81) owing to the limitation of computational works. In this case, the values of ζ_{max} at the

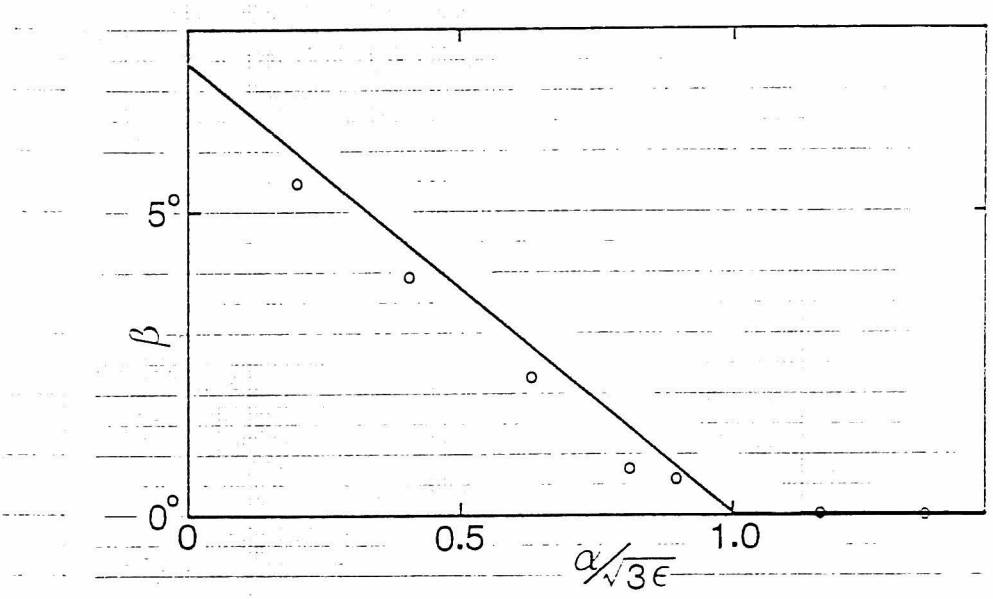

Fig.16. The values of β in Fig.10(c) for $\varepsilon = 0.05$. ○: Calculated results. ———: Theoretical values predicted by Miles.

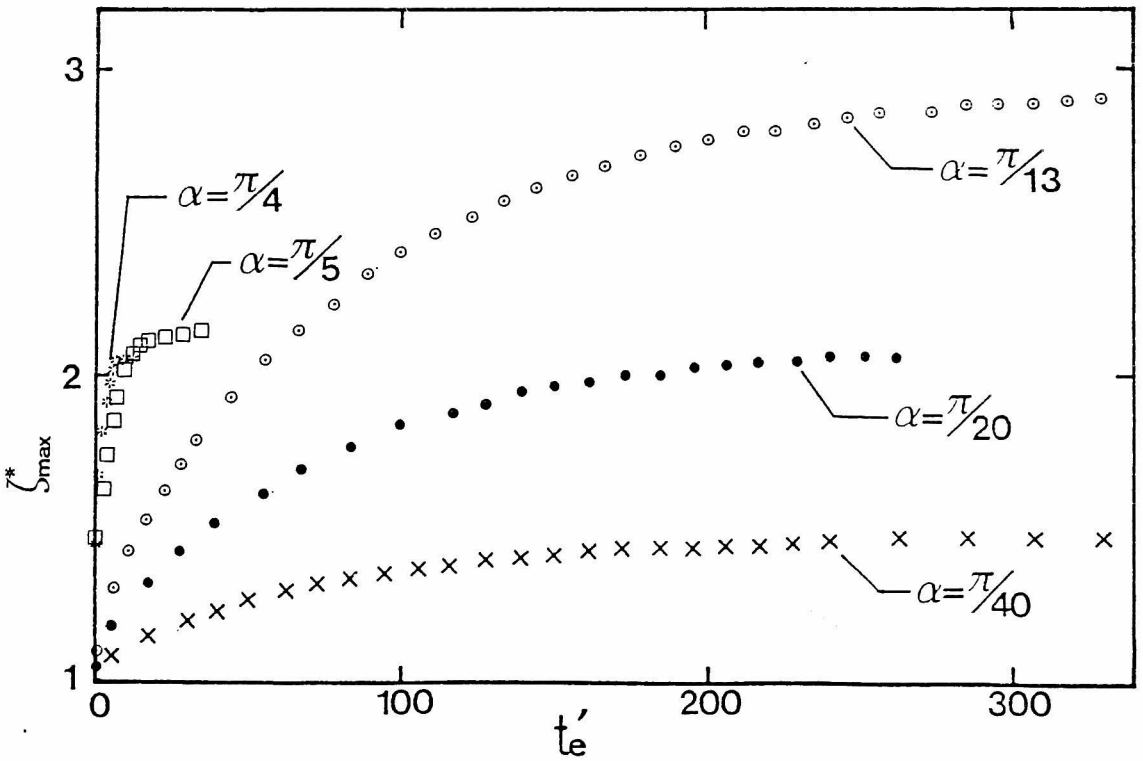

Fig.17. Time evolution of maximum run-up at the wall for $\varepsilon = 0.05$. Horizontal co-ordinate is the non-dimensional interaction time $t'_e = t_e\sqrt{ag}/h$. (t_e is the interaction time of an incident wave with an oblique wall. When the crest line of an incident wave passes through the line x = 0 in Fig.11 far from the corner, t_e is chosen as 0.).

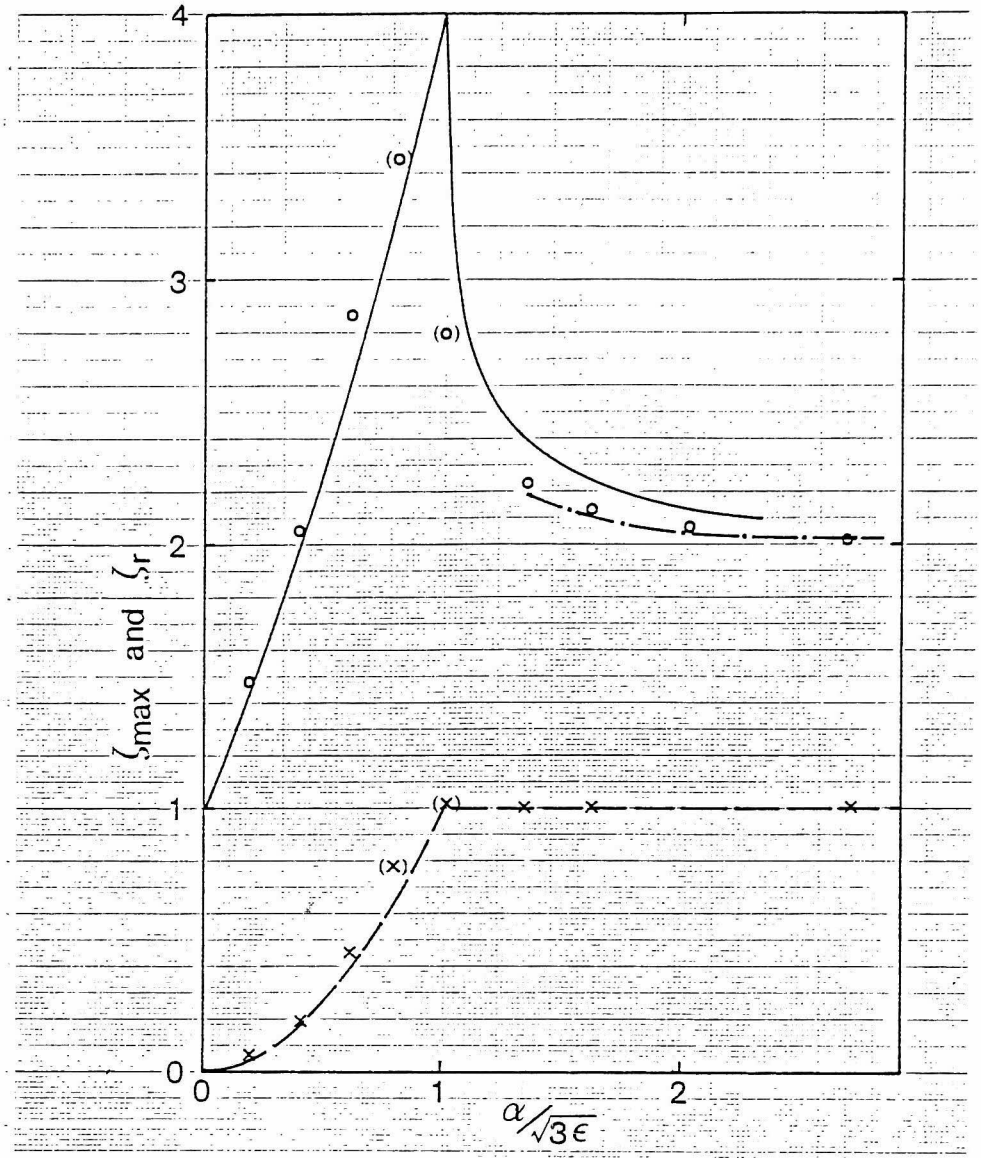

Fig.18. The maximum run-up at the wall and the amplitudes of reflected waves for $\varepsilon = 0.05$. O: Calculated maximum run-up. (O): Calculated unsaturated maximum run-up at the largest time of the computation. ———: Theoretically predicted maximum run-up for grazing reflection. —·—: Theoretically predicted maximum run-up for non-grazing reflection. X: Calculated amplitudes of reflected waves. (X): Unsaturated amplitudes of reflected waves at the largest time of the computation. — — —: Theoretically predicted amplitudes of reflected waves.

largest time of the computation are considerably larger than 2 and are increasing slowly (see Fig.18). Then ζ_{max} is inferred to be close to that of Miles' prediction.

The value of $\zeta^*_{max}(t)$ at the largest observation time in Melville's experiment was much smaller than the theoretical value although measured $\zeta^*_{max}(t)$ increased slowly at that time for most cases. Furthermore, measured $\zeta^*_{max}(t)$ increased monotonically as α increased.

The values of $\zeta^*_{max}(t)$ in Melville's experiments and in the corresponding calculations are shown as a function of the co-ordinate along an oblique wall in Fig.19. The measured values agree fairly well with the calculated values. However, the calculated values of $\zeta^*_{max}(t)$ continue to increase for the interaction time of 7 or 9 times as long as the largest interaction time in the experiments. Therefore, if the experiment with a little larger observation time is made, a little larger value of $\zeta^*_{max}(t)$ may be obtained (although much larger observation time does not necessarily give the much larger value of it as is discussed in § 3.4.6).

3.4.3 The behaviour of reflected waves

Figure 20 shows the examples of profiles of the surface elevation along the crest line of a reflected wave (and a Mach stem). At the first stage of interaction of an incident wave with a wall, the profile such as the broken line is obtained. The amplitude of a reflected wave is not defined for this case. After the sufficiently long interaction time, the profile such as the solid line appears. We define the surface elevation at the point P of locally minimum gradient as the amplitude of a

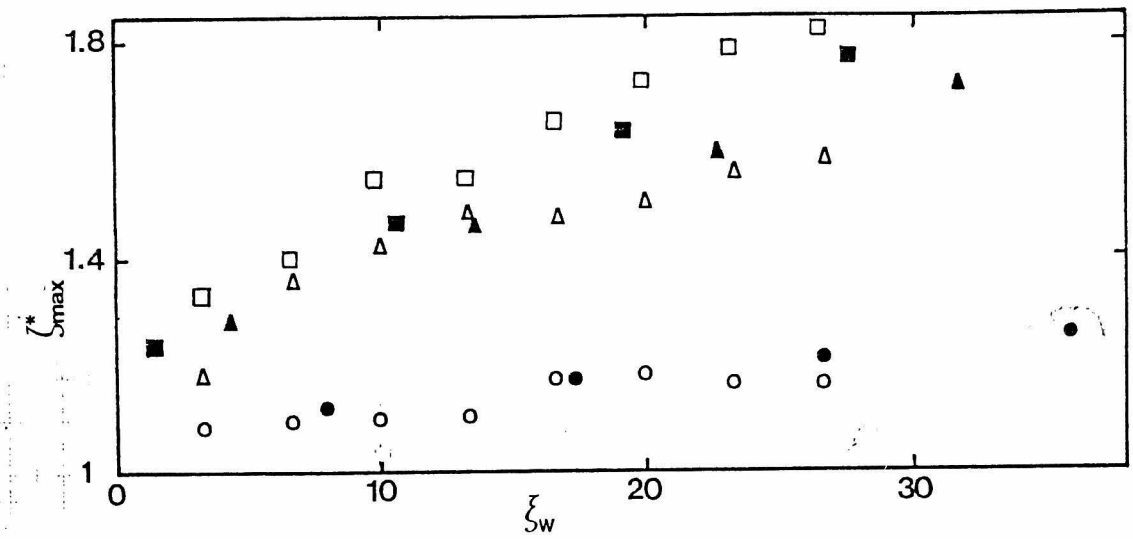

Fig.19. Maximum run-up at the wall in the present calculations and in Melville's experiments for each value of the non-dimensional distance divided by h along an oblique wall from the corner. Open symbols denote experimental results. Solid symbols denote calculated results. ● and ○: $\varepsilon = 0.1$, $\alpha = 10°$ (experiment), 9° (calculation). ▲ and △: $\varepsilon = 0.1$, $\alpha = 25°$ (experiment), 25.7° (calculation). ■ and □: $\varepsilon = 0.1$, $\alpha = 30°$.

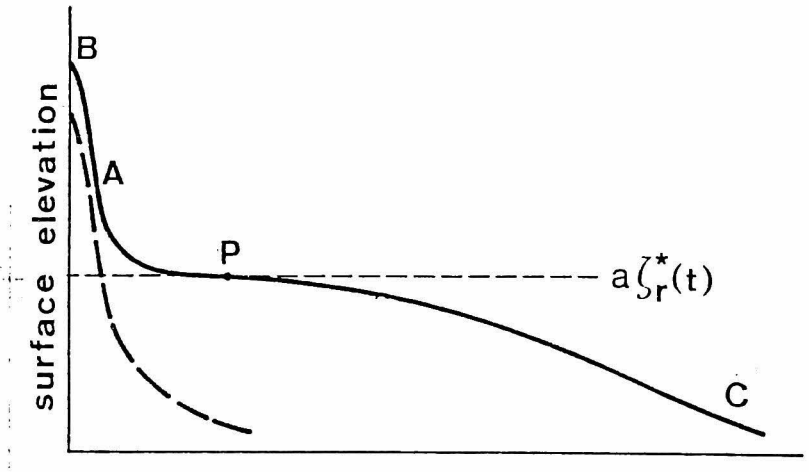

Fig.20. Representative profiles of the surface elevation along the crest line of a reflected wave (and a Mach stem). The horizontal co-ordinate is the distance from the point of maximum run-up at the wall along the crest line of a reflected wave (and a Mach stem). — — —: The profile at small interaction time . ————: The profile at the larger interaction time (B, A and C correspond to those in Fig.10(b) and (c)).

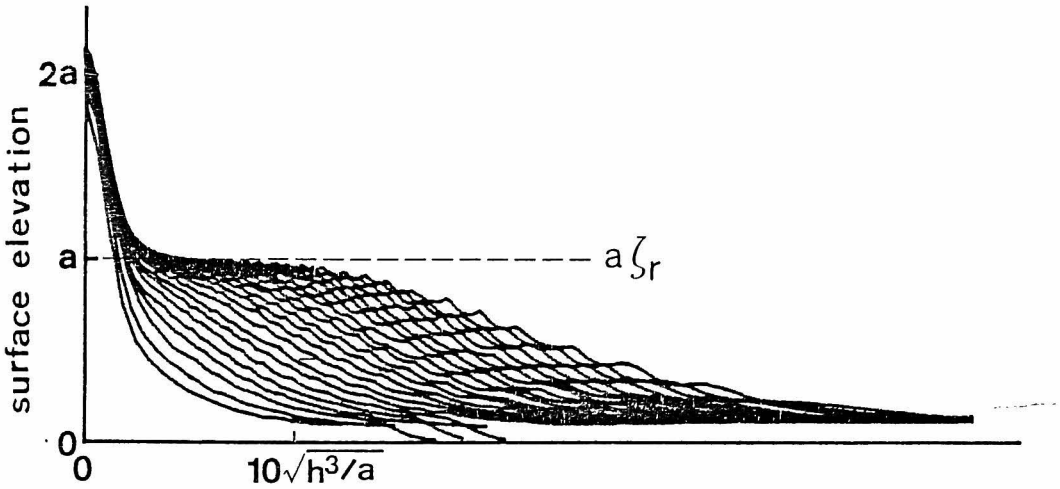

Fig.21. Time evolution of the profile of the surface elevation along the crest line of a reflected wave. ε = 0.05 and $\alpha=\pi$ 5 ($\alpha/\sqrt{3\varepsilon}$ = 1.62) corresponding to regular reflection. Horizontal co-ordinate is the same as that in Fig.20. The lines are for the interaction time t_e = $5.08h/\sqrt{ag}$, $6.47h/\sqrt{ag}$, ... of the same interval.

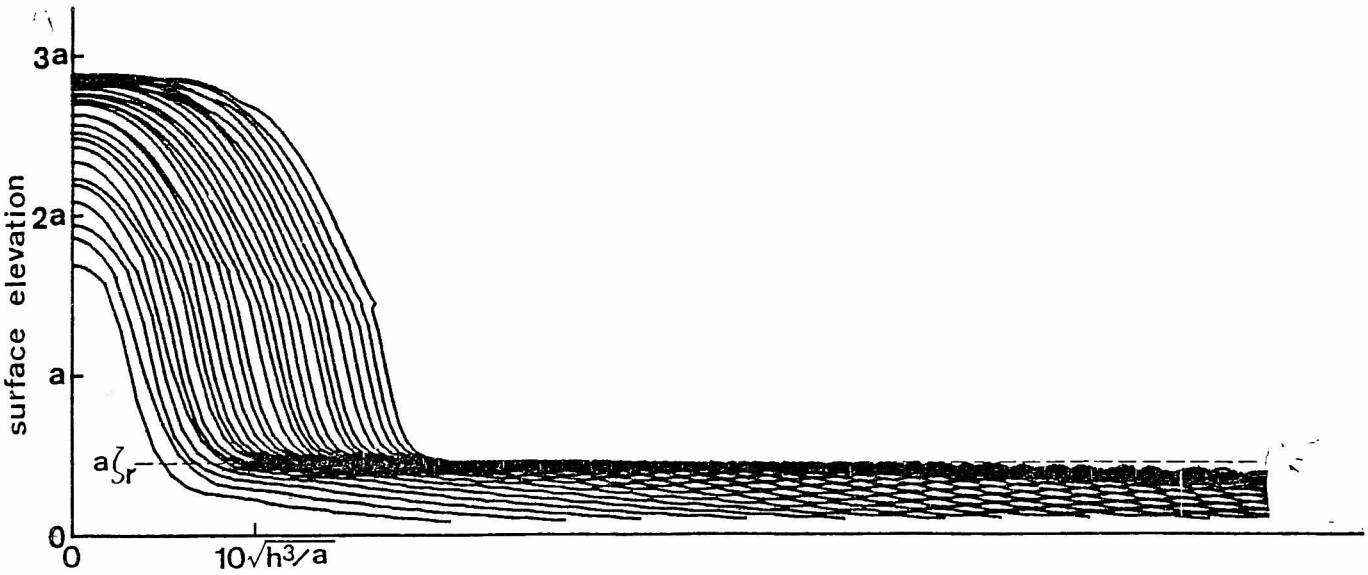

Fig.22. Time evolution of the profile of the surface elevation along the crest line of a Mach stem and a reflected wave. ε = 0.05 and $\alpha = \pi/13$ ($\alpha/\sqrt{3\varepsilon}$ =0.62) corresponding to Mach reflection. Horizontal co-ordinate is the same as that in Fig.20. The lines are for the interaction time t_e = $27.95h/\sqrt{ag}$, $39.13h/\sqrt{ag}$, ... of the same interval.

reflected wave at that time and write it as $a\zeta^*_r(t)$.

The obtained values of $a\zeta^*_r(t)$ increase monotonically with the time and approach to certain values. We define this asymptotic value as the amplitude of a reflected wave in stationary state and write it as $a\zeta_r$. The value of it is shown in Fig.18 for $\varepsilon = 0.05$. It is equal to the amplitude of an incident wave if $\alpha > \sqrt{3\varepsilon}$, and decreases to zero as α decreases from $\sqrt{3\varepsilon}$ to zero in agreement with Miles' prediction $\zeta_r = \alpha^2/(3\varepsilon)$.

Time evolutions of profiles of the surface elevation along reflected waves (and Mach stems) are shown in Figs.21 and 22. When $\alpha > \sqrt{3\varepsilon}$, a Mach stem is not generated as is shown in Fig.21. This corresponds to the regular reflection. On the other hand, if $\alpha < \sqrt{3\varepsilon}$ a Mach stem elongates with the time. This represents the Mach reflection pattern (see Fig.22) The position of the tip of a reflected wave can not be determined definitely because the surface elevation decreases very slowly along the crest line of a reflected wave at the region far from the wall.

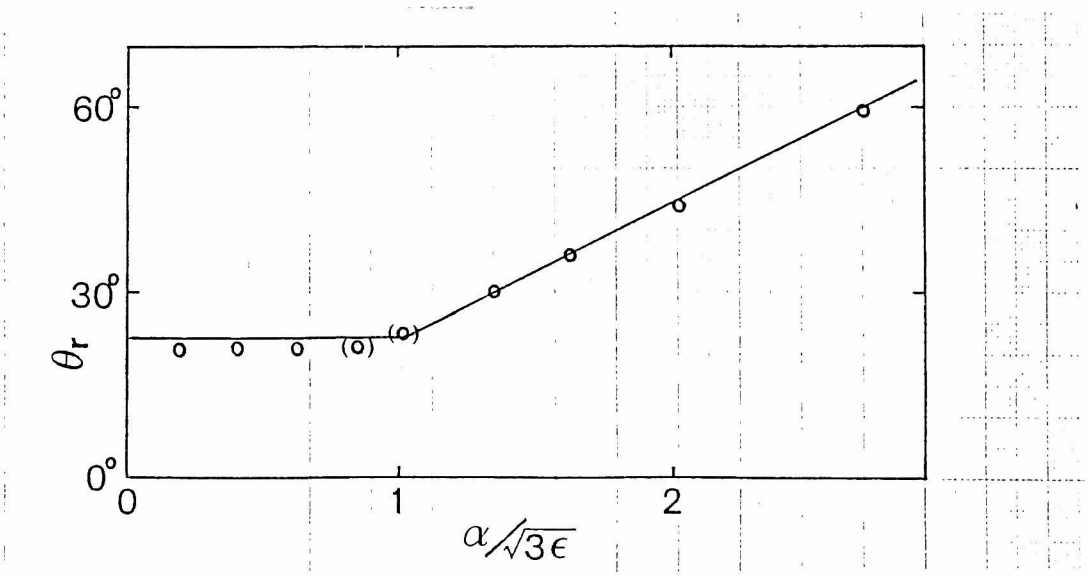

Fig.23. The angle of reflection for $\varepsilon = 0.05$. O: Calculated results. (O): The unsaturated values at the largest time of the computation. ——: Theoretically predicted values.

The angle of reflection θ_r (see Fig.10(c)) takes approximately constant value after sufficiently large interaction time and is shown in Fig.23 for ε = 0 05. If $\alpha>\sqrt{3\varepsilon}$, then θ_r is almost the same as the angle of incidence. On the other hand, the value of θ_r is independent of α and agrees well with Miles' prediction $\theta_r=\sqrt{3\varepsilon}$ if $\alpha<\sqrt{3\varepsilon}$.

Figure 24 shows the profile of the surface elevation across the crest line of a reflected wave. When $\alpha>\sqrt{3\varepsilon}$ the profile which agrees well with that of an incident wave is obtained asymptotically (see the circles and a solid line in Fig.24(a)) Figures 24 (b) and (c) correspond to the case of Mach reflection. The profiles agree approximately with those of Miles' prediction

$$\zeta' = \frac{\alpha^2}{3\varepsilon}\mathrm{sech}^2\left[\frac{\alpha}{(3\varepsilon)^{1/2}}(\xi'-\xi_0)\right]$$

after the sufficiently large interaction time, where $l\xi'$ is the horizontal co-ordinate along the normal to the crest line of a reflected wave. The profiles for insufficient interaction time are not symmetric and represent the more rapid decrease at the backward side of waves as is shown by the triangles in Fig.24

Melville obtained "reflected wave amplitudes" which are considerably smaller than the theoretical values except for small α. The effect of viscosity seems negligible for his observation time as will be discussed in § 3.4.6. I infer that "the reflected wave amplitude" obtained by him is the surface elevation at some point on the crest line of the reflected wave at an insufficient interaction time from the following two reasons: First, the profiles such as the broken line in Fig.20

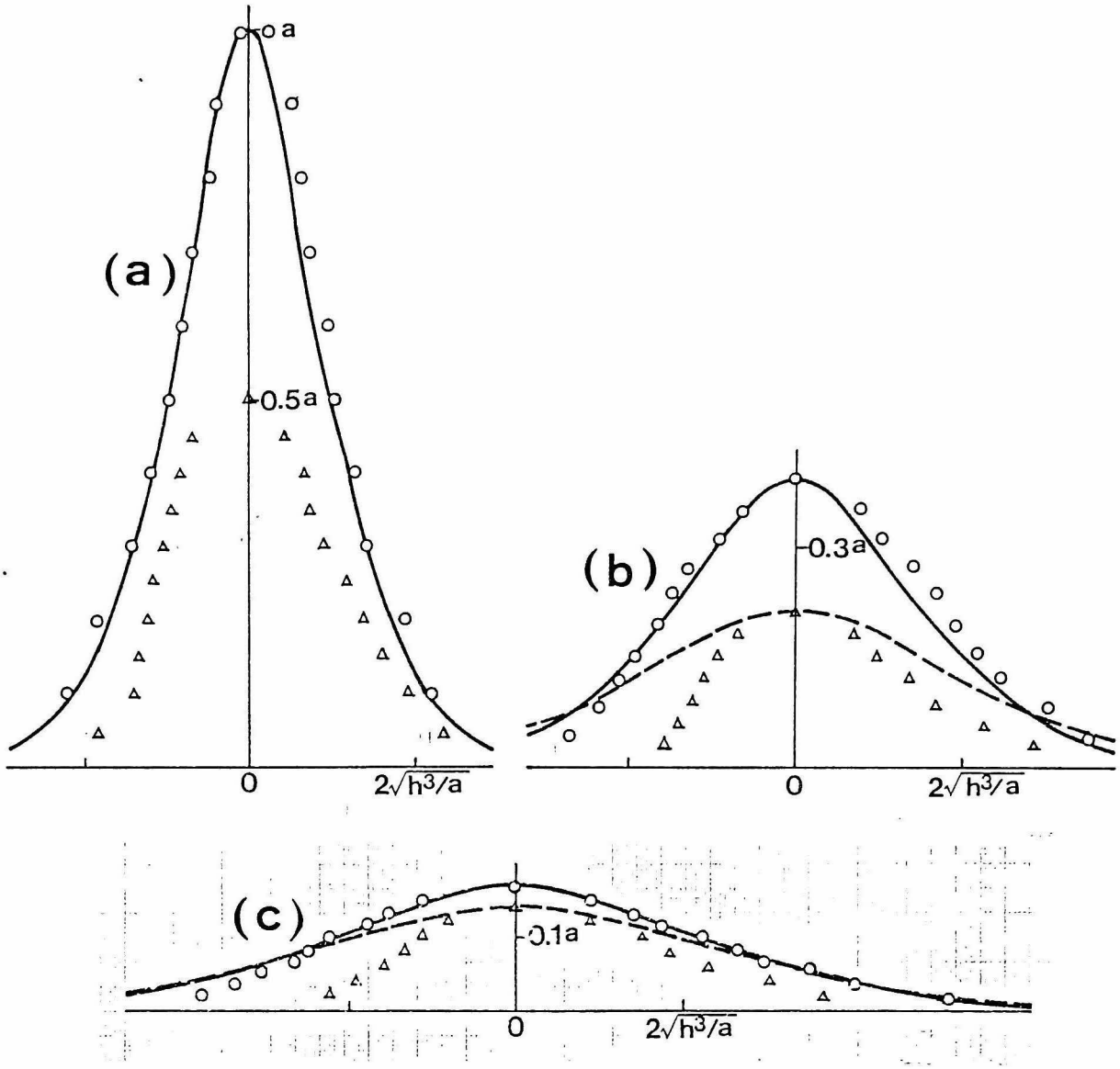

Fig.24. Profiles of the surface elevation across the crest line of a reflected wave for $\varepsilon = 0.05$. Circles denote the profiles of sufficiently developed reflected waves at the section where the maximum values of them agree with the theoretically predicted values. Triangles denote the profiles of insufficiently developed reflected waves. Solid lines denote the profiles of an incident wave (in (a)) and of the reflected wave in Miles' prediction (in (b) and (c)). Broken lines denote the profile of a Boussinesq solitary wave of the same amplitude as the profile of triangles. (a), $\alpha=\pi/6$, corresponding to regular reflection; △, $t_e = 16.8h/\sqrt{ag}$; ○, $t_e = 72.7h/\sqrt{ag}$. (b), $\alpha = \pi/13$, corresponding to Mach reflection; △, $t_e = 39.1h/\sqrt{ag}$; ○, $t_e = 274h/\sqrt{ag}$. (c), $\alpha=\pi/20$, corresponding to Mach reflection; △, $t_e = 83.9h/\sqrt{ag}$; ○, $t_e = 330h/\sqrt{ag}$.

are obtained in the present calculations for ε and α corresponding to his experiments at the interaction time estimated crudely from the contents of his paper (see Fig.25 for examples). Secondly, the much narrower profile than a Boussinesq solitary wave of a reflected wave measured by him is also obtained for the reflected wave at insufficient interaction time as is shown by the broken line and triangles in Figs.24 (b) and (c). Therefore, the larger interaction time seems to be required for the measurement of fully developed reflected waves although the viscous effect may not be negligible then.

Melville considered the model with a reflected wave of finite length. In this model it is assumed that the surface elevation varies as a step function along the crest line of a reflected wave and that the incident and reflected waves and the Mach stem have the solitary wave profiles. He determined the length of the reflected wave by means of the conservation of mass and energy. The result is inconsistent with the conservation of momentum in the neighbourhood of the tip of the reflected wave. For this reason, Melville suggested that Miles' solution does not appear asymptotically. However, the result of the present calculations differs from the assumption in this model, and the calculated amplitude of the reflected wave agrees with Miles' model. The above inconsistency seems due to the defect of the model itself.

3.4.4 The behaviour of troughs

In the present calculations a trough appears behind a reflected wave (and a Mach stem). The depth of it at the wall attains a maximum value ad_t at the time $T_t h/\sqrt{ag}$, and then

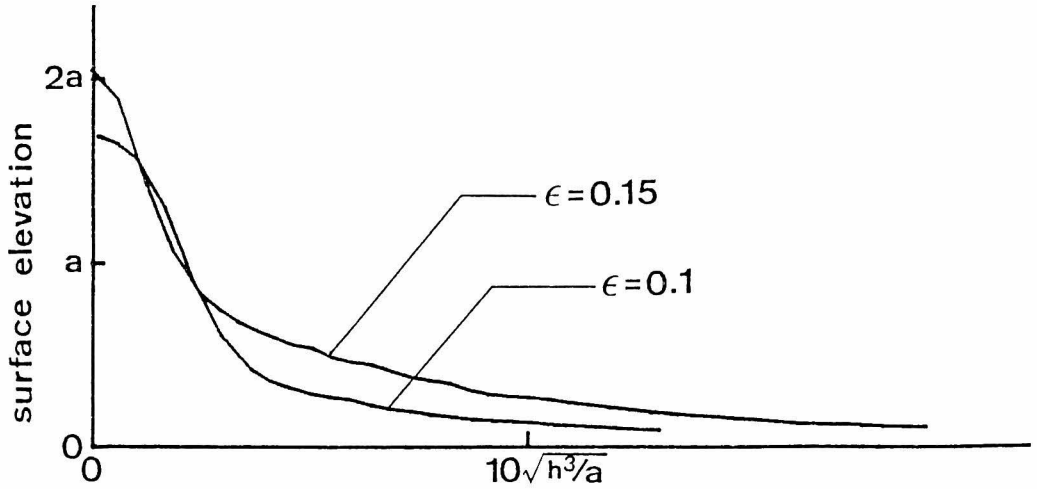

Fig.25. The profiles of the surface elevation along the crest line of a reflected wave at the time which is inferred to be the largest observation time in Melville's experiment. Horizontal co-ordinate is the same as that in Fig.20. One line is for $\varepsilon = 0.1$, $\alpha = \pi/7$ and interaction time $t_e = 7.96\, h/(ag)^{1/2}$. Another line is for $\varepsilon = 0.15$, $\alpha = \pi/5$ and $t_e = 9.17h/\sqrt{ag}$.

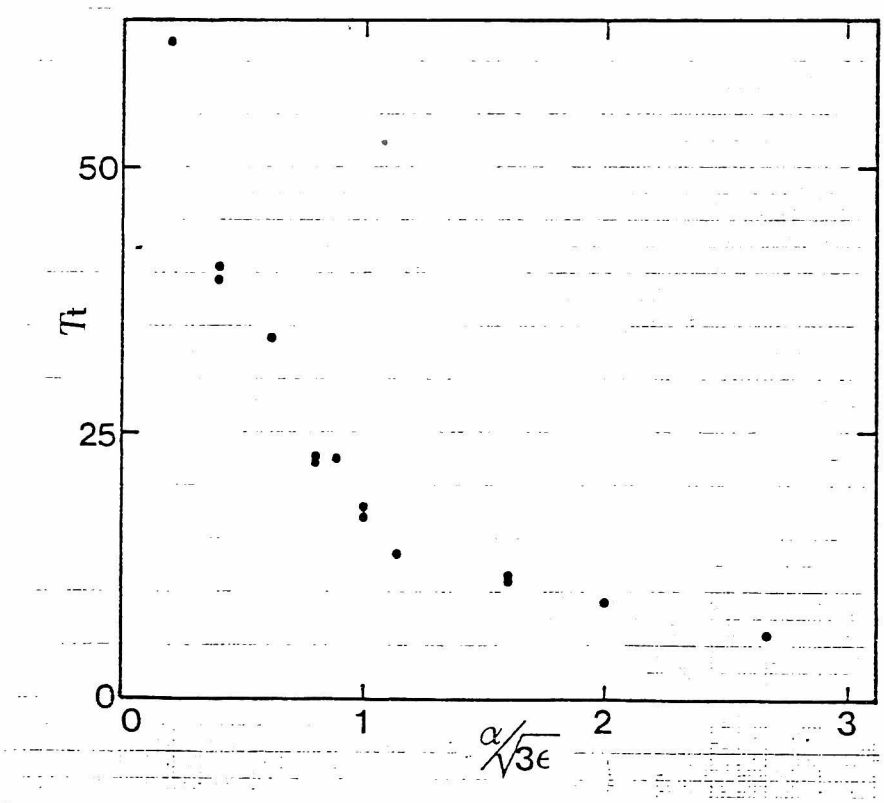

Fig.26. The time required for the attainment of the largest depth of a trough at the wall. $\varepsilon = 0.05$.

decreases slowly. The time is measured from the instance when the incident wave passes through the line $x = 0$ in Fig.11. The values of T_t are shown in Fig.26 for $\varepsilon = 0.05$. They increases rapidly as α decreases to zero. The values of d_t are shown in Fig.27 for $\varepsilon = 0.05$. They are about 0.3 independent of α if $\alpha > \sqrt{3\varepsilon}$; on the contrary, if $\alpha < \sqrt{3\varepsilon}$, they decreases to zero as α decreases to zero (corresponding to a wave moving parallel to the wall). The trough travels more slowly than the point of maximum run-up. The delay of the trough to the crest increases as α increases. The trough was observed also in the experiment made by Perroud [87] for $\alpha > 20^\circ$ although available data for quantitative comparison were not given.

3.4.5 **Mach stem**

In all the solutions representing the Mach reflection pattern, the surface elevation on the wall OA in Fig.11 have the sech^2 profile which was predicted by Miles as the profile of a Mach stem. As an example, the result for $\alpha = \pi/20$ and $\varepsilon = 0.05$ is shown in Fig.28 with the predicted values.

3.4.6 **The estimation of the effect of viscosity**

Although the accurate estimation of the viscous effect on the oblique reflection phenomena is difficult, the crude estimation may be possible if the theory for the viscous damping of a one-dimensional solitary wave is used.

Keulegan [91] examined the viscous attenuation of a one-dimensional solitary wave in a channel of constant depth and width. He derived an inverse-fourth-power decay law for a

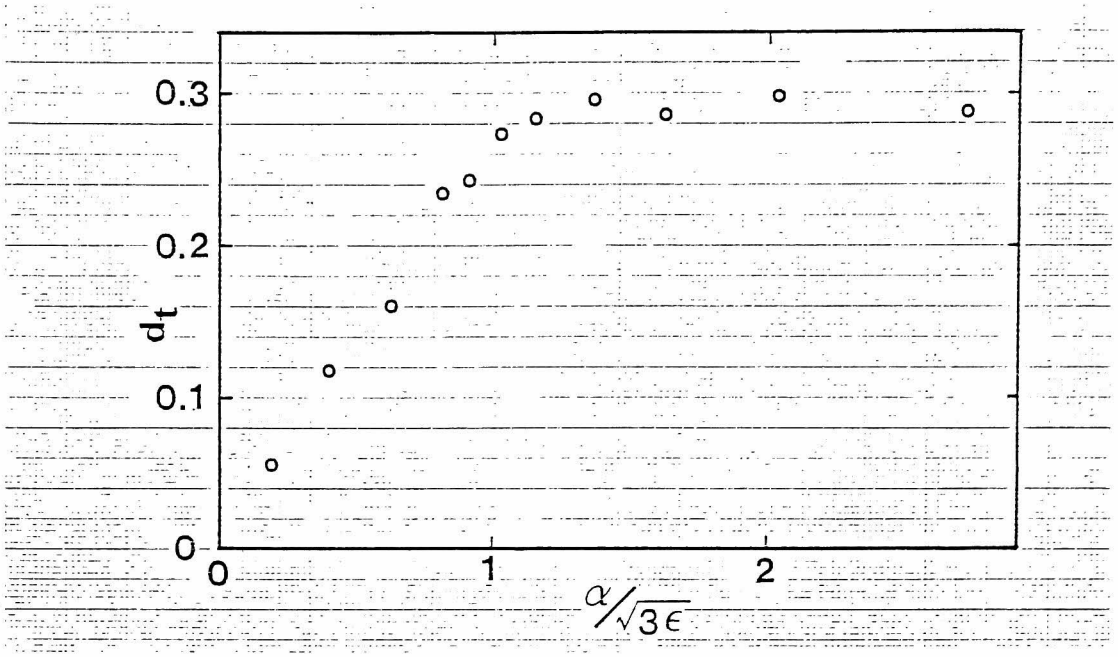

Fig.27. The largest values of the depth of a trough behind a wave for ε = 0.05.

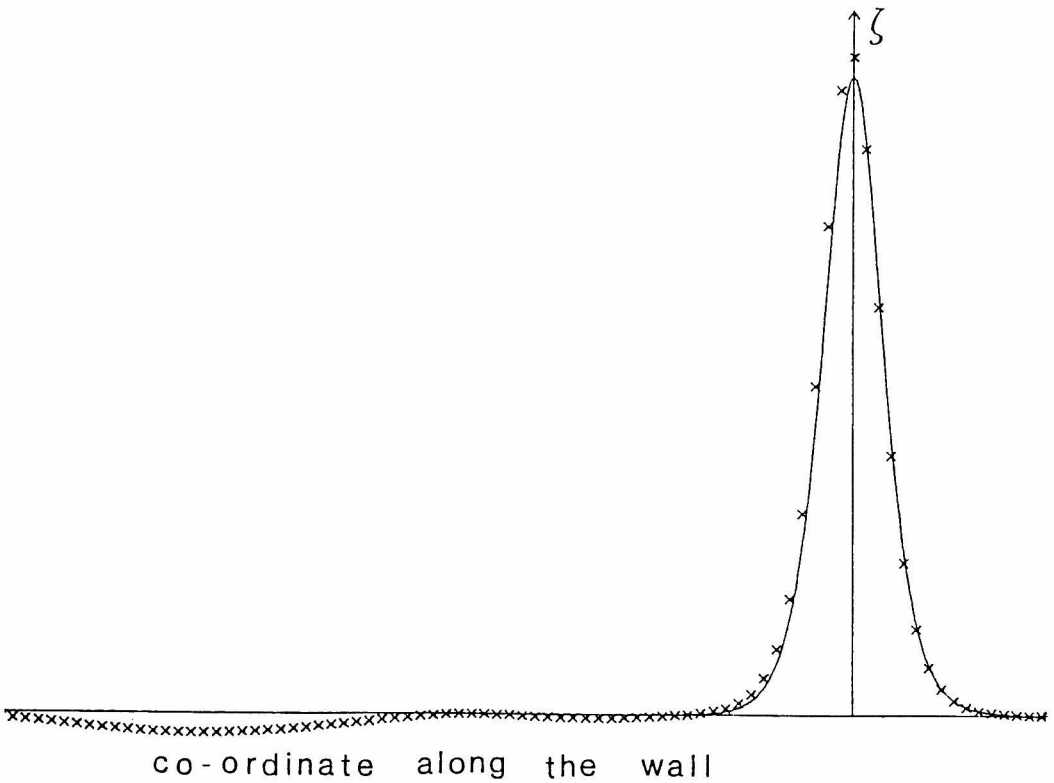

Fig.28. Free-surface displacement on the wall for ε = 0.05, δ = 0.01 and $\alpha=\pi/20$. The wave is traveling to the right. ×: Calculated results at t' = 105. ———: The profile of the Mach stem of the same parameters predicted by Miles.

shallow water solitary wave of small amplitude on the assumptions that the flow is laminar and that the thickness of boundary layers is much smaller than the water depth and that the dissipative and dispersive effect of viscosity on wave form (except for the amplitude) can be neglected. This law is written as

$$\frac{p(t)}{p(0)} = \frac{1}{(1+\gamma t)^4} , \tag{3.6}$$

where $p(t)$ is the amplitude of a solitary wave at the time t, and

$$\gamma = \frac{1}{12}(1+\frac{2h}{b})(\frac{p(0)g\nu^2}{h^6})^{1/4} , \tag{3.7}$$

where h and b are the depth and the width of a channel, and ν is the kinematic viscosity. This law was derived also by Ott and Sudan [92] and by Kakutani and Matsuuchi [93]. Miles[94] also obtained a similar law. In his equation also the effect of surface contamination is taken into consideration, so eq.(3.7) is modified as

$$\gamma = 0.0839(1+\frac{2h}{b}+\kappa)(\frac{p(0)g\nu^2}{h^6})^{1/4} , \tag{3.8}$$

where κ is a surface-contamination parameter and is chosen as 1 in the following.

We use the Miles' formula (3.6) and (3.8) for the estimation of viscous effect on the oblique reflection phenomena as a crude approximation. Melville's experiments were made with h = 20, 30cm and ε = 0.1, 0.15. The interaction time in his experiment is inferred to be about 4 seconds. If t = 4sec., h = 30 cm, $p(0)$ = 3cm, ν = 0.01cm^2/s and b = ∞, Miles' formula give

the damping of 1.2% of an initial wave amplitude. If t = 4sec., h = 20cm, $p(0)$ = 3cm and $b = \infty$, the damping of 2.2% is given. Therefore, the viscous effect seems negligible in his experiment although maximum run-up at the wall may be affected also by the viscous dissipation in the boundary layer at a side wall.

In the present calculations for ε = 0 05, the interaction time required for the attainment of the stationary state depends on α intensely as is shown in Fig 17. If $\alpha/\sqrt{3\varepsilon}$ is larger than 1.5, then $\zeta^*_{max}(t)$ is saturated approximately in the interaction time less than $20h/\sqrt{ag}$, and the representative rate of increase of $\zeta^*_{max}(t)$ is fairly large On the other hand, if $\alpha/\sqrt{3\varepsilon}$ is less than 0.81, the interaction time required for the saturation of $\zeta^*_{max}(t)$ is very large (more than $200h/\sqrt{ag}$), and the representative rate of increase of it is small.

Interaction times $20h/\sqrt{ag}$ and $200h/\sqrt{ag}$ correspond to 15sec. and 150sec. respectively if we use h = 30cm and a = 1.5cm. If h = 30cm, $p(0)$ = 1.5cm and $b = \infty$, Miles' formula with t = 15sec. and t = 150sec. give the damping of 4% and 30% of an initial wave amplitude. Therefore, if h is 30cm, the viscous effect on the oblique reflection phenomena seems approximately negligible for $\alpha/\sqrt{3\varepsilon}>1.5$. In other words measured $\zeta^*_{max}(t)$ is expected to increase rapidly to the value close to that obtained from the inviscid theory before the viscous effect reduce the wave amplitude appreciably. However, for the Mach reflection case of $\alpha/\sqrt{3\varepsilon}<0.81$, the viscous effect is significant if h is 30cm. That is, the viscous effect on $\zeta^*_{max}(t)$ becomes non-negligible before $\zeta^*_{max}(t)$ increases sufficiently, so $\zeta^*_{max}(t)$ tends to the considerably smaller value than that of inviscid theory, and then decreases.

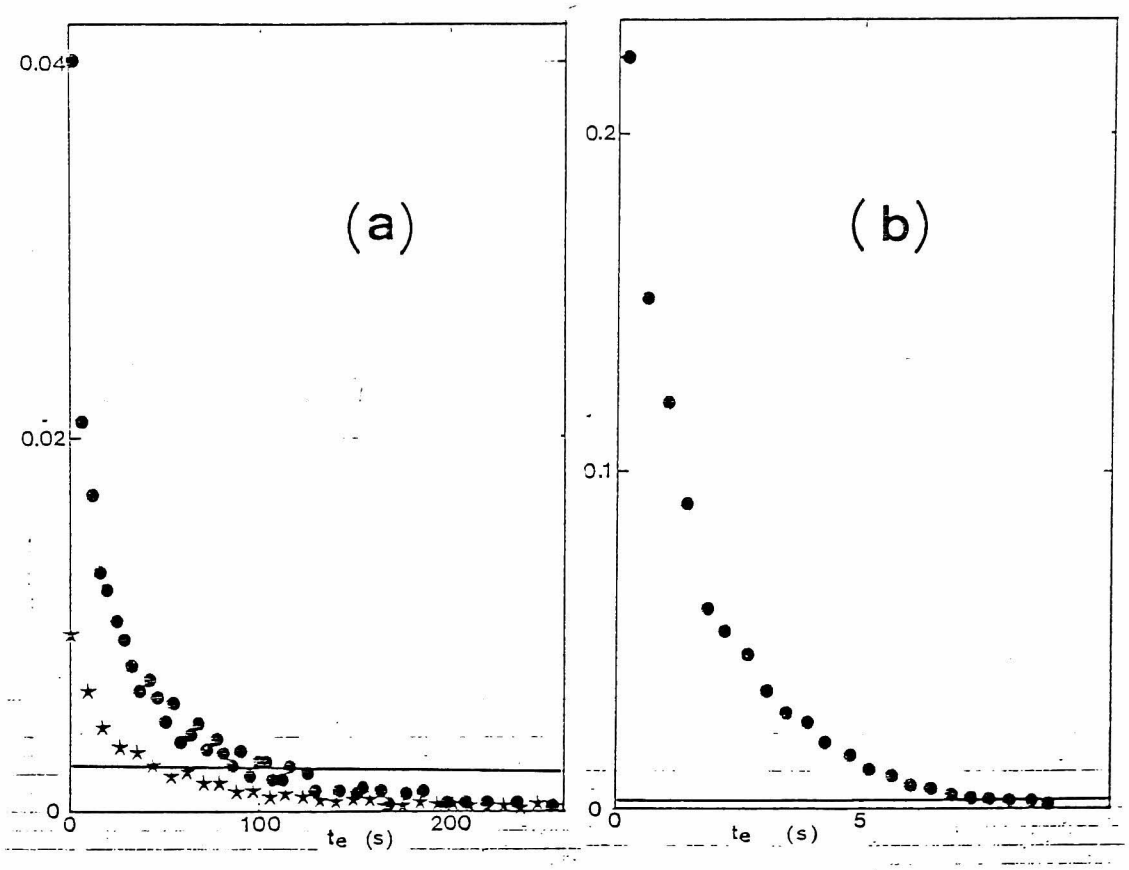

Fig.29. The rate of increase of maximum run-up at the wall in inviscid calculations and the estimated rate of decrease of it due to viscosity for h = 30cm, and ε = 0.05. Circles and stars denote $(d\zeta^*_{max}(t)/dt)/\zeta^*_{max}(t)$. They are shown as a function of interaction time t_e. Solid line denotes $-(dp(t)/dt)/p(t)$ based on eqs.(3.6) and (3.8). (a), Circles are for $\alpha=\pi/13$ and stars are for $\alpha=\pi/40$, both corresponding to Mach reflection. (b), Circles are for $\alpha=\pi/4$ corresponding to regular reflection.

Figures 29 (a) and (b) show the viscous effect a little more definitely. The circles and stars represent the rate of increase of calculated $\zeta^*_{max}(t)$ per 1 second for ε = 0.05 and h = 30cm. The solid line shows the rate of decrease of $p(t)$ per 1 second based on eqs.(3.6) and (3.8) with h = 30cm, $p(0)$ = 1.5cm and $b = \infty$ (this seems to be underestimation of viscous effect in consideration of the existence of a side wall and the larger

values of $\zeta^*_{max}(t)$ than 1 in the real problem). These rates are normalized by the values of ζ^*_{max} and p at the time when they are calculated. When $\alpha = \pi/4$ ($\alpha/\sqrt{3\varepsilon} = 2.0$), the rate of increase of $\zeta^*_{max}(t)$ is much larger than the viscous damping rate for the most time of evolution. On the contrary, if α is $\pi/13$ or $\pi/40$ ($\alpha/\sqrt{3\varepsilon} = 0.62$ or 0.20), viscous damping overcome the increase of $\zeta^*_{max}(t)$ at the considerably smaller interaction time than that required for the attainment of stationary state in inviscid calculations.

Consequently, the large values of ζ_{max} which were obtained in the inviscid calculations for $\alpha \sim \sqrt{3\varepsilon}$ seem unrealizable for small ε in the laboratory experiments with the apparatus of ordinary dimensions. The viscous effect seems relatively small for the large scale wave in the ocean. Therefore, the maximum run-up at the wall may become much larger than twice of the incident wave amplitude in the ocean.

Appendix

Calculations were made in a rectangular region in the (ξ, η)-plane $(-\xi_1 \leqq \xi \leqq \xi_2,\ -L \leqq \eta \leqq 0)$ which was transformed from the region OABCD in the (x, y)-plane shown Fig.11. This transformation is made by the following Schwartz-Christoffel transformation:

$$\frac{d\nu}{d\mu} = -\frac{\pi}{L}(\nu-1)^{1-\alpha/\pi}\nu^{\alpha/\pi}, \qquad (3.A.1)$$

where

$$\mu = x + iy, \quad i^2 = -1, \quad \nu = \exp(-\frac{\pi}{L}w) + 1, \quad w = \xi + i\eta.$$

If α can be written as

$$\alpha = \frac{n_1}{m_1}\pi \qquad (m_1, n_1 : \text{positive integers}), \tag{3.A.2}$$

then eq.(3.A.1) can be integrated to give

$$\mu = \frac{L}{\pi}\sum_{r=0}^{m_1-1}\exp\left(\frac{2\pi r i n_1}{m_1}\right)\ln\left[\chi - \exp\left(\frac{2\pi r i}{m_1}\right)\right], \tag{3.A.3}$$

where

$$\chi = \left(1 - \frac{1}{\nu}\right)^{1/m_1} \qquad \left(0 \leqq \arg\chi \leqq \frac{\pi}{m_1}\right),$$

$$-\pi < \arg\left[\chi - \exp\left(\frac{2\pi r i}{m_1}\right)\right] \leqq \pi.$$

The corner O in Fig.11 corresponds to the point $w = -Li$ in the (ξ, η)-plane under this expression.

In this (ξ, η)-plane, the evolution eqs.(3.1) and (3.2) are written as

$$\frac{\partial \zeta}{\partial t} + p_1\left[\Delta_w f + \varepsilon\nabla_w(\zeta\nabla_w f) - \frac{1}{6}\delta\left(p_2\Delta_w f + p_1\Delta_w^2 f + p_3\Delta_w\frac{\partial f}{\partial \xi}\right.\right.$$

$$\left.\left. + p_4\Delta_w\frac{\partial f}{\partial \eta}\right)\right] = 0, \tag{3.A.4a}$$

$$\frac{\partial}{\partial t}\left(f - \frac{1}{2}\delta p_1\Delta_w f\right) + \zeta + \frac{1}{2}\varepsilon p_1(\nabla_w f)^2 = 0, \tag{3.A.4b}$$

where

$$\nabla_w = \left(\frac{\partial}{\partial \xi}, \frac{\partial}{\partial \eta}\right), \qquad \Delta_w = \frac{\partial^2}{\partial \xi^2} + \frac{\partial^2}{\partial \eta^2},$$

$$p_1 = |F_1|^2, \quad p_2 = 4|E_1|^2, \quad p_3 = 4\mathrm{Re}(F_1E_1^*), \quad p_4 = 4\mathrm{Im}(F_1E_1^*),$$

$$F_1 = \left(\frac{\nu}{\nu-1}\right)^{n_1/m_1}, \quad E_1 = \frac{n_1\pi}{m_1L}\nu^{n_1/m_1-1}(\nu-1)^{-n_1/m_1}.$$

Here the primes in nondimensionalized variables were omitted. Since the coefficients p_2, p_3, p_4 diverge as μ tends to zero, we removed the boundary AOD in Fig.11 inward by a small amount L_r (thus the actual calculation region is $-L+L_r \leqq \eta \leqq 0$).

The finite-difference scheme which we used as an approximation of eqs (3.A.4) is

$$\frac{1}{2\Delta t}(\zeta^{n+1} - \zeta^{n-1}) + p_1\{(1 - \frac{1}{6}\hat{\delta}p_2)(U_\xi f + U_\eta f)$$
$$+ \varepsilon A_{\xi/2}(\zeta A_{\xi/2} f) + \varepsilon A_\eta(\zeta A_\eta f) - \frac{1}{6}\hat{\delta}[p_1(B_\xi^2 f + B_\eta^2 f + 2B_\xi B_\eta f)$$
$$+ p_3(B_\xi A_\xi f + B_\eta A_\xi f) + p_4(A_\eta B_\xi f + A_\eta B_\eta f)]\} = 0, \qquad (3.A.5a)$$

$$\frac{1}{2\Delta t}[f^{n+1} - f^{n-1} - \frac{1}{2}\hat{\delta}p_1(B_\xi f^{n+1} + B_\eta f^{n+1} - B_\xi f^{n-1} - B_\eta f^{n-1})]$$
$$+ \zeta + \frac{1}{2}\varepsilon p_1[(A_\xi f)^2 + (A_\eta f)^2] = 0, \qquad (3.A.5b)$$

where Δt is the time increment for one time step, and $f^{n\pm1}$ and $\zeta^{n\pm1}$ are the values of f and ζ at $t = (n\pm1)\Delta t$ (f^n and ζ^n are abbreviated to f and ζ) The symbols A_ξ, B_ξ etc. denote spatial difference operators defined in the following. We define $f_{k,j}$ as the value of f at the point (ξ_k, η_j), where (ξ_k, η_j) is the (ξ, η) co-ordinate of the intersection of the k-th mesh line of constant ξ and the j-th mesh line of constant η. We introduce the operators T_ξ and T_η which are defined as

$$T_\xi^m f_{k,j} = f_{k+m,j}, \quad T_\eta^m f_{k,j} = f_{k,j+m}.$$

In the ξ direction, we used the following spatial differences :

$$A_\xi = \frac{1}{2\Delta\xi}(T_\xi - T_\xi^{-1}), \quad A_{\xi/2} = \frac{1}{\Delta\xi}(T_\xi^{1/2} - T_\xi^{-1/2}),$$

$$B_\xi = \frac{1}{\Delta\xi^2}(T_\xi - 2 + T_\xi^{-1}),$$

$$U_\xi = \frac{1}{\Delta\xi^2}(-\frac{1}{12}T_\xi^2 + \frac{4}{3}T_\xi - \frac{5}{2} + \frac{4}{3}T_\xi^{-1} - \frac{1}{12}T_\xi^{-2}),$$

where $\Delta\xi$ is a mesh size in the ξ direction. Moreover, we used the following formula :

$$\zeta_{k+1/2,j} = \frac{1}{2}(\zeta_{k,j} + \zeta_{k+1,j}) \quad etc.$$

In the η direction, we used the non-uniform mesh size of exponential stretch in order to save computational works. The spacing of each mesh line of constant η is written as

$$\Delta\eta_j = \eta_{j+1} - \eta_j = \eta_0\gamma^{j-3},$$

where η_0 is a positive constant and γ is a constant which is slightly larger than 1 We used the formula of A_η, B_η etc which are in principle equivalent to A_ξ, B_ξ etc. and can be reduced to those corresponding to A_ξ, B_ξ etc. if $\gamma = 1$. For example,

$$A_\eta = \frac{1}{\Delta\eta_j}[\frac{1}{1+\gamma}T_\eta + (\gamma - 1) - \frac{\gamma^2}{1+\gamma}T_\eta^{-1}],$$

$$B_\eta = \frac{1}{\Delta\eta_j^2}[\frac{2\gamma}{1+\gamma}T_\eta - 2\gamma + \frac{2\gamma^2}{1+\gamma}T_\eta^{-1}].$$

We added a virtual mesh outside the true boundary. The values at virtual mesh points were chosen so as to satisfy the boundary conditions (3.3) at the true boundary. We used the conditions

$A_\xi f = 0, \quad A_\xi \zeta = 0$ at the boundary of constant ξ,

and

$A_\eta f = 0, \quad A_\eta \zeta = 0$ at the boundary of constant η,

corresponding to the boundary conditions (3.3a) and (3.3c). At the boundary BC in Fig.11 (corresponding to $\eta=0$), the condition (3.3b) corresponds to

$$\frac{\partial^3 f}{\partial \eta^3} = 0,$$

so we used the condition

$A_\eta B_\eta f = 0$ at the boundary BC.

On the other hand, the condition (3.3b) for the boundary AOD in Fig 11 (corresponding to $\eta=-L+L_r$) is written as

$$\frac{\partial^3 f}{\partial \eta^3} = R_1 \frac{\partial^2 f}{\partial \eta^2} + R_2 \frac{\partial f}{\partial \xi},$$

where

$$R_1 = \frac{3 n_1 \pi}{m_1 L} \mathrm{Im}\left(\frac{1}{\nu}\right),$$

$$R_2 = -\frac{n_1 \pi^2}{m_1 L^2} \mathrm{Im}\left(\frac{\nu + n_1/m_1 - 1}{\nu^2}\right) - 2\left(\frac{n_1 \pi}{m_1 L}\right)^2 \mathrm{Re}\left(\frac{1}{\nu}\right) \mathrm{Im}\left(\frac{1}{\nu}\right).$$

Therefore, we used the condition

$$A_\eta B_\eta f = R_1 B_\eta f + R_2 A_\xi f,$$

at the boundary of $\eta=-L+L_r$. Similar condition was imposed on the boundary of constant ξ.

The values of ζ^{n+1} can be calculated explicitly from the values of ζ^{n}, ζ^{n-1} and f^{n} by the use of eq.(3.A.5a). However, the values of f^{n+1} can not be calculated explicitly in eq.(3.A.5b), so we used the iterative method which is called 'successive line overrelaxation method' (see Varga [90] for particulars).

Chapter 4

The Resonant Interaction between a Long Internal Gravity Wave and a Surface Gravity Wave Packet I. Shallow-Fluid Case.

§ 4.1. Introduction

It is well known that a strong interaction between long and short waves occurs when the phase speed of the long wave and the group velocity of the short wave are matched, and can be interpreted as a limiting case of the three-wave resonant interaction [95], [96] This interaction between a long gravity wave and a capillary-gravity wave was investigated by Djordjevic and Redekopp [69] for water of finite depth. The same kind of interaction between long and short internal waves was investigated by Grimshaw [70]. Both of them derived the coupled equations of the form

$$i\frac{\partial A}{\partial \tau} + \gamma\frac{\partial^2 A}{\partial \xi^2} = \alpha AB, \tag{4.1a}$$

$$\frac{\partial B}{\partial \tau} = \beta\frac{\partial}{\partial \xi}(|A|^2), \tag{4.1b}$$

where A is proportional to the complex amplitude of a short wave, and B denotes an appropriate quantity associated with a long wave, and α, β and γ are constants. The variables ξ and τ are the appropriately stretched spatial and time coordinates in the frame moving at the group velocity of a short wave.

The model equations for the interaction of a Langmuir wave with an ion-sound wave in a plasma

$$i\frac{\partial E}{\partial t} + \frac{1}{2}\frac{\partial^2 E}{\partial x^2} = nE, \tag{4.2a}$$

$$\frac{\partial n}{\partial t} + \frac{\partial n}{\partial x} = -\frac{\partial}{\partial x}(|E|^2), \tag{4.2b}$$

which are reduced to eqs.(4.1) through the transformation $\phi = Ee^{i(t/2-x)}$, $\xi = x-t$ and $\tau = t$, were solved exactly by Yajima and Oikawa [97] by using the inverse scattering method and shown to have the N-soliton solutions. The equations (4.1) were also solved by Ma [98] in the similar way. Ma and Redekopp [99] gave some another solutions of eqs.(4.1).

In this chapter, we examine the interaction between a long internal wave and a short surface wave in a two layer fluid under the assumption that the fluid depth is sufficiently small in comparison with the wavelength of the internal wave. Then it is found that the equations describing the interaction become the same form as eqs.(4.1). The derivation of these interaction equations is given in § 4.2.

Koop and Redekopp [100] made the experiments on the resonant interaction between long and short internal waves in a rigid-lid three layer fluid. They mainly investigated the interaction of wavetrains. Here, we examine numerically the resonant interaction of long and short waves with localized distributions. It is shown in § 4.3 that asymptotic states for a class of initial short wave packets consist of coupled-soliton solution and a steady solution composed of a long wave alone and a dispersing wave composed of short wave alone. The interaction between a soliton and a steady long wave is also examined.

A supplementary comment is made in § 4.4.

§ 4.2. Formulation and Reduced Interaction Equations

We consider the wave propagation in a two-layer fluid which consists of the upper layer with the density $\rho_1 \equiv \rho_2(1-\Delta)$ and the thickness h_1 and the lower layer with the density ρ_2 ($> \rho_1$) and the thickness h_2 (see Fig.2). The fluids are assumed to be inviscid and incompressible, and their motions to be two-dimensional and irrotational. If the disturbed free surface is specified by $z=h_1+\zeta_1(x,t)$, the disturbed interface by $z=\zeta_2(x,t)$ and the velocity potentials in the upper and lower layers by $\phi_1(x,z,t)$ and $\phi_2(x,z,t)$, and there is the flat rigid boundary at $z=-h_2$, the basic equations and the boundary conditions are given by eqs.(1.15).

Linear approximation of eqs.(1.15) yields the solution (1.16) and dispersion relation (1 17). The relation (1 17) gives the surface mode and the internal mode. We consider the interaction of a surface mode and an internal mode in the shallow fluid. We assume that $\varepsilon \equiv a/\lambda \ll 1$, $\lambda/h_1 \sim 1$, $h_2/h_1 \sim 1$ and $\lambda/l \ll 1$. Here a and λ are a characteristic amplitude and a characteristic length scale of the surface wave, respectively, and l is a characteristic length scale of the internal wave. We expand the solution in the following form :

$$\phi_j = \sum_{n=0}^{\infty} \varepsilon^{(2+n)/3} \phi_j^{(n)}, \qquad (j=1,2) \tag{4.3a}$$

$$\zeta_j = \sum_{n=0}^{\infty} \varepsilon^{(2+n)/3} \zeta_j^{(n)} . \qquad (j=1,2) \tag{4.3b}$$

The variables $\zeta_j^{(n)}$ (and $\phi_j^{(n)}$) are regarded as functions of the

stretched coordinates

$$\xi = \varepsilon^{2/3}(x - c_g t), \quad \tau = \varepsilon^{4/3} t, \tag{4.4}$$

as well as x, t (and z). Substituting eq.(4.3a) into eqs.(1.15) and equating the coefficients of like powers of ε, we obtain a linear boundary value problem for $\phi_j^{(n)}$ from the terms of $O(\varepsilon^{(n+2)/3})$. Both for $\phi_j^{(0)}$ and for $\phi_j^{(1)}$, the equations and the boundary conditions are given by the linearized forms of eqs.(1.15). We assume that $\phi_j^{(0)}$ ($j=1,2$) consist of a long wave alone and $\phi_j^{(1)}$ ($j=1,2$) a short wave alone. Therefore, we take

$$\phi_j^{(0)} = \Phi_j(\xi,\tau), \quad \zeta_j^{(0)} = 0, \quad (j=1,2) \tag{4.5}$$

and

$$\begin{cases} \phi_1^{(1)} = \dfrac{i\omega}{k} A(\xi,\tau) e^{i\theta} \{\sinh k(h_1-z) - \dfrac{gk}{\omega^2}\cosh k(h_1-z)\} + \text{c.c.}, \\ \zeta_1^{(1)} = A(\xi,\tau) e^{i\theta} + \text{c.c.}, \\ \phi_2^{(1)} = -\dfrac{i\omega}{k\sinh kh_2}(\cosh kh_1 - \dfrac{gk}{\omega^2}\sinh kh_1) A(\xi,\tau) e^{i\theta}\cosh k(z+h_2) + \text{c.c.}, \\ \zeta_2^{(1)} = (\cosh kh_1 - \dfrac{gk}{\omega^2}\sinh kh_1) A(\xi,\tau) e^{i\theta} + \text{c.c.}, \end{cases} \tag{4.6}$$

from eqs.(1.16), where $\theta = kx - \omega t$, and k and ω satisfy the dispersion relation of the surface mode (relation (1.17) with plus sign), and c.c. denotes the complex conjugate of the preceding term. It is noted that the long wave given by eqs.(4.5) gives rise to a horizontal velocity of $O(\varepsilon^{4/3})$. In $O(\varepsilon^{4/3})$, we obtain

$$\begin{cases} \phi_1^{(2)} = \Phi_1^{(2)}(\xi,\tau), \qquad \phi_2^{(2)} = \Phi_2^{(2)}(\xi,\tau), \\ \zeta_1^{(2)} = \dfrac{c_g}{g}\dfrac{\partial\Phi_1}{\partial\xi}, \qquad \zeta_2^{(2)} = \dfrac{c_g}{\Delta g}\left[\dfrac{\partial\Phi_2}{\partial\xi} - (1-\Delta)\dfrac{\partial\Phi_1}{\partial\xi}\right]. \end{cases} \tag{4.7}$$

The condition for no-secularity in $O(\varepsilon^{5/3})$ yields

$$c_g = \frac{d\omega}{dk}. \tag{4.8}$$

In $O(\varepsilon^2)$, we find that Φ_1 and Φ_2 must satisfy

$$\begin{cases} (gh_1 - c_g^2)\dfrac{\partial^2\Phi_1}{\partial\xi^2} + gh_2\dfrac{\partial^2\Phi_2}{\partial\xi^2} = 0, \\ (\Delta gh_1 - c_g^2)\dfrac{\partial^2\Phi_1}{\partial\xi^2} + c_g^2\dfrac{\partial^2\Phi_2}{\partial\xi^2} = 0. \end{cases} \tag{4.9}$$

The compatibility condition for these equations becomes

$$c_g^2 = c_p^2, \tag{4 10}$$

where c_p is the phase speed of the internal wave in the long wave limit and is given by

$$c_p = \{ [h_1 + h_2 - \sqrt{(h_1+h_2)^2-4\Delta h_1 h_2}\,] g / 2 \}^{1/2}. \tag{4.11}$$

We assume k to satisfy the resonance condition $c_g = c_p$. The condition for no-secularity in $O(\varepsilon^{7/3})$ leads to

$$i\frac{\partial A}{\partial\tau} + \frac{1}{2}\omega''\frac{\partial^2 A}{\partial\xi^2} = -\alpha AB, \tag{4 12a}$$

where $B=\zeta_2^{(2)}$, and $\omega'' = d^2\omega/dk^2$. The constant α is given by

eq.(4.A.1) in Appendix A. In deriving eq (4.12a), we have used the relations

$$\zeta_1^{(2)} = -\frac{c_g^2}{gh_1-c_g^2}\zeta_2^{(2)}, \quad \frac{\partial\Phi_1}{\partial\xi} = -\frac{gc_g}{gh_1-c_g^2}\zeta_2^{(2)}, \quad \frac{\partial\Phi_2}{\partial\xi} = \frac{c_g}{h_2}\zeta_2^{(2)}.$$

The compatibility condition in $O(\varepsilon^{8/3})$ yields

$$\frac{\partial B}{\partial\tau} = \beta\frac{\partial}{\partial\xi}(|A|^2), \tag{4.12b}$$

where β is given by eq.(4.A.2) in Appendix A. The equations (4.12) give the desired coupled set of equations Numerical computation shows that α and β are positive. The constant ω'' is negative as shown easily. Since $gh_1-c_g^2>0$, the signs of $\zeta_1^{(2)}$ and $\zeta_2^{(2)}$ are opposite each other.

The equations (4.12) are equivalent to eqs.(4.1) which are exactly solvable by using the inverse scattering method [97], [98] and have the N-soliton solution [97], [99]. The soliton solution of eqs.(4.12) propagates to the positive ξ direction and is accompanied by the depression of the interface as seen from eqs.(4.15). The solution of eqs (4.12) has the similarity in the sense that if $A=f(\xi,\tau)$ and $B=g(\xi,\tau)$ satisfy these equations, $A=r^{3/2}f(r\xi,r^2\tau)$ and $B=r^2g(r\xi,r^2\tau)$ also satisfy them. Here r is an arbitrary positive constant. The latter can be obtained by replacing scaling parameter ε with $\varepsilon'=r^{-3/2}\varepsilon$. Therefore this similarity is trivial.

The equations (4.12) can be reduced to the forms

$$i\frac{\partial S}{\partial T} - \frac{\partial^2 S}{\partial X^2} = -LS, \tag{4.13a}$$

$$\frac{\partial L}{\partial T} = \frac{\partial}{\partial X}(|S|^2), \tag{4.13b}$$

by an appropriate scale transformation. These equations have an infinite set of conservation laws [97], [98]. The first four conserved quantities are written as

$$\begin{cases} I_1 = \int_{-\infty}^{\infty} L dX, \qquad I_2 = \int_{-\infty}^{\infty} |S|^2 dX, \\ I_3 = \int_{-\infty}^{\infty} \{L^2 - i\,(S^*\frac{\partial S}{\partial X} - S\frac{\partial S^*}{\partial X})\}\, dX, \\ I_4 = \int_{-\infty}^{\infty} (|\frac{\partial S}{\partial X}|^2 + L|S|^2) dX. \end{cases} \tag{4.14}$$

The soliton solution of eqs.(4.13) are written as

$$S = \sqrt{2p}q\,\mathrm{sech}q(X - pT - X_0)\exp\{i\{-\frac{p}{2}X + (-q^2 + \frac{1}{4}p^2)T + \theta_0\}\}, \tag{4.15a}$$

$$L = -2q^2\,\mathrm{sech}^2 q(X - pT - X_0), \tag{4.15b}$$

where p and q are arbitrary positive constants, and X_0 and θ_0 are arbitrary real constants. The 2-soliton solution of eqs.(4.13) reduces to the breather solution [99] when two constituent solitons have the same velocity. The breather solution is written as

$$\begin{cases} S = \frac{G}{F}, \\ L = -2\frac{\partial^2}{\partial X^2}(\ln F). \end{cases} \tag{4.16}$$

where

$$F = 1+a_1\exp(2q_1\varphi)+a_2\exp(2q_2\varphi-2d_0)+\mathrm{Re}\{a_3\exp[(q_1+q_2)\varphi-d_0+i(q_1^2-q_2^2)(T-T_0)]\}+a_4\exp[2(q_1+q_2)\varphi-2d_0],$$

$$G = \sqrt{2}\exp\{i[-\frac{1}{2}p\varphi-(q_1^2+\frac{1}{4}p^2)(T-T_0)+\theta_0]\}\{\exp(q_1\varphi)+\exp[q_2\varphi-d_0+i(q_1^2-q_2^2)(T-T_0)]+b_1\exp[(2q_1+q_2)\varphi-d_0+i(q_1^2-q_2^2)(T-T_0)]+b_2\exp[(q_1+2q_2)\varphi-2d_0]\},$$

$$\varphi = X-pT-X_0.$$

Here $a_1\sim a_4$, b_1 and b_2 are constants depending on p, q_1 and q_2, and are given in Appendix B. The positive constant p specifies the velocity of the "center of mass" of the breather solution as is expected from the following relations for eqs.(4.16)

$$I_L\equiv-\int_{-\infty}^{\infty}L\,dX=4(q_1+q_2), \tag{4.17a}$$

$$\frac{\partial}{\partial T}\int_{-\infty}^{\infty}XL\,dX=-4p(q_1+q_2). \tag{4.17b}$$

Furthermore, q_1 and q_2 are arbitrary positive constants and play the similar role as q in eqs.(4.15). Among the other real arbitrary constants d_0, X_0, T_0 and θ_0, d_0 gives a measure of the distance of two constituent solitons. As is shown easily, $|S|$

and L for the breather solution are periodic in time with the period

$$T_P = \frac{2\pi}{|q_1^2 - q_2^2|}. \tag{4 18}$$

The uniform amplitude periodic solutions to eqs.(4.13) are unstable for modulational perturbations with small wavenumbers [69], [99].

§ 4.3. Numerical Study of the Reduced Interaction Equations

Although eqs (4.13) are formally solvable by the inverse scattering method, it seems difficult to obtain the solution explicitly on this method for general initial-value problems. Therefore, we solve the equations by a finite-difference method and examine the properties of the solutions starting from localized initial distributions.

We adopt the following centered time and centered space explicit scheme for the numerical integration of eqs.(4.13) :

$$\frac{1}{2\Delta T}(U_j^{n+1} - U_j^{n-1}) = \frac{1}{\Delta X^2}(V_{j+1}^n - 2V_j^n + V_{j-1}^n) - L_j^n V_j^n, \tag{4.19a}$$

$$\frac{1}{2\Delta T}(V_j^{n+1} - V_j^{n-1}) = -\frac{1}{\Delta X^2}(U^n{}_{j+1} - 2U_j^n + U_{j-1}^n) + L_j^n U_j^n, \tag{4 19b}$$

$$\frac{1}{2\Delta T}(L_j^{n+1} - L_j^{n-1}) = \frac{1}{2\Delta X}[(U_{j+1}^n)^2 + (V_{j+1}^n)^2 - (U_{j-1}^n)^2 - (V_{j-1}^n)^2], \tag{4.19c}$$

where $S = U + iV$, and U_j^n is the value of U at $T = n\Delta T$, $X = j\Delta X$ etc. The

periodic boundary condition with sufficiently large period d is used. The spatial mesh size ΔX was chosen so as to keep the variations of $I_1 \sim I_4$ in eqs.(4.14) sufficiently small. The time increment ΔT was determined from the criterion $\Delta T < \Delta X^2/4$ based on the linear stability analysis.

4.3.1 **The dependence of the solution on the initial wavenumber**

At first, the property of the solution starting from

$$S = \mathrm{sech}(X-X_0)e^{icx}, \tag{4.20a}$$

$$L = 0, \tag{4.20b}$$

is examined. Here c and X_0 are real constants. This initial condition is adopted as the representative of the short wave packet of the wavenumber deviating from the resonant one by small amount $\varepsilon^{2/3}c$.

Figure 30 shows the evolution of the solution for exactly resonant case c=0. The positive and negative parts of L are generated at the first stage owing to the effect of the short wave packet. The positive part of L remains there without propagation and the value of $|S|$ at the corresponding location tends to zero, while the negative part of L is coupled with a part of the short wave packet to propagate to the positive X direction. These behaviours of the short wave packet can be explained from the fact that eq.(4.13a) is the Schrödinger equation with the potential L. After sufficient evolution time, the solution separates into three parts : (i) the negative part of L coupled with a hump of $|S|$ propagating to the positive X direction, (ii) the solution composed of a steady positive part

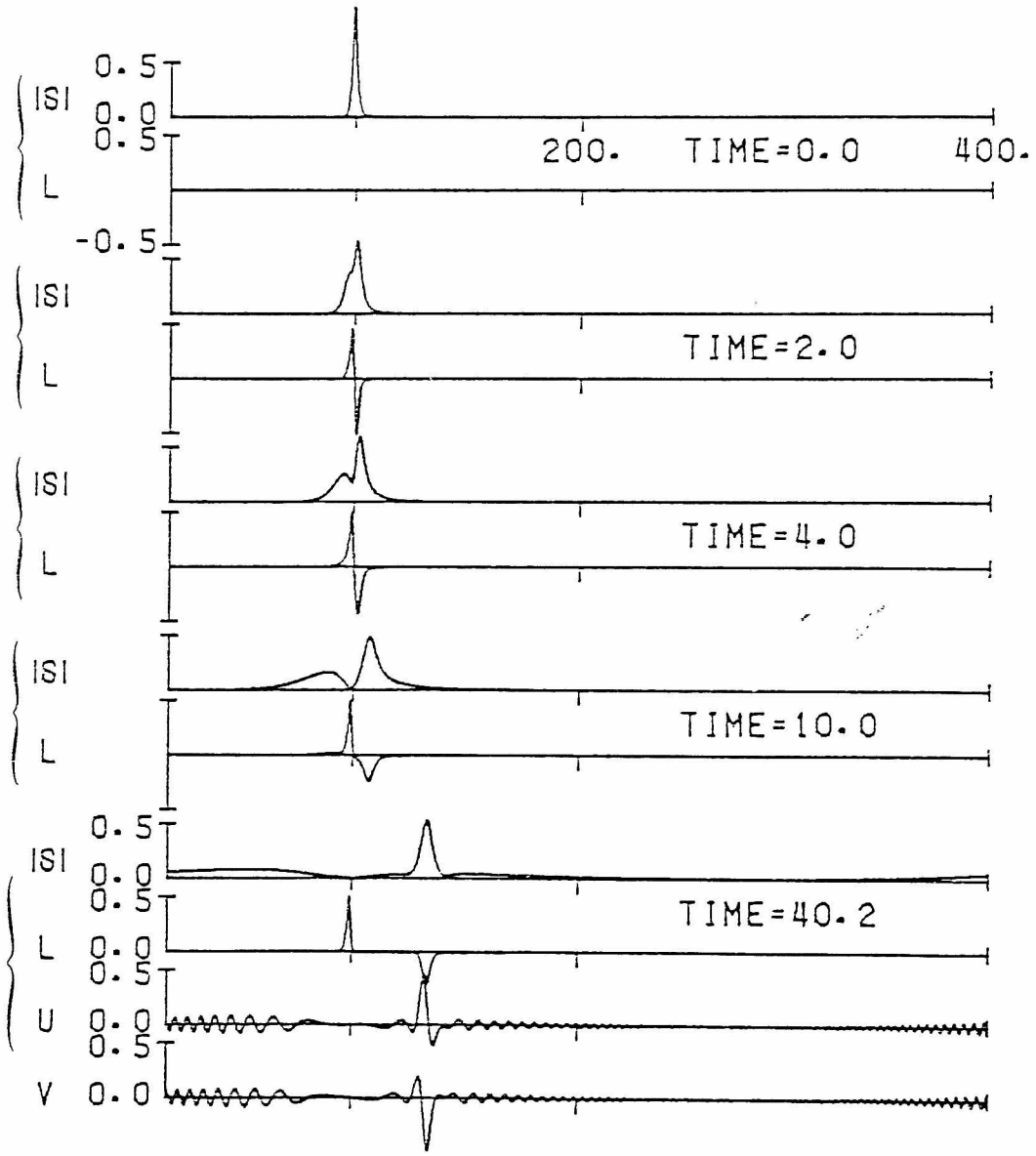

Fig.30. Time development of the solution for the initial data (4.20) with c = 0. S = U + iV. ΔX = 0.2. Since the periodic boundary condition with the period d = 400 is used, the short wave dispersing to the left appears from the right end.

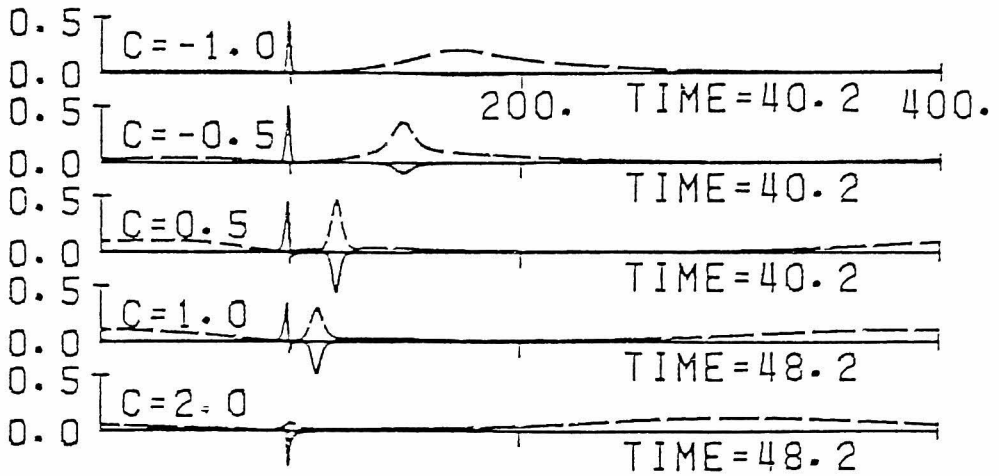

Fig.31. The solution for the initial data (4.20) with several values of c. ——:|S| . ———:L. X_0 = 90. d = 400. ΔX = 0.2. For $c \geqq -0.5$ the short wave dispersing to the left appears from the right end.

of L alone, (iii) the solution composed of only the short wave packet which disperses to both directions.

The solutions for $c \neq 0$ are shown in Fig.31 They also separate into these three parts as long as $|c|$ is not so large. The solution for $c \leqq -1$ seems not to contain the coupled part(i) because the amplitude of short wave packet decreases monotonically. For large positive c, the evolution of the negative part of L is so slow that the definite coupled part(i) is not obtained in the ordinary evolution time. Fairly large part of the initial short wave packet evolves to part(i) for small $|c|$, while most of it evolves to part(iii) for large $|c|$. The peak of $|S|$ of the part(iii) for large $|c|$ moves at the speed $-2c$ as is expected from eq.(4.13a) with L=0. The larger steady positive part of L is generated by the short wave packet of the wavenumber more close to the resonant one.

For $-0.75 \leqq c \leqq 1.5$ the coupled part(i) of the solution

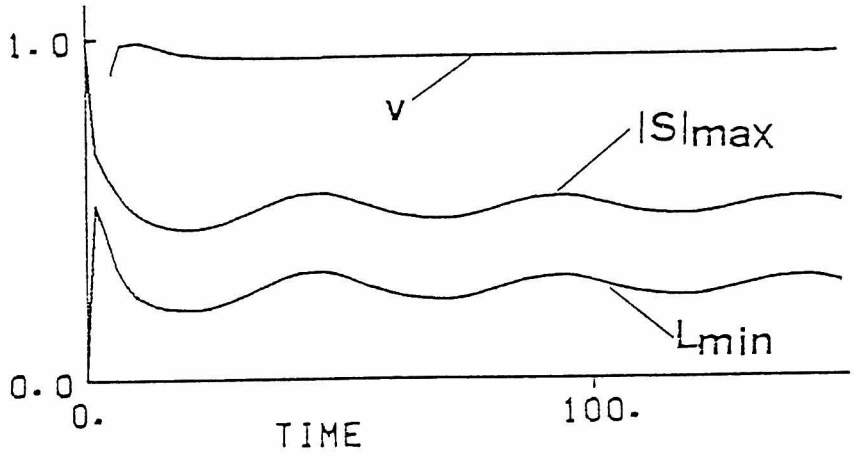

Fig.32. Time development of $|S|_{max}$, L_{min} and v for the initial data (4.20) with c = 0. The amplitude of the oscillation of v is very small.

looks like a 1-soliton solution (4.15). However, $|S|_{max} \equiv \max|S(X,T)|$, $L_{min} \equiv -\min L(X,T)$, and the velocity of the negative part of L, v, calculated from the data of the part(i) oscillate slowly in time with decreasing amplitudes as illustrated in Fig.32. This kind of oscillation has been found for the nonlinear Schrödinger equation [18]. The relation $|S|_{max}^2 = vL_{min}$, which must be satisfied by the 1-soliton solution (4 15), is approximately satisfied at any time. This oscillation can be considered as the result of the interaction between a 1-soliton and a dispersing short wave (part(iii)). Therefore, one soliton is expected to emerge asymptotically. The values of parameters p and q of the soliton will be calculated from $|S|_{max}$ and L_{min} averaged over a period of oscillation, the averaged values being practically constant. The dependence of p and q on

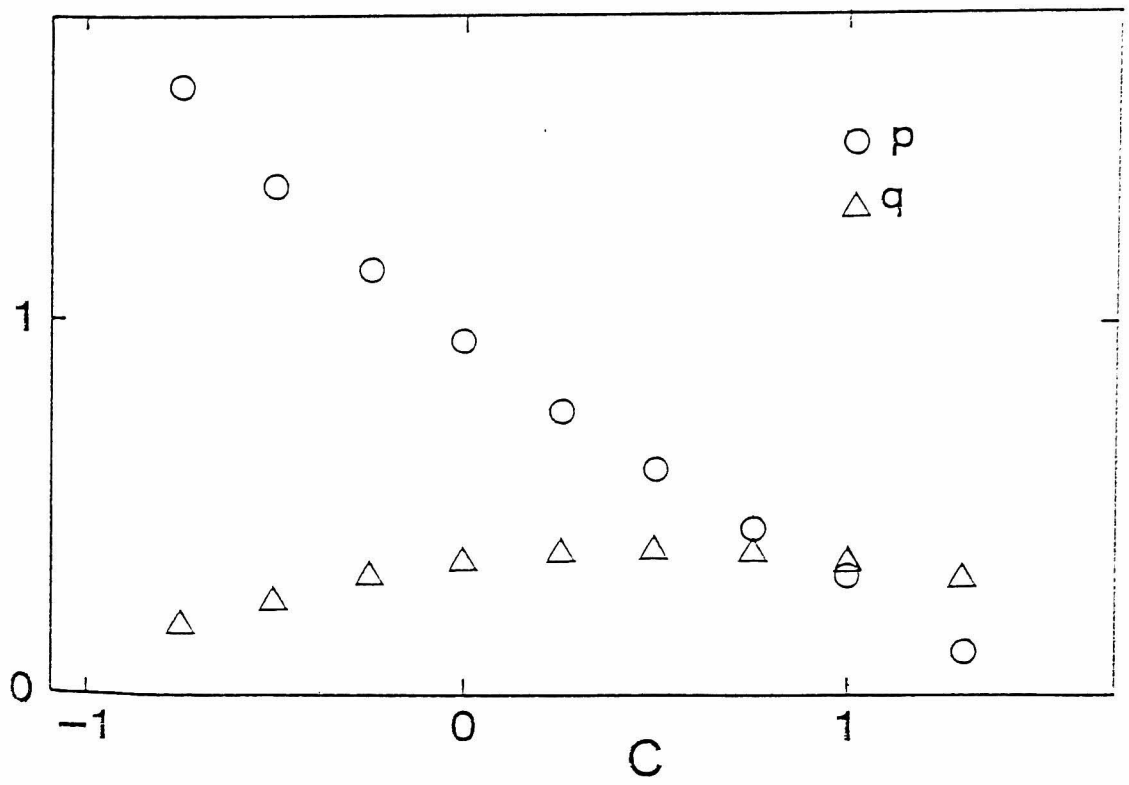

Fig.33. Dependence of the parameters p and q of the asymptotic 1-soliton solution (4.15) on c.

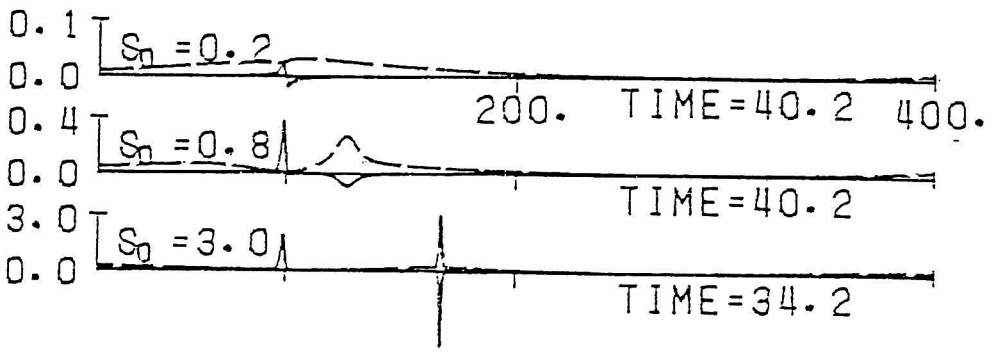

Fig.34. The solution for the initial data (4.21) with several values of S_0. ——— : $|S|$. ——— : L. $X_0 = 90$. d = 400. For $S_0 \leqq 3$ only the state of one negative peak of L is observed.

c are shown in Fig.33. The slower soliton emerges from the initial value of larger c. The dependence of q on c is relatively weak.

4.3.2. **The dependence on the initial amplitude of a short wave packet**

In this subsection we examine the dependence of the asymptotic properties of the solution on the amplitude of the initial wave packet of the resonant wavenumber. Therefore, the solution starting from the initial condition,

$$\begin{cases} S = S_0 \mathrm{sech}(X - X_0), \\ L = 0, \end{cases} \tag{4.21}$$

is studied. Here S_0 is a positive constant. As is shown in Figs.34 and 35, the solution again eventually separates into three parts(i)(ii)(iii) introduced in the preceding subsection. The larger steady positive part of L is generated for larger S_0. The time developments of the solutions shown in Fig.34 suggest that one soliton emerges for $0.5 \leqq S_0 \leqq 3$ and that no soliton for $S_0 = 0.2$. On the other hand, it is suggested that the breather solution (4.16) is generated for $3.5 \leqq S_0 \leqq 4$ because the state of one negative peak of L and that of two negative peaks of L are observed alternately. This breather-like evolution is illustrated in Fig.35.

For $S_0 \geqq 0.5$ $|S|_{\max}$ and $L_{\min}$ defined in § 4.3.1 oscillate in time with slowly decreasing amplitudes within the computation time, while they decrease monotonically for $S_0 = 0.2$. In the case $0.5 \leqq S_0 \leqq 3$, the parameters p and q of the asymptotic soliton solution (4.15) can be estimated in the similar way to the case in § 4.3.1. The parameters p, q_1 and q_2 of the asymptotic

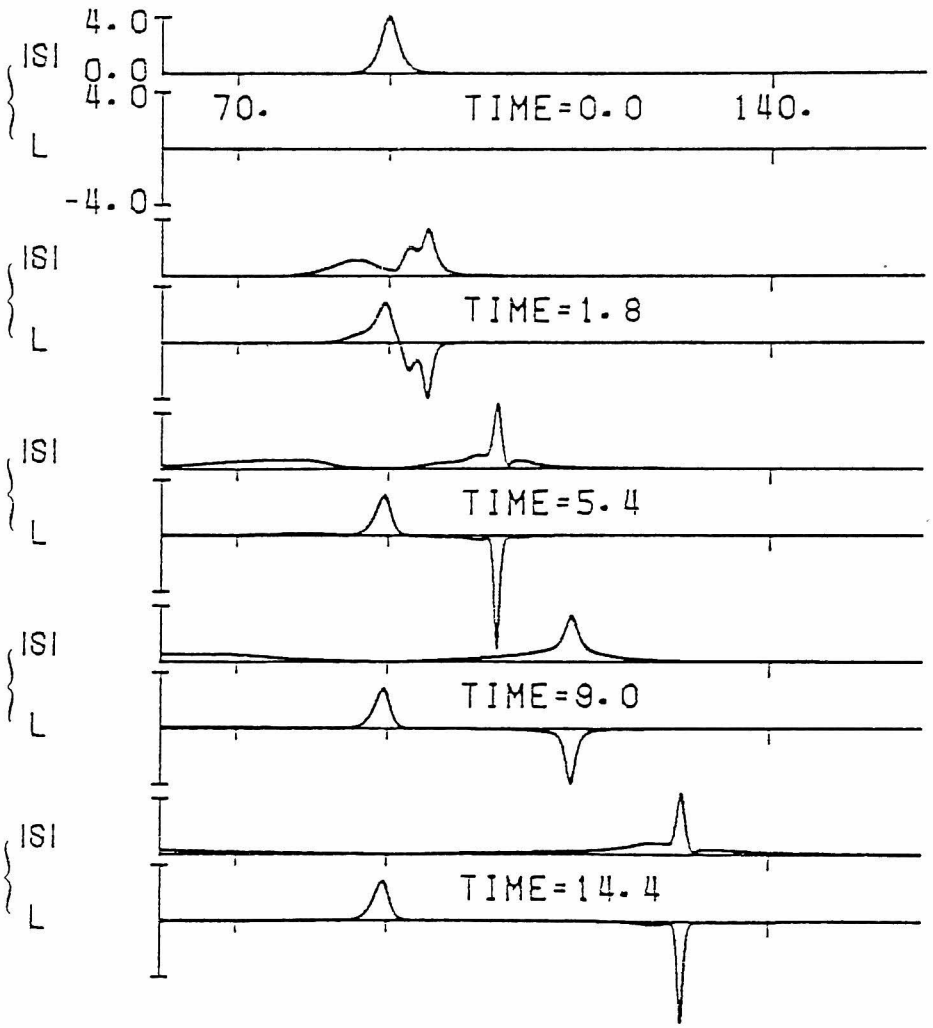

Fig.35. Time development of the solution for the initial data (4.21) with S_0 = 4. d =200. ΔX = 0.025. Breather solution for which $|S|_{max}$ and L_{min} oscillate in time with the period 2.24 emerges asymptotically. The solutions at t = 5.4 and at t = 14.4 have two negative peaks of L, while the solution at t = 9.0 has one negative peak of L.

breather solution (4.16) for $3.5 \leqq S_0 \leqq 4$ were estimated by using the relations (4.17) and (4.18). The computed values of the left hand sides of eqs.(4.17) are approximately constant in time. We adopted the period of the oscillations of $|S|_{max}$ and L_{min} as the approximate value for T_p. This period is also approximately constant in time. The parameters p and q (or q_1, q_2) for the

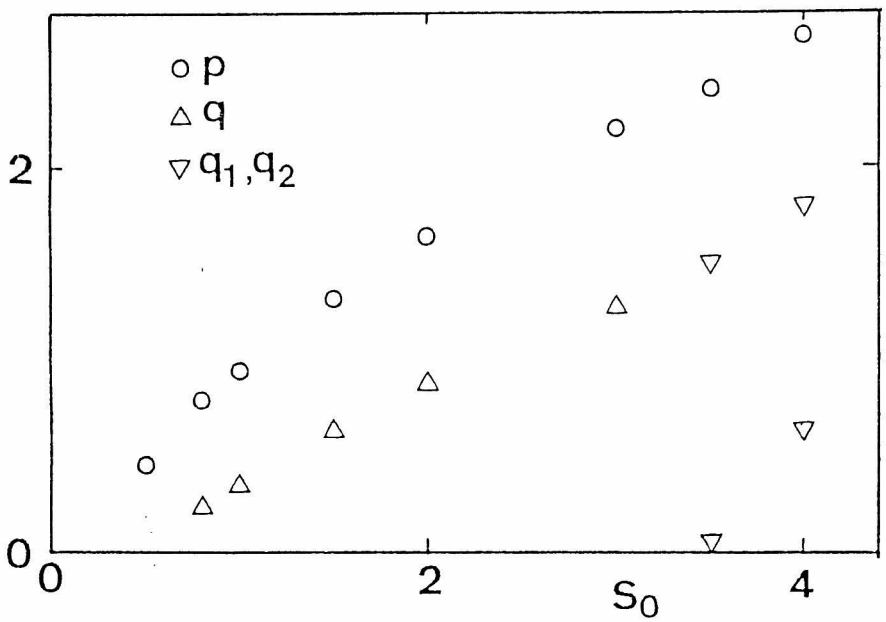

Fig.36 Dependence of the parameters p, q, q_1 and q_2 of the asymptotic 1-soliton solution (4.15) or the breather solution (4.16) on S_0.

asymptotic soliton (or breather solution) are plotted in Fig.36. The faster soliton (or breather solution) is generated for larger S_0. The extrapolation of p and q to small S_0 suggests that no soliton emerges for $S_0<0.2$. This is consistent with the behaviour of the solution for $S_0=0.2$. Furthermore, the values of q, q_1 and q_2 suggest that two or more solitons including the breather solution emerge for $S_0>3.4$.

4.3.3. The interaction of a coupled soliton and a steady localized long wave

In this subsection we mainly examine the interaction between the soliton solution (4.15) and the steady long wave solution of the form

$$\begin{cases} S = 0, \\ L = b\,\mathrm{sech}^2\kappa(X-X_1), \end{cases} \tag{4.22}$$

where b and X_1 are real constants, and κ is a positive constant

In the special case of $b=-n(n+1)\kappa^2$, ($n=1,2,\ldots$), eq.(4.22) represents the steady n-soliton solution as is shown in Appendix C, so the interaction of it with an incident coupled soliton is already known theoretically [97], [99]. Both an incident coupled soliton and the steady 1-soliton, (4.22) with $b=-2\kappa^2$, suffer only the phase shifts from the interaction between them. The phase shifts Δ_1 and Δ_2 of the incident soliton (4.15) and the steady 1-soliton, respectively, are written as

$$\Delta_1 = \frac{1}{2q}\ln\left[\frac{4(q+\kappa)^2+p^2}{4(q-\kappa)^2+p^2}\right] > 0, \tag{4.23a}$$

$$\Delta_2 = -\frac{q\Delta_1}{\kappa} < 0. \tag{4.23b}$$

A positive (negative) phase shift means a position phase shift to the right (left). However, if $n \geqq 2$, a steady n-soliton solution suffers the change of its shape from the interaction because each constituent soliton undergoes a different phase shift.

Since theoretical results are not obtained for $b \neq -n(n+1)\kappa^2$ or for more general steady long wave solution, the interaction is examined numerically. An incident coupled soliton suffers only the phase shift from the interaction with the solution (4.22) as is illustrated in Fig.37, and the phase shift Δ_1 is positive for $b < 0$ and negative for $b > 0$. Furthermore, it is likely that Δ_1 is positive for the arbitrary steady localized negative long wave, and is negative for the arbitrary positive one.

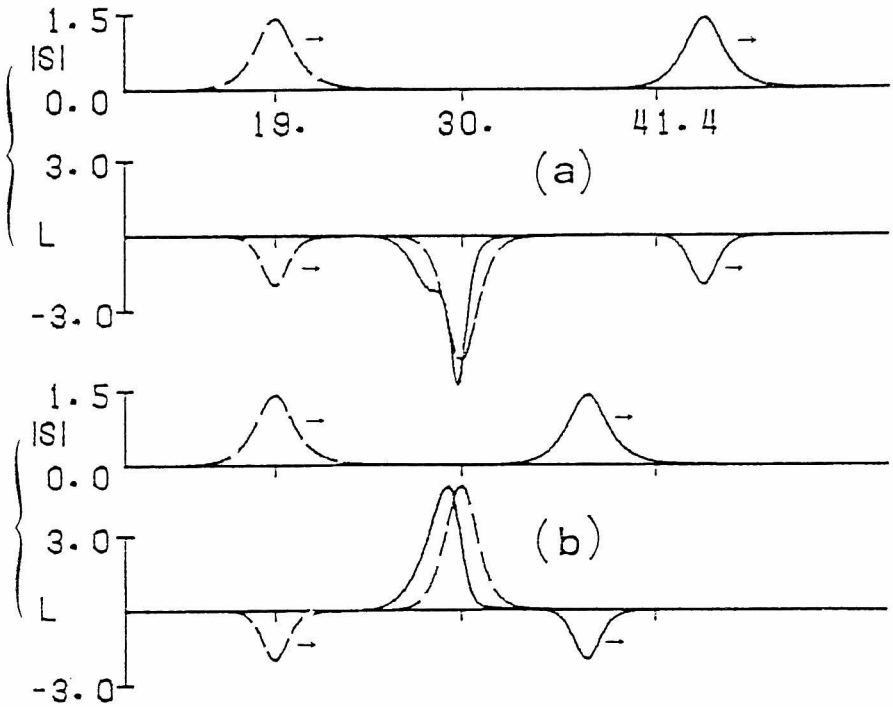

Fig.37. The interaction between the soliton solution (4.15) with p = q = 1 and the steady long wave solution (4.22) with κ = 0.8, b = −5 for (a), and κ = 0.8, b = 5 for (b). ——: t = 0. ——: t = 22.4.

Figure 38 represents the dependence of Δ_1 for the coupled soliton with $p=q=1$ on the area $I_s=2b/\kappa$ and the steepness $b\kappa$ of the solution (4.22). For sufficiently small $|I_s|$, Δ_1 is close to $-2I_s/5$ for any values of $b\kappa$. Furthermore, the relation $\Delta_1 = -2I_s/5$ is likely to be satisfied even for the steady long wave of arbitrary shape of sufficiently small area I_s. The value of Δ_1/I_s in the limit $|I_s|\to 0$ can be predicted for general values of p and q from the relation (4.23a) on the assumption that $\kappa \ll q$, and is written as

$$\frac{\Delta_1}{I_S} = -\frac{2}{p^2+4q^2}. \qquad (4.24)$$

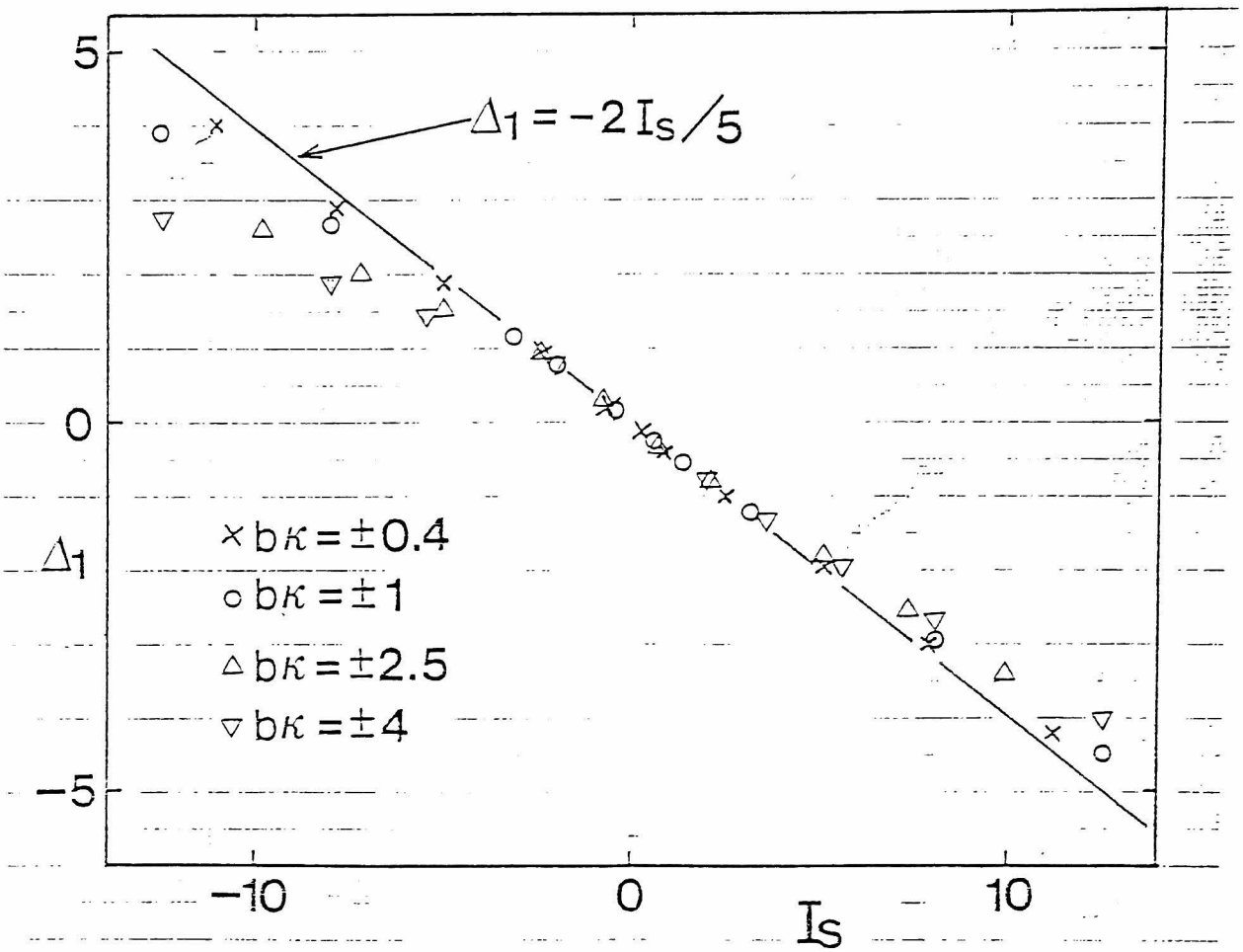

Fig.38. The phase shift of the soliton solution (4.15) with p = q = 1 owing to the interaction with the steady long wave solution (4.22). I_S(= $2b/\kappa$) is the area of the steady long wave.

Several computations for different p and q support that this relation is valid for sufficiently small $|I_s|$. Figure 38 also shows that if $|I_s|$ is not so small then Δ_1 depends on the shape of the steady long wave as well as I_s. For arbitrary values of b and κ, $|\Delta_1/I_s|$ does not exceed 2/5. These results suggest that $|\Delta_1|$ of the soliton (4.15) due to the interaction with the steady long wave of arbitrary shape and area I_s is at most $2|I_s|/(p^2+4q^2)$.

A steady long wave in general suffers the change of its

shape in addition to the shift of its position from the interaction with a coupled soliton as is illustrated in Fig.37 As the measure of the shift of the steady long wave, we calculate the following quantity from the steady part of L

$$\tilde{\Delta}_2 \equiv \left[\int_{-\infty}^{\infty} XL\,dX \Big/ \int_{-\infty}^{\infty} L\,dX\right]_{T_1=T_2} - \left[\int_{-\infty}^{\infty} XL\,dX \Big/ \int_{-\infty}^{\infty} L\,dX\right]_{T=T_1}, \tag{4.25}$$

where T_1 and T_2 are the instants sufficiently before and after the interaction respectively. The value of $\tilde{\Delta}_2$ is negative both for any positive long wave and for any negative one. The values of Δ_1 and $\tilde{\Delta}_2$ associated with the interaction between the soliton 4.15) and an arbitrary steady long wave of an area I_s must satisfy

$$I_S\tilde{\Delta}_2 - 4q\Delta_1 = 0. \tag{4.26}$$

The derivation of the relation (4.26) from eq.(4.13b) is given in Appendix D. By using the preceding results about the sign of Δ_1, it follows from (4.26) that $\tilde{\Delta}_2$ is negative.

§4 4. Supplementary Discussion

In this section we make a brief comment on the previous results about the evolution of a short wave and a long wave starting from a short wave packet of near-resonant wavenumber.

The short wave packet and the long wave corresponding to the coupled part(i) stated in §4.3 keep the assumed scale

$$\lambda_s = O(a_s^{-2/3}), \tag{4.27a}$$

$$\lambda_l = O(a_l^{-1/2}), \tag{4.27b}$$

$$a_l = O(a_s^{4/3}), \tag{4.27c}$$

where a_s and a_l are the amplitudes of a short and a long wave, and λ_s and λ_l are the length scales of a short wave packet and a long wave. Here all the variables are nondimensionalized by the water depth. However, the short wave packet corresponding to part(iii) disperses and becomes not to satisfy the initial relation (4.27a This short wave packet is expected to continue to disperse until the relation $\lambda_s=O(a_s^{-1})$ is satisfied. The short wave packet satisfying this relation is governed by the nonlinear Schrödinger equation (1.11). Although the long wave corresponding to the part(ii) does not propagate in the assumed nondimensional time scale of $O(a_l^{-1})$, it is known [49] to be governed by the K-dV equation (1.13) in the slower time scale of $O(a_l^{-3/2})$. The steady n-soliton solution, (4.22) with $b = -n(n+1)\kappa^2$, may be considered as the degenerate case of the n-soliton solution of the K-dV equation.

Appendix A

The coupling constants α and β in eqs.(4.12) are given by

$$\frac{\alpha}{(g/h_1^3)^{1/2}} = K\Omega\left[\Delta\left(1-\frac{K^2}{\Omega^4}\right)(\sigma_2-\sigma_1)+\frac{2\Delta}{\Omega V_g}\left(\frac{K}{\Omega^2}\sigma_1-1\right)+\frac{V_g^2}{V_g^2-1}\left\{\left(1-\frac{K^2}{\Omega^4}\right)(\sigma_1+\sigma_2\right.\right.$$
$$\left.-\Delta\sigma_2\left(1+\frac{K}{\Omega^2}\sigma_1\right)\right)-\frac{2}{\Omega V_g}\left((1-\Delta)(1+\sigma_1\sigma_2)+\frac{\Delta K}{\Omega^2}\sigma_1\left(1-\frac{K}{\Omega^2}\sigma^2\right)\right)\left.\right\}\left.\right]/\left[4\left(1+(1\right.$$
$$\left.-\Delta)\sigma_1\sigma_2\right)-\frac{2K}{\Omega^2}(\sigma_1+\sigma_2)\left.\right], \qquad (4.A.1)$$

$$\frac{\beta}{(g/h_1)^{1/2}} = -\frac{\delta}{2(\Delta\delta-V_g^4)}\left[(1-\Delta)V_g\left(\Omega^2-\frac{K^2}{\Omega^2}\right)-2(1-\Delta)\frac{KV_g^2}{\Omega}-2\Omega V_g^2(1-\Delta)(\sigma_3\right.$$
$$\left.-\frac{K}{\Omega^2}\sigma_4)(\sigma_4-\frac{K}{\Omega^2}\sigma_3)-\left\{\Omega^2V_g(V_g^2-1)\left(\frac{1}{\sigma_2^2}-1\right)+\frac{2\Omega}{\sigma^2}(V_g^2-\Delta)\right\}(\sigma^3-\frac{K}{\Omega^2}\sigma_4)^2\right], \qquad (4.A.2)$$

where

$$K=kh_1, \quad \Omega=\omega\sqrt{h_1/g}, \quad V_g=\frac{c_g}{(gh_1)^{1/2}}, \quad \delta=\frac{h_2}{h_1},$$

$$\sigma_1 = \tanh K, \quad \sigma_2 = \tanh\delta K, \quad \sigma_3 = \cosh K, \quad \sigma_4=\sinh K.$$

Appendix B

The coefficients in the representation (4 16) of the breather solution are written as

$$a_1 = \frac{1}{4pq_1^2}, \qquad a_2 = \frac{1}{4pq_2^2},$$

$$a_3=\frac{2}{\nu_1^2\mu_1}\ , \qquad a_4=a_1a_2\left(\frac{\nu_2}{\nu_1}\right)^4\left|\frac{\mu_2}{\mu_1}\right|^2,$$

$$b_1 = a_1\left(\frac{\nu_2}{\nu_1}\right)^2\frac{\mu_2^*}{\mu_1}\ , \qquad b_2 = a_2\left(\frac{\nu_2}{\nu_1}\right)^2\frac{\mu_2^*}{\mu_1^*}\ .$$

where

$$\mu_1 = p-i(q_1-q_2), \quad \mu_2 = p+i(q_1+q_2),$$

$$\nu_1 = q_1+q_2, \quad \nu_2 = q_1-q_2.$$

Appendix C

The eigenvalue problem in the inverse scattering method associated with eqs.(4.13) is written as [97], [98]

$$\frac{\partial V_1}{\partial X} = -3i\zeta V_1 - \frac{1}{2^{1/2}}SV_2 - iLV_3, \tag{4.C.1a}$$

$$\frac{\partial V_2}{\partial X} = -2i\zeta V_2 - \frac{1}{2^{1/2}}S^*V_3, \tag{4.C.1b}$$

$$\frac{\partial V_3}{\partial X} = -i\zeta V_3 + iV_1, \tag{4.C.1c}$$

where ζ is the eigenvalue. If we assume that $S=0$, eqs.(4.C.1a) and (4.C.1c) reduce to the equation

$$-\frac{\partial^2 u}{\partial X^2} + Lu = \zeta^2 u, \tag{4.C.2}$$

where

$$u = V_3 e^{2i\zeta X}.$$

This is the Schrödinger equation of eigenvalue ζ^2 and potential L. When L take the form (4.22) this equation can be transformed to Legendre's associated differential equation, and it is known [101] that n discrete eigenvalues exist and the reflection coefficient vanishes when $b=-n(n+1)\kappa^2$, ($n=1,2,\ldots$). From this result it is shown that the solution (4.22) satisfying $b=-n(n+1)\kappa^2$ belongs to the steady n-soliton solution.

Appendix D

For the localized distribution of S and L, the integration of eq.(4.13b) gives

$$\frac{\partial}{\partial T}\int_{-\infty}^{\infty} XL\,dX=-\int_{-\infty}^{\infty} |S|^2 dX. \qquad (4.D\ 1)$$

We assume that

$$|S|=f(X-pT),\ L=L_1(X)+g(X-pT),\ \text{for}\quad T\to-\infty, \qquad (4.D.2a)$$

and

$$|S|=f(X-pT-\Delta_1),\ L=L_2(X)+g(X-pT-\Delta_1),\quad \text{for}\quad T\to+\infty \qquad (4.D.2b)$$

where f and g represent the soliton solution (4.15). Integrating eq.(4.D.1) from $T=T_1$ to $T=T_2$, and using the asymptotic forms (4.D.2), we obtain

$$\int_{-\infty}^{\infty} XL_2(X)dX - \int_{-\infty}^{\infty} XL_1(X)dX = 4q\Delta_1. \qquad (4.D.3)$$

Therefore, $\tilde{\Delta}_2$ defined in eq.(4.25) can be written as

$$\tilde{\Delta}_2 = \frac{4q\Delta_1}{I_S}, \qquad (4.D.4)$$

where

$$I_S = \int_{-\infty}^{\infty} L_1(X)dX.$$

Chapter 5

The Resonant Interaction between a Long Internal Gravity Wave and a Surface Gravity Wave Packet II. Deep-Fluid Case.

§ 5.1 Introduction

The long-short resonant interaction discussed in the preceding chapter was restricted to the case in which a long wave is not dispersive. It is also possible to consider the resonant interaction between a dispersive short wavetrain and a "dispersive" long wave. Benney [96] discussed this interaction between a short capillary-gravity wave and a long gravity wave in deep water.

In this chapter, we examine the interaction between a long internal wave and a short surface wave in two-layer fluid under the assumption that $h_1 \ll l \ll h_2$. Here l is a characteristic length scale of a long wave, and h_1 and h_2 are the water depths of the upper and lower layers respectively (see Fig.2). The equations describing the interaction are derived in § 5.2. They have the extra term representing the dispersion of a long wave in comparison with the eqs.(4.12) for shallow-fluid case discussed in the preceding chapter. It is difficult to find analytical solutions of the derived interaction equations. Therefore, we computed solitary wave solutions of them numerically in § 5.3. It is suggested that the solitary wave solutions are specified by two independent parameters. The interaction equations seem to have only four conserved quantities. This suggests that the

equations are not completely integrable and that the obtained solitary wave solutions do not behave as solitons.

§ 5.2 Formulation and Reduced Interaction Equations

We consider the wave propagation in a two-layer fluid which consist of the "shallow" upper layer and the "deep" lower layer. The same symbols as those in chapter 4 are used for the densities, water depths, displacements of free-surface and interface and the velocity potentials (see Fig.2). Then the basic equations and boundary conditions are again given by eqs.(1.15). The linear dispersion relation (1.17) reduces to

$$\omega = \sqrt{gk} \tag{5.1a}$$

$$\omega = \left[\frac{\Delta gk\sigma}{1+(1-\Delta)\sigma}\right]^{1/2}, \qquad (\ \sigma=\tanh kh\ ), \tag{5.1b}$$

for $h_1=h$ and $h_2\to\infty$. The linear dispersion relation for the surface mode (5.1a) is the same as that for surface gravity waves in deep water.

We assume that $\varepsilon \equiv a/\lambda \ll 1$, $\lambda/h_1 \sim 1$, $\lambda/l \ll 1$ and $h_2 = \infty$. Here a and λ are a characteristic amplitude and a characteristic length scale of the surface wave, respectively. From now on, we omit the subscript from h_1. The vertical length scale of long wave component in the lower layer is the same as the horizontal one. This suggests that it is necessary to introduce the stretched coordinate $Z = \varepsilon^{2/3}z$ in addition to ξ and τ defined in § 4.2. In the linear approximation, the boundary conditions at the interface require the continuity of the

vertical velocity there. This suggests that the leading term of the velocity potential of the long wave component in the lower layer is $O(\varepsilon^{4/3})$ because the vertical velocity of the long wave component in the upper layer is expected to be $O(\varepsilon^2)$ from the results in shallow-fluid case. Therefore, we assume that the solution is of the form :

$$\phi_1 = \sum_{n=0}^{\infty} \varepsilon^{(2+n)/3} \phi_1^{(n)}, \tag{5.2a}$$

$$\phi_2 = \sum_{n=1}^{\infty} \varepsilon^{(2+n)/3} \phi_2^{(n)}, \tag{5.2b}$$

$$\zeta_1 = \sum_{n=0}^{\infty} \varepsilon^{(2+n)/3} \zeta_1^{(n)}, \tag{5.2c}$$

$$\zeta_2 = \sum_{n=1}^{\infty} \varepsilon^{(2+n)/3} \zeta_2^{(n)}, \tag{5.2d}$$

Introducing $Z = \varepsilon^{2/3} z$ as well as the variables ξ and τ given by eqs.(4.4), we regard the long wave component of $\phi_2^{(n)}$ as a function of ξ, Z and τ. We assume that $\phi_1^{(0)}$ consists of a long internal mode alone and $\phi_1^{(1)}$ and $\phi_2^{(1)}$ consist of a short surface mode alone. Therefore, we take

$$\phi_1^{(0)} = \Phi_1(\xi, \tau), \qquad \zeta_1^{(0)} = 0, \tag{5.3}$$

and

$$\begin{cases} \phi_j^{(1)} = -\dfrac{i\omega}{k} A(\xi, \tau) e^{i\theta} e^{k(z-h)} + \text{c.c.}, \quad (j=1,2) \\ \zeta_1^{(1)} = A(\xi, \tau) e^{i\theta} + \text{c.c.}, \qquad \zeta_2^{(1)} = \zeta_1^{(1)} e^{-kh}, \\ \theta = kx - \omega t \end{cases} \tag{5.4}$$

by taking the limit $h_2 \to \infty$ in the linear solution (1.16). Here k

and ω satisfy the dispersion relation of the surface mode (5.1a). In $O(\varepsilon^{4/3})$, we obtain

$$\begin{cases} \phi_1^{(2)} = \Phi_1^{(2)}(\xi,\tau), \qquad \phi_2^{(2)} = \Phi_2^{(2)}(\xi,Z,\tau), \\ \zeta_1^{(2)} = \dfrac{c_g}{g}\dfrac{\partial\Phi_1}{\partial\xi}, \qquad \zeta_2^{(2)} = -\dfrac{c_g(1-\Delta)}{\Delta g}\dfrac{\partial\Phi_1}{\partial\xi}. \end{cases} \tag{5.5}$$

The condition for no-secularity in $O(\varepsilon^{5/3})$ yields

$$c_g = \frac{d\omega}{dk} = \frac{\omega}{2k}. \tag{5.6}$$

From the compatibility condition in $O(\varepsilon^2)$ we obtain

$$c_g^2 = \Delta gh = c_p^2, \tag{5.7}$$

where $c_p=(\Delta gh)^{1/2}$ is the phase speed of the internal wave in the long wave limit, $l/h\to\infty$. We assume that k satisfies the resonance condition $c_g=c_p$. In this order of ε we furthermore obtain

$$\left[\frac{\partial}{\partial Z}\Phi_2^{(2)}\right]_{Z=0} = (1-\Delta)h\frac{\partial^2\Phi_1}{\partial\xi^2}, \qquad \frac{\partial}{\partial Z}\Phi_2^{(2)}\to 0 \quad (Z\to-\infty). \tag{5.8}$$

In $O(\varepsilon^{7/3})$, the condition for no-secularity leads to

$$i\frac{\partial A}{\partial\tau} + \frac{1}{2}\omega''\frac{\partial^2 A}{\partial\xi^2} = -\alpha AB, \tag{5.9}$$

where $B=\zeta_2^{(2)}$, and

$$\omega'' = \frac{d^2\omega}{dk^2} = -\frac{\omega}{4k^2} < 0,$$

$$\alpha = \frac{2\Delta k\omega(1-e^{-2kh})}{1-\Delta(1-e^{-2kh})} > 0.$$

In $O(\varepsilon^{8/3})$, we obtain from the compatibility condition

$$2\frac{\partial^2\Phi_1}{\partial\xi\partial\tau} + c_g\left[\frac{\partial^2}{\partial\xi^2}\Phi_2^{(2)}\right]_{Z=0} + 4\Delta\omega^2(1-e^{-2kh})\frac{\partial}{\partial\xi}(|A|^2) = 0, \qquad (5.10)$$

and also

$$\frac{\partial^2}{\partial\xi^2}\Phi_2^{(2)} + \frac{\partial^2}{\partial Z^2}\Phi_2^{(2)} = 0. \qquad Z<0 \qquad (5.11)$$

From eqs.(5.11) and (5.8) we can represent the second term of eq.(5.10) by means of Φ_1. Substituting this into eq (5.10) and using eqs.(5.5) we obtain

$$\frac{\partial B}{\partial\tau} + \gamma H\left(\frac{\partial^2 B}{\partial\xi^2}\right) = \beta\frac{\partial}{\partial\xi}(|A|^2), \qquad (5\ 12)$$

where H represents the Hilbert transform

$$H(f) = \frac{1}{\pi}P\int_{-\infty}^{\infty}\frac{f(\xi')}{\xi'-\xi}d\xi',$$

where P denotes the Cauchy principal value. The constants β and γ are written as

$$\beta = (1-\Delta)\omega(1-e^{-2kh}) > 0, \qquad \gamma = \frac{1}{2}(1-\Delta)h\sqrt{\Delta gh} > 0.$$

From eqs.(5.5), we obtain

$$\zeta_1^{(2)} = -\frac{\Delta}{1-\Delta}\zeta_2^{(2)}, \qquad \frac{\partial \Phi_1}{\partial \xi} = -\frac{2\Delta\omega}{1-\Delta}\zeta_2^{(2)}.$$

The signs of $\zeta_1^{(2)}$ and $\zeta_2^{(2)}$ are opposite each other.

The equations (5.9) and (5.12) are to be compared with eqs.(4.12). The extra term in eq.(5.12) represents the dispersion of the internal wave in a deep fluid. The solution of eqs.(5.9) and (5.12) has the same similarity as that of eqs.(4.12). That is, if $A=f(\xi,\tau)$ and $B=g(\xi,\tau)$ satisfy these equations, $A=r^{3/2}f(r\xi,r^2\tau)$ and $B=r^2g(r\xi,r^2\tau)$ also satisfy them. Here r is an arbitrary positive constant. This similarity is predicted from the procedure for the derivation of the equations.

The equations (5.9) and (5.12) can be reduced to the forms

$$i\frac{\partial S}{\partial T} - \frac{\partial^2 S}{\partial X^2} = -LS, \tag{5.13a}$$

$$\frac{\partial L}{\partial T} + \delta \mathrm{H}\left(\frac{\partial^2 L}{\partial X^2}\right) = \frac{\partial}{\partial X}(|S|^2), \tag{5.13b}$$

by an appropriate scale transformation. The coefficient δ ($= (1-\Delta)/(2\Delta)$) is a positive constant. In contrast with eqs (4.13), these equations seem to have only the following four conserved quantities,

$$I_1=\int_{-\infty}^{\infty} L\,dX, \quad I_2=\int_{-\infty}^{\infty} |S|^2 dX, \tag{5.14a,b}$$

$$I_3=\int_{-\infty}^{\infty} \left[L^2 - i\left(S^*\frac{\partial S}{\partial X} - S\frac{\partial S^*}{\partial X}\right)\right] dX, \tag{5.14c}$$

$$I_4 = \int_{-\infty}^{\infty} \left[\left|\frac{\partial S}{\partial X}\right|^2 + L|S|^2 - \frac{\delta}{2}L\mathrm{H}\left(\frac{\partial L}{\partial X}\right)\right] dX. \tag{5.14d}$$

The uniform amplitude periodic solutions to eqs.(5.13) are given by

$$S = S_0 e^{iL_0 T}, \quad L = L_0 \qquad (S_0, L_0: \text{ real constants}). \tag{5.15}$$

We consider the following perturbed solution

$$S = (S_0 + \varepsilon' a)\exp(iL_0 T + i\varepsilon'\theta), \quad L = L_0 + \varepsilon' b, \tag{5.16}$$

where ε' is a small parameter. Substituting these into eqs.(5.13) and assuming the solution of the form

$$(a, \theta, b) = (\hat{a}, \hat{\theta}, \hat{b})\exp[i(\kappa X - \nu T)] \qquad (\kappa > 0),$$

we obtain as the condition for instability

$$\kappa^3 < 27 S_0^2 [(\delta^2+3)(\sqrt{\delta^2+3}-\delta)+12\delta]^{-1}. \tag{5.17}$$

Therefore, the uniform amplitude periodic solutions to eqs.(5.13) are unstable for modulational perturbations with small amplitudes similarly to the shallow-fluid case.

§ 5.3 Numerical Study of the Reduced Interaction Equations

In contrast with the case of shallow fluid, it is difficult to find analytical solutions to the reduced interaction equations for deep fluid (5.13). Therefore, several numerical computations are made in order to examine the properties of the solutions including whether the solitary wave solution exists.

At first, eqs.(5.13) with δ=1 are solved numerically for the initial condition

$$S = \sqrt{2}\,\mathrm{sech}\,(X-30)\,e^{-(1/2)iX}, \tag{5.18a}$$

$$L = 0. \tag{5.18b}$$

We use the explicit scheme which is the same as eqs.(4.19) except for the addition of the following term to the left hand side of eq.(4.19c)

$$\frac{\delta}{\Delta X^2}(Q^n_{j+1}-2Q^n_j+Q^n_{j-1}),$$

where $Q = \mathrm{H}(L)$. Since the periodic boundary condition with a period d is adopted, the representation of Q is modified as

$$Q = \frac{1}{d}\mathrm{P}\int_0^d L(X',T)\cot\frac{\pi}{d}(X'-X)\,dX'.$$

The formula based on the Taylor series of L around $X'=X$ is used for the above integration over the range $X-3\Delta X \leqq X' \leqq X+3\Delta X$, and Simpson's rule is used for the other integration range.

Figure 39 shows the evolution of the solution starting from eqs.(5.18). The most remarkable difference from the shallow-water case is the shedding of the wavetrain of L to the negative X direction caused by the effect of the dispersion term in eq.(5.13b). The negative part of L generated first propagates to the positive X direction together with a hump of $|S|$. The heights of these peaks are oscillating with decreasing amplitudes in the computation time. Figure 40 shows the

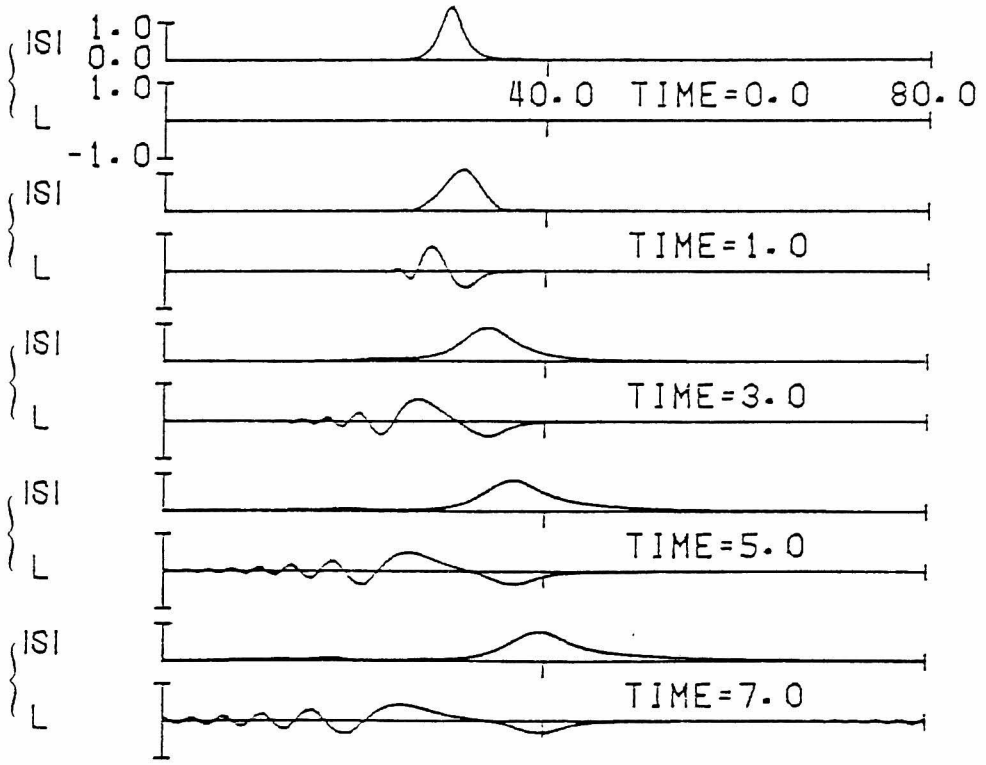

Fig.39.Time development of the solution for the initial data (5.18). δ = 1. ΔX = 0.2.

evolution of the solution starting from eq.(5.18a) and

$$L = -2\mathrm{sech}^2(X-30). \tag{5.19}$$

The behaviour of the solution is similar to that in Fig.39 These results suggest that a solitary wave solution of eqs.(5.13) exists and that a class of the initial conditions evolve to it asymptotically.

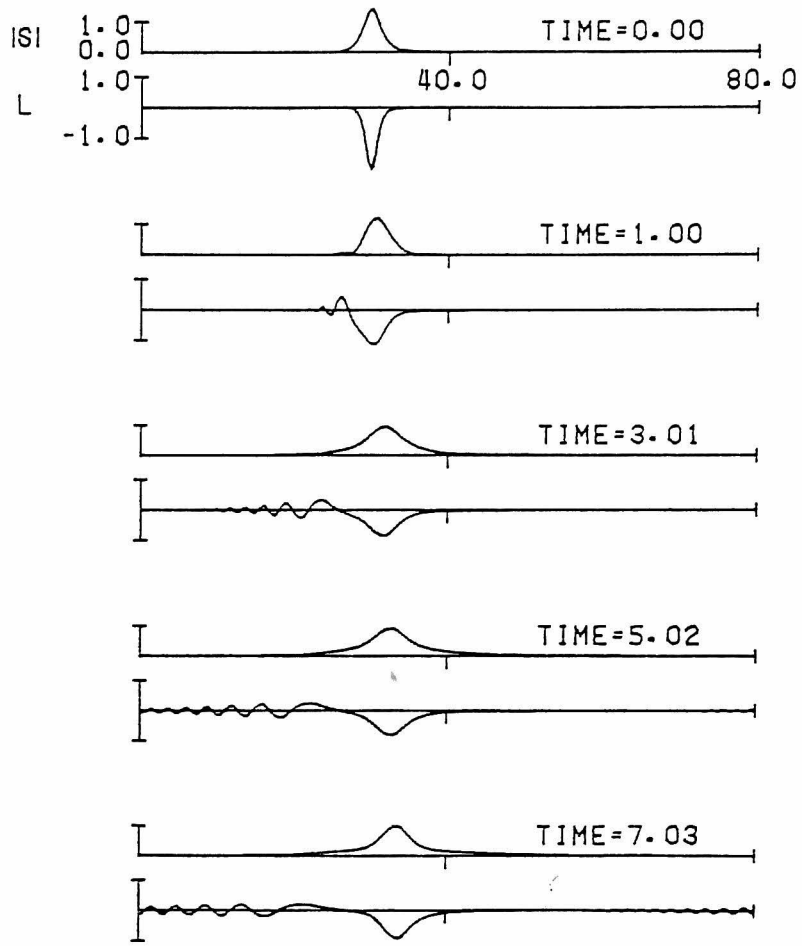

Fig.40. Time development of solution for the initial data (5.18a), (5.19). $\delta = 1$.

Therefore, we consider the solution of the form

$$S = f(X-vT)e^{i\varphi}, \tag{5.20a}$$

$$L = g(X-vT), \tag{5.20b}$$

$$\frac{\partial \varphi}{\partial X} = h(X-vT), \tag{5.20c}$$

where f, g and h are real functions, and v is a constant. The

functions f and g are assumed to vanish as $|X-vT|\to\infty$. Substitution of eqs.(5.20) into eqs.(5.13) gives the results

$$\frac{\partial\varphi}{\partial X} = h = -\frac{1}{2}v, \tag{5.21a}$$

$$\frac{\partial\varphi}{\partial T} = \text{const.}(\equiv\mu), \tag{5.21b}$$

and the equations for f and g

$$f'' + (\mu-\frac{1}{4}v^2)f = fg, \tag{5.22a}$$

$$-vg + \delta H(g') = f^2, \tag{5.22b}$$

where the prime denotes the differentiation with respect to $X - vT$. We obtained explicitly two solitary wave solutions which satisfy eqs.(5.21) and (5.22) for $\delta=1$ by a trial and error method. These solutions give $(v,\mu)=(0.66,-0.54)$ and $(v,\mu)=(1.64,0.47)$. Figure 41 represents the profiles of $|S|$ and L of them.

The two solitary wave solutions belong to different family of the similarity solutions stated in §5.2. Therefore, it is suggested that the solitary wave solution of eqs.(5.13) is specified by two independent parameters.

We can find only four conserved quantities (5.14) for eqs.(5.13). This suggests that eqs.(5.13) are not completely integrable and that steady solitary wave solutions do not behave as solitons.

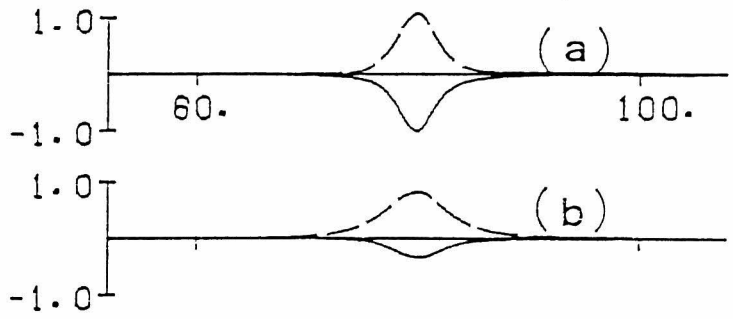

Fig.41. Two examples of the steady solitary wave solution to (5.13) with $\delta = 1$. ——: $|S|$. ——: L. The velocity of the solution, v, is 0.66 and 1.64 for (a) and (b) respectively.

Chapter 6

Concluding Remarks

In the present chapter, the results obtained in the previous chapters are summarized and some related remarks are presented.

In chapter 2, the one-dimensional reflection of a solitary wave in shallow water at the rigid vertical wall is examined numerically by an improved MAC (Marker and Cell) method. The problem is equivalent to that of head-on collision between two solitary waves of the same amplitudes. The phase shift associated with the reflection and the slight distortion of the reflected wave is found for any small but finite values of ε. Here ε is the amplitude of an incident wave nondimensionalized by the water depth h.

The larger phase shift associated with the reflection is obtained for the larger ε. Furthermore, the phase shift tends to zero as ε decreases to zero. This tendency is consistent with the existing theory based on the perturbation method. On the contrary, the experiments made by Maxworthy [57] give the phase shift independent of ε. Although he suggested that this discrepancy between the theory and his experiment is due to the inappropriate scaling adopted in the theory or to the truncation of the perturbation calculation at the insufficient order, the results in the present thesis indicate that the theory based on the perturbation method is valid for sufficiently small ε in the framework of the inviscid theory.

The distortion of the reflected wave nondimensionalized by h is found to be at most of $O(\varepsilon^3)$. This result is consistent with the existing second-order theories [55], [56] which predict no distortion. Although the third-order theory by Su and Mirie [84] predicted the distortion of $O(\varepsilon^3)$, the wave form of the reflected wave predicted by them is not similar to that in the present thesis. Therefore, a new perturbation method may be required for the description of the distortion of a reflected wave.

In chapter 3, the reflection of an obliquely incident solitary wave at the rigid vertical wall is examined. This problem has a close relation to the problem of two-dimensional interaction of solitary waves. The equations which govern the two-dimensional shallow-water wave motion are derived by taking only the terms of lowest order of nonlinearity and dispersion, and are solved numerically.

The solution for the reflection problem depends strongly on the ratio of the angle of incidence α to $\varepsilon^{1/2}$. When $\alpha > (3\varepsilon)^{1/2}$, the regular reflection pattern composed of an incident wave and a reflected wave of the same amplitudes emerges asymptotically. If $\alpha \gg \varepsilon^{1/2}$ the incident and the reflected waves intersect approximately at the point on the wall implying that the solution can be approximated by the superposition of incident and reflected waves. However, if α decreases to $(3\varepsilon)^{1/2}$, the position at which the incident and the reflected waves intersect becomes more distant from the wall.

On the other hand, if $\alpha < (3\varepsilon)^{1/2}$ "a Mach reflection pattern" (geometrically similar to the corresponding shock-wave

reflection pattern) composed of three obliquely oriented solitary waves is obtained as an asymptotic solution. This solution has the reflected wave of the amplitude smaller than that of an incident wave, and "the Mach stem" perpendicular to the wall, as well as the incident wave. As α tends to zero, the amplitude of a reflected wave and a Mach stem decreases to zero and εh, respectively, consistent with what is expected as the solution for the propagation of a solitary wave along the wall.

Other interesting behaviour of the solution is the large values of the maximum run-up at the wall for $\alpha \sim (3\varepsilon)^{1/2}$. Even the value larger than $3.4\varepsilon h$ is obtained, although the linear theory predicts $2\varepsilon h$ for any values of non-zero α. This phenomena is one remarkable manifestation of nonlinear effect.

The aforementioned asymptotic solution for $\alpha < (3\varepsilon)^{1/2}$ agrees well with the solution composed of three resonantly interacting solitary waves predicted by Miles [62]. Therefore, it is confirmed that the predicted solution emerges asymptotically as the solution for the initial-value problem of oblique reflection with $\alpha < (3\varepsilon)^{1/2}$.

Recently Melville [63] made an experiment on this problem. Although he obtained the results indicating the emergence of the Mach reflection pattern for $\alpha < (3\varepsilon)^{1/2}$, he could not observe the large maximum run-up at the wall for $\alpha \sim (3\varepsilon)^{1/2}$ in contradiction to the Miles' solution. The experiment with the larger dimension may be required for the observation of the large maximum run-up at the wall in consideration of the fairly large evolution time required for the attainment of the stationary state in the present numerical calculation.

In chapters 4 and 5, the long-short wave interactions between a long internal gravity wave and a short surface gravity wave packet in two-layer fluid are examined. This interaction occurs when the phase speed of an internal wave coincides with the group velocity of a surface wave packet. The equations which govern the time evolution of the long wave and the short wave packet are derived by the reductive perturbation method.

In chapter 4 the shallow-fluid case, in which the wavelength l of an internal wave is much larger than the fluid depths, is considered. The governing equations for this case are solved numerically for several initial localized distributions.

It is found that the coupled soliton [97], [99] composed of the depression of a long wave and a hump of short wave packet emerges asymptotically from a wide class of initial distributions of short wave packet. A part of the initial short wave packet does not couple with the depression of a long wave and disperses. The short wave corresponding to this part seems to become to be governed by the nonlinear Schrödinger equation (1.11) after sufficiently large evolution time. The solution composed of the elevation of a long wave alone is also found in the asymptotic state. Although this solution is stationary in the assumed time scale, the long wave corresponding to this part is expected to be governed by the K-dV equation (1.13) in the slower time scale.

In chapter 5, the deep-fluid case, in which l is much larger than the fluid depth of the upper layer and is much smaller than that of the lower layer, is considered. The governing equations for this case have the extra term

representing the dispersion of the internal waves in comparison with those for shallow-fluid case. Solitary wave solutions to the equations are computed numerically, since it seems difficult to find analytical solutions to them. It is suggested that the solitary wave solutions are specified by two independent parameters.

The governing equations for this case seem to have only four conserved quantities. This suggests that the equations are not completely integrable and that the obtained solitary wave solutions do not behave as solitons.

References

[1] Stokes,G.G. : "On the theory of oscillatory waves" Trans. Cambridge Philos. Soc. 8 (1847) 441.

[2] Stokes,G.G. : "Supplement to a paper on the theory of oscillatory waves" Mathematical & Physical Papers 1 (1880) 314 Cambridge, England.

[3] De,S.C. : "Contributions to the theory of Stokes waves" Proc. Cambridge Philos. Soc. 51 (1955) 713.

[4] Chappelear,J.E. : "Direct numerical calculation of wave properties" J. Geophys. Res. 66 (1961) 501.

[5] Schwartz,L.W. : "Computer extension and analytic continuation of Stokes' expansion for gravity waves" J. Fluid Mech. 62 (1974) 553

[6] Wilton,J.R. : "On deep water waves" Philos. Mag. (6) 27 (1914) 385.

[7] Longuet-Higgins,M.S. : "Integral properties of periodic gravity waves of finite amplitude" Proc. Roy. Soc. London Ser.A. 342 (1975) 157.

[8] Benjamin,T.B. and Feir,J.E. : "The disintegration of wavetrains on deep water Part 1 Theory" J. Fluid Mech. 27 (1967) 417.

[9] Lighthill,M.J. : "Contributions to the theory of waves in nonlinear dispersive systems" J. Inst. Math. Appl. 1 (1965) 269. ; "Some special cases treated by the Whitham theory" Proc. Roy. Soc. London Ser.A 299 (1967) 28.

[10] Whitham,G.B. : "Variational methods and applications to water waves" Proc. Roy. Soc. London Ser.A 299 (1967) 6;

"Nonlinear dispersion of water waves" J. Fluid Mech. 27 (1967) 399.

[11] Whitham,G.B. :"Non-linear dispersive wave" Proc. Roy. Soc. London Ser.A 283 (1965) 238; "A general approach to linear and non-linear dispersive waves using a Lagrangian" J. Fluid Mech. 22 (1965) 273. 570 10

[12] Benjamin,T.B. : "Instability of periodic wave trains in nonlinear dispersive systems" Proc. Roy. Soc. London Ser.A 299 (1967) 59.

[13] Hasimoto,H. and Ono,H. : "Nonlinear modulation of gravity waves" J. Phys. Soc. Jpn. 33 (1972) 805.

[14] Benney,D.J. and Newell,A.C. : "The propagation of nonlinear wave envelopes" J. Math. Phys. 46 (1967) 133.

[15] Taniuti,T. and Yajima,N. : "Perturbation method for a nonlinear wave modulation. I" J. Math. Phys. 10 (1969) 1369.

[16] Zakharov,V.E. and Shabat,A.B. : "Exact theory of two-dimensional self-focusing and one-dimensional self-modulating waves in nonlinear media" Zh. Eksp. Teor. Fiz. 61 (1971) 118. Transl. in Sov. Phys. JETP 34 (1972) 62.

[17] Yuen,H.C. and Lake,B.M. : "Nonlinear deep water waves : Theory and experiment" Phys. Fluids 18 (1975) 956.

[18] Satsuma,J. and Yajima,N. : "Initial value problems of one-dimensional self-modulation of nonlinear waves in dispersive media" Suppl. Prog. Theor. Phys. 55 (1974) 284.

[19] Yuen,H.C. and Ferguson,W.E.Jr. : "Relationship between Benjamin-Feir instability and recurrence in the nonlinear Schrödinger equation" Phys. Fluids 21 (1978) 1275.

[20] Ursell,F. : "The long-wave paradox in the theory of

gravity waves" Proc. Cambridge Philos. Soc. 49 (1953) 685.

[21] Boussinesq,M.J. : "Théorie des ondes et des remous qui se propagent le long d'un canal rectangulaire horizontal, en communiquant au liquide contenu dans ce canal des vitesses sensiblement pareilles de la surface au fond" J. Math. Pures Appl. (2) 17 (1872) 55. Transl. A.C.J. Vastano, J.C.H. Mungall, Texas A&M Univ. Ref.76-2-T (March,1976).

[22] Rayleigh,Lord : "On waves" Phil. Mag. 1 (1876) 257. Sci. Pap. 1 251.

[23] Korteweg,D.J. and de Vries,G. : "On the change of form of long waves advancing in a rectangular canal and on a new type of long stationary wave" Phil. Mag. (5) 39 (1895) 422 .

[24] Zakharov,V.E. : "Kinetic equation for solitons" Soviet Physics JETP 33 (1971) 538.

[25] Wadati,M. and Toda,M. : "The exact N-soliton solution of the Korteweg-de Vries equation" J. Phys. Soc. Jpn. 32 (1972) 1403.

[26] Tanaka,S. : "On the N-tuple wave solutions of the Korteweg-de Vries equation" Publ. Res. Inst. Math. Sci. 8 (1972/1973) 419.

[27] Gardner,C.S., Greene,J.M., Kruskal,M.D. and Miura,R.M. : "Korteweg-de Vries equation and generalizations. VI. Methods for exact solution" Comm. Pure Appl. Math. 27 (1974) 97.

[28] Miura,R.M. : "The Korteweg-de Vries equation : A survey of results" SIAM Review 18 (1976) 412.

[29] Nekrasov,A.I. : "On waves of permanent type" Izv. Ivan. Voznesensk. politekh. Inst. 3 (1921) 52.

[30] Levi-Civita,T. : "Détermination rigoureuse des ondes

permanentes d'ampleur finie" Math. Ann. 93 (1925) 264.

[31] Yamada,H. : "On the highest solitary wave" Rep. Res. Inst. Appl. Mech. Kyushu Univ. 5 (1957) 53.

[32] Yamada,H. : "On approximate expressions of solitary wave" Rep. Res. Inst. Appl. Mech. Kyushu Univ. 6 (1958) 35.

[33] Yamada,H., Kimura,G. and Okabe,J.-I. : "Precise determination of the solitary wave of extreme height on water of a uniform depth" Rep. Res. Inst. Appl. Mech. Kyushu Univ. 16 (1968) 15.

[34] Byatt-Smith,J.G.B. : "An exact integral equation for steady surface waves" Proc. R. Soc. London Ser.A 315 (1970) 405.

[35] Packham,B.A. : "The theory of symmetrical gravity waves of finite amplitude. II The solitary wave" Proc. Roy. Soc. London Ser.A 213 (1952) 238.

[36] Byatt-Smith,J.G.B. and Longuet-Higgins,M.S. : "On the speed and profile of steep solitary waves" Proc. R. Soc. London Ser.A 350 (1976) 175.

[37] Laitone,E.V. : "The second approximation to cnoidal and solitary waves" J. Fluid Mech. 9 (1960) 430.

[38] Chappelear,J.E. : "Shallow-water waves" J. Geophys. Res. 67 (1962) 4693.

[39] Fenton,J.D. : "A high-order cnoidal wave theory" J. Fluid Mech. 94 (1979) 129.

[40] Fenton,J.D. : "A ninth-order solution for the solitary wave" J. Fluid Mech. 53 (1972) 257.

[41] Longuet-Higgins,M.S. and Fenton,J.D. : "On the mass, momentum, energy and circulation of a solitary wave II"

Proc. Roy. Soc. London Ser.A 340 (1974) 471.

[42] Benjamin,T.B. : "The stability of solitary waves" Proc. Roy. Soc. London Ser.A 328 (1972) 153.

[43] Jeffrey,A. and Kakutani,T. : "Stability of the Burgers shock wave and the Korteweg-deVries soliton" Indiana Univ. Math. J. 20 (1970) 463.

[44] Kadomtsev,B.B. and Petviashvili,V.I. : "On the stability of solitary waves in weakly dispersing media" Sov. Phys. Dokl. 15 (1970) 539.

[45] Oikawa,M., Satsuma,J. and Yajima,N. : "Shallow water waves propagating along undulation of bottom surface" J. Phys. Soc. Jpn. 37 (1974) 511.

[46] Crapper,G.D. : "An exact solution for progressive capillary waves of arbitrary amplitude" J. Fluid Mech. 2 (1957) 532.

[47] Harrison,W.J. : Proc. London Math. Soc. (2) 7 (1909) 107.

[48] Wilton,J.R. : "On ripples" Philos. Mag.(6) 29 (1915) 688.

[49] Kakutani,T. and Yamasaki,N. : "Solitary waves on a two-layer fluid" J. Phys. Soc. Jpn. 45 (1978) 674.

[50] Walker,L.R. : "Interfacial solitary waves in a two-fluid medium" Phys. Fluids 16 (1973) 1796.

[51] Tanaka,M. : "Nonlinear self-modulation of interfacial waves" J. Phys. Soc. Jpn. 51 (1982) 2016.

[52] Zabusky,N.J. and Galvin,C.J. : "Shallow-water waves, the Korteweg-deVries equation and solitons" J. Fluid Mech. 47 (1971) 811.

[53] Hammack,J.L. and Segur,H. : "The Korteweg-deVries equation and water waves. Part.2. Comparison with experiments" J.

Fluid Mech. 65 (1974) 289.

[54] Weidman,P.D. and Maxworthy,T. : "Experiments on strong interactions between solitary waves" J. Fluid Mech. 49 (1971) 625.

[55] Byatt-Smith,J.G.B. : "An integral equation for unsteady surface waves and a comment on the Boussinesq equation" J. Fluid Mech. 49 (1971) 625.

[56] Oikawa,M. and Yajima,N. : "Interactions of solitary waves --- A perturbation approach to nonlinear systems ---" J. Phys Soc. Jpn. 34 (1973) 1093.

[57] Maxworthy,T. : "Experiments on collisions between solitary waves" J. Fluid Mech. 76 (1976) 177.

[58] Miles,J.W. : "Obliquely interacting solitary waves" J. Fluid Mech. 79 (1977) 157.

[59] Chen,H.-H. : "A Bäcklund transformation in two dimensions" J. Math. Phys. 16 (1975) 2382.

[60] Satsuma,J. : "N-soliton solution of the two-dimensional Korteweg-deVries equation" J. Phys. Soc. Jpn. 40 (1976) 286.

[61] Hirota,R. : "Direct method of finding exact solutions of nonlinear evolution equations" *Bäcklund transformations, the Inverse Scattering Method, Solitons, and Their Applications*, ed. R. M. Miura, (Springer, Berlin, 1976) p.40.

[62] Miles,J.W. : "Resonantly interacting solitary waves" J. Fluid Mech. 79 (1977) 171.

[63] Melville,W.K. : "On the Mach reflexion of a solitary wave" J. Fluid Mech. 98 (1980) 285.

[64] McGoldrick,L.F. : "Resonant interactions among capillary-gravity waves" J. Fluid Mech. 21 (1965) 305.

〔65〕 Ball,F.K. : "Energy transfer between external and internal gravity waves" J. Fluid Mech. 19 (1964) 465.

〔66〕 Thorpe,S.A. : "On wave interactions in a stratified fluid" J. Fluid Mech. 24 (1966) 737.

〔67〕 Bretherton,F.P. : "Resonant interactions between waves. The case of discrete oscillations" J. Fluid Mech. 20 (1964) 457.

〔68〕 Hasselmann,K. : "A criterion for non-linear wave stability" J. Fluid Mech. 30 (1967) 737.

〔69〕 Djordjevic,V.D. and Redekopp,L.G. : "On two-dimensional packets of capillary-gravity waves" J. Fluid Mech. 79 (1977) 703.

〔70〕 Grimshaw,R.H.J. : "The modulation of an internal gravity-wave packet, and the resonance with the mean motion" Studies Appl. Math. 56 (1977) 241.

〔71〕 McGoldrick,L.F. : "An experiment on second order capillary-gravity resonant interactions" J. Fluid Mech. 40 (1970) 251.

〔72〕 Simmons,W.F. : "A variational method for weak resonant wave interactions" Proc. Roy. Soc. London Ser.A 309 (1969) 551.

〔73〕 Nayfeh,A.H. : "Third-harmonic resonance in the interaction of capillary and gravity waves" J. Fluid Mech. 48 (1971) 385.

〔74〕 McGoldrick,L.F. : "On the rippling of small waves, a harmonic nonlinear nearly resonant interaction" J. Fluid Mech. 52 (1972) 725.

〔75〕 Phillips,O.M. : "On the dynamics of unsteady gravity waves

of finite amplitude Part 1. The elementary interactions" J. Fluid Mech. 9 (1960) 193.

〔76〕 Hasselmann,K. : "On the non-linear energy transfer in a gravity-wave spectrum. Part 1. General theory" J. Fluid Mech. 12 (1962) 481.

〔77〕 Longuet-Higgins,M.S. : "Resonant interactions between two trains of gravity waves" J. Fluid Mech. 12 (1962) 321.

〔78〕 Longuet-Higgins,M.S. and Smith,N.D. : "An experiment on third-order resonant wave interactions" J. Fluid Mech. 25 (1966) 417.

〔79〕 McGoldrick,L.F., Phillips,O.M., Huang,N.E. and Hodgson,T.H. "Measurements of third-order resonant wave interactions" J. Fluid Mech. 25 (1966) 437.

〔80〕 Benney,D.J. : "Non-linear gravity wave interactions" J. Fluid Mech. 14 (1962) 577.

〔81〕 Phillips,O.M. : "Wave interactions - the evolution of an idea" J. Fluid Mech. 106 (1981) 215.

〔82〕 Miles,J.W. : "Solitary waves" Ann. Rev. Fluid Mech. 12 (1980) 11.

〔83〕 Benney,D.J. and Luke,J.C. : "On the interactions of permanent waves of finite amplitude" J. Math. and Phys. 43 (1964) 309.

〔84〕 Su,C.H. and Mirie,R.M. : "On head-on collisions between two solitary waves" J. Fluid Mech. 98 (1980) 509.

〔85〕 Chan,R.K.-C. and Street,R.L. : "A computer study of finite-amplitude water waves" J. Comp. Phys. 6 (1970) 68.

〔86〕 Yajima,N., Oikawa,M. and Satsuma,J. : "Interaction of ion-acoustic solitons in three-dimensional space" J. Phys.

Soc. Jpn. 44 (1978) 1711.

[87] Perroud,P.H. : "The solitary wave reflection along a straight vertical wall at oblique incidence" Ph. D. Thesis, Univ. of California, Berkeley, 1957.

[88] Wiegel,R.L. : *Oceanographical Engineering* (Prentice-Hall, Englewood Cliffs, 1964) Chap.3, p.72.

[89] Lin,C.C. and Clark,A. : "On the theory of shallow water waves" Tsing Hua J. Chinese Studies 1 (1959) 54.

[90] Varga,R.S. : *Matrix Iterative Analysis* (Prentice-Hall, Englewood Cliffs, 1962) Chap. 6.

[91] Keulegan,G.H. : "Gradual damping of solitary waves" J. Res. Natl. Bur. Stand. 40 (1948) 487.

[92] Ott,E. and Sudan,R.N. : "Damping of solitary waves" Phys. Fluids 13 (1970) 1432.

[93] Kakutani,T. and Matsuuchi,K. : "Effect of viscosity on long gravity waves" J. Phys. Soc. Jpn. 39 (1975) 237.

[94] Miles,J.W. : "Damping of weakly nonlinear shallow-water waves" J. Fluid Mech. 76 (1976) 251.

[95] Phillips, O.M. : *The Dynamics of the Upper Ocean, 2nd ed.* (Cambridge University Press, Cambridge 1977) p.80.

[96] Benney,D.J. : "Significant interactions between small and large scale surface waves" Studies Appl. Math. 55 (1976) 93.

[97] Yajima,N. and Oikawa,M. : "Formation and interaction of sonic-Langmuir solitons -inverse scattering method- " Prog. Theor. Phys. 56 (1976) 1719.

[98] Ma,Y.-C. : "The complete solution of the long-wave-short-wave resonance equations " Studies Appl. Math. 59 (1978) 201.

〔99〕 Ma,Y.-C. and Redekopp,L.G. : " Some solutions pertaining to the resonant interaction of long and short waves " Phys. Fluids 22 (1979) 1872.

〔100〕 Koop,C.G. and Redekopp,L.G. : " The interaction of long and short internal gravity waves , theory and experiment" J. Fluid Mech. 111 (1981) 367.

〔101〕 Landau,L. and Lifschitz,E. : *Quantum mechanics, nonrelativistic theory* (Pergamon Press, New York, 1958).